THEORETICAL AND EXPERIMENTAL STUDIES OF THE IMPEDANCE CHARACTERISTICS OF HUMAN SKIN

A THESIS

SUBMITTED TO THE DEPARTMENT OF ELECTRONICS

AND THE COMMITTEE ON GRADUATE STUDIES

OF THE CHINESE UNIVERSITY OF HONG KONG

IN PARTIAL FULFILLMENT OF THE REQUIREMENTS

FOR THE DEGREE OF

MASTER OF PHILOSOPHY

BY

POON CHI-SANG

MAY, 1977.


香港中文大學
UNIVERSITY
LIBRARY
SYSTEM
THE CHINESE UNIVERSITY OF HONG KONG

ABSTRACT

The impedance of the skin was found to possess frequency-dependent properties. The magnitude-frequency plot of the impedance resembled that of an RC parallel netwok, but the straight line slope at intermediate frequencies was less than unity. In the complex plane the impedance exhibited a circular-arc locus with the centre displaced from the real axis. These effects could be described by an equivalent model consisting of a constant phase polarization admittance of the form $(j\omega C)^{\alpha}$ and a shunt resistance. From the stripping experiments it was found that the impedance was caused by the laminae structure of the epidermal stratum corneum, and in particular, those cell layers nearest to the surface had the predominant effects. Hence the existence of a 'barrier layer' was disqualified. In palmar areas the shunt resistance was determined by the resistance of the filled sweat ducts, and the presence of some partially filled ducts resulted in a low-frequency departure in the complex impedance locus.

For the given form of impedance function, the voltage transient response was shown to be a bounded and well-defined

function of time, and could be evaluated numerically at discrete time intervals. A simple scheme was developed to infer the parameters of the impedance function from the experimental response curve. The method ultilized the convergence property of the response curves and by a normalization process (both in magnitude and in time scale) the experimental curve could be compared to a set of computed response curves.

The effects of some physical factors were also studied. Two processes were shown to be essential in producing variations of the skin impedance: the effects of sweating and effective surface area. In thermoneutral conditions the effect of the sweat glands was small except in palmar areas. However, in a rigorous state of sweating palmar sweat glands were found to be inhibited by a duct-blocking mechanism. On the other hand, instability of the impedance when using a dry electrode could result from imperfect electrode contact with the skin, producing pressure and movement artifacts.

To investigate the objective existence of 'good conductance points' and their correlates with the acupuncture loci, a more reliable method using solvent-activated silver tape electrode was developed in lieu of Nakatani's Ryodoraku method. Tiny spots of higher conductance were located on the forearm, but the patterns of these spots were found to be random in nature. It was shown that such good conductance spots were created by thermal damage of the

skin tissues when localized current density was built up by a high excitation voltage.

As the skin was made up of a number of cellular laminae the impedance of skin was closely related to the impedance of a single cell. In Part II of the report an attempt was made to derive the diffusion impedance across a cell membrane. It was found that the conventional assumption of microscopic electroneutrality was inconsistent with the electrodiffusion model. In fact, the transport of ions could take place in another state involving a space charge effect. At low frequencies the set up of the space charge was such that local gain of the cation density was coupled to an equal loss in anion density, or vice versa. Under this condition the impedance was shown to be frequency dependent. Moreover, an inductive effect was also possible for a very thin membrane. These results had been confirmed experimentally by other workers.

ACKNOWLEDGEMENT

The author wishes to express his deep appreciation to Mr. Thomas T.C. Choy, supervisor, for his suggestion of the topic of this thesis and also for his continual guidance and counsel, both technical and personal, throughout the course of the investigation.

TABLE OF CONTENTS

PART I

PART II

P A R T O N E

CHAPTER ONE MORPHOLOGY AND PHYSICAL PROPERTIES OF HUMAN SKIN

Histologically the skin is divided into two major parts: the epidermis which forms the outermost lining over the entire body, and the dermis or corium directly underneath. Below the dermis lies the subcutaneous tissue which is mainly made of fat. A typical cross-section of the human skin is as shown in Fig. 1.1a, and Fig. 1.1b shows the relative thickness of each layer and their percentage water contents.

As a boundary between the body and its environment, the skin carries out important functions such as: (a) protection; (b) sensation; (c) excretion; (d) temperature regulation; and (e) food reserve. Most of these functions are attributable primarily to the epidermis or its appendageal glands. The main functions usually attributed to the dermis are simply its strength support to the epidermis, the appendages, and to the associated nerves, blood and lymphatic vessels.

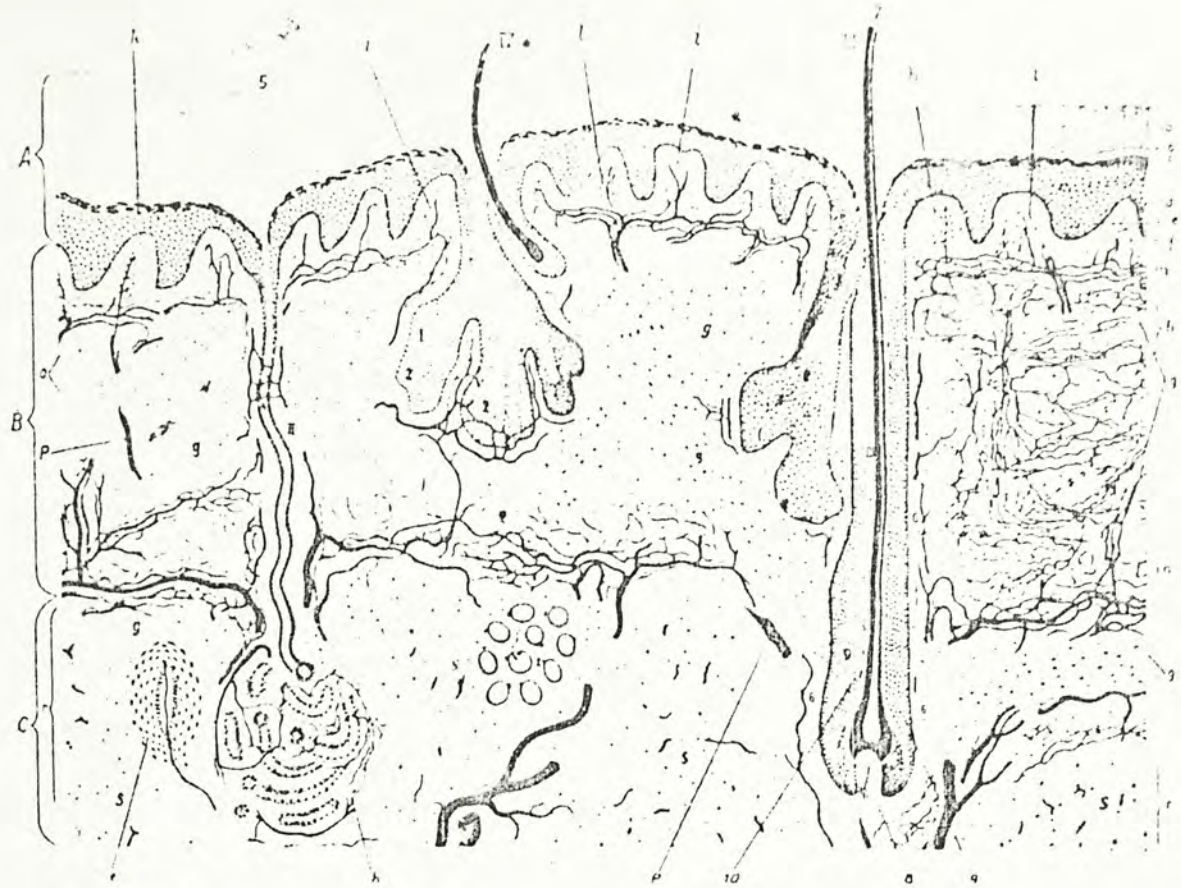

FIG. 1.a Scheme of cross-section of human skin. *A*, epidermis; *B*, dermis; *C*, subdermis; *a*, horny layer; *b*, stratum lucidum; *c*, granular layer; *d*–*e*, mucous layer; *f*, basal layer; *g*, collagenous fibers; *h*, elastic fibers; *i*, papillary capillaries; *I*, sebaceous gland; *II*, eccrine sweat gland; *III*, terminal hair with small sebaceous gland; *IV*, downy hair with large sebaceous gland; *1*, basal layer of sebaceous gland; *2*, sebaceous-gland cells; *4*, sweat-gland duct with capillaries; *5*, sweat-duct pore; *7*, hair; *9*, external root sheath of hair; *10*, internal root sheath of hair (transitorial layer of hair follicle). From Rothman (122). (Drawing by B. Keilitz, Chromolith. Urban & Schwarzenberg, Vienna. Reproduced by permission of Springer Verlag.) (1)

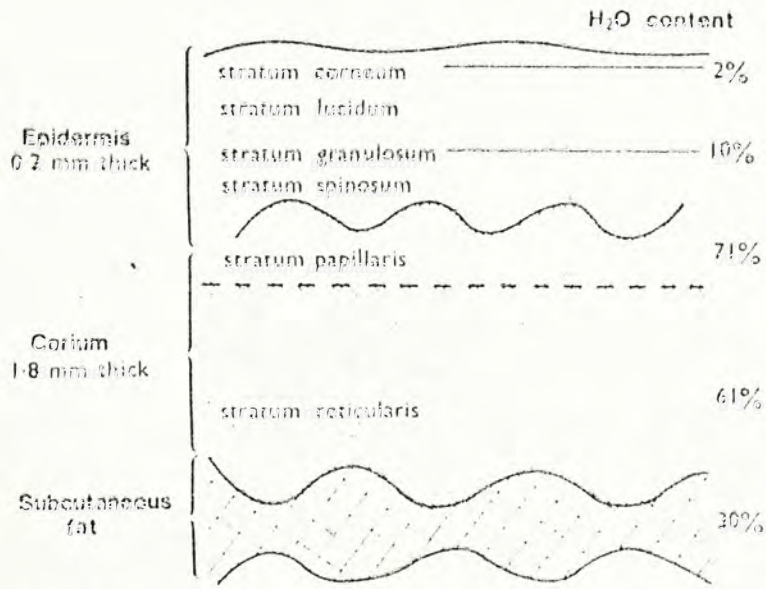

FIG. 1.b The water contents of the different layers of both epidermis and dermis are indicated. The greater water content of the dermal stratum papillaris is especially notable (modified after fig. 73, p. 234 of *Die Normale und Pathologische Physiologie der Haut* by Günter Stüttgen 1965). (2)

1.1 THE DERMIS

The dermis is a structure of connective and elastic tissue and living cells, nourished by a rich vascular supply consisting of arteries and a venous plexus in the lowest part, as well as abundant superficial capillary networks. Also found within the dermis are numerous nerve fibers, sense organs, smooth muscle fibers, and glands.

The vascular system, together with its extensive capillary network and the lymphatic system, drains the entire region with water and a rich supply of electrolytes. It is thus expected that the dermis should be a region of high electrical conductivity. Experimental results show that the resistance of the dermis, together with other parts of the deep tissue, is of the order of 500 Ω (3). The actual value depends on the path length between electrodes, and is usually negligible compared with the impedance of the epidermis. Thus the dermis and the deep tissue are considered as internal links of electric current throughout the body.

1.2 THE EPIDERMIS

The epidermis may be subdivided into four different layers. The deepest layer, composed of fully living cells, is known as the stratum germinativum (or stratum basale). Active cell division takes place here serving as a main source of the overlying cells.

Immediately superficial to the stratum germinativum is the stratum granulosum, which consists of two to five layers of spindle-shaped cells arranged with their long axes parallel to the surface of the skin. The cytoplasm of these cells contains pigment granules. Above the stratum granulosum are the stratum lucidum and stratum corneum, which are composed of dead cells with no organelles. These cells are flat polygons often less than 1 μm thick. The thickness of the stratum corneum varies considerably over the body surface. On the forehead it varies between 20 and 40 μm in thickness; on the palm and sole it is 400 to 700 μm. The stratum lucidum lies immediately below the stratum corneum, and is about 10 μm in thickness. This layer of cells is only found in the palms and soles where the stratum corneum is thickest.

Cells produced in the stratum germinativum continually migrates towards the surface of the skin, replacing those cells above them and undergoing the sequence of changes which characterize the other strata. Finally they are shed at the surface of the stratum corneum. In man all the cells of the epidermis are replaced about once every month; the time taken for the cells of the stratum corneum and the stratum lucidum to be shed is about two days.

1.3 SWEAT GLANDS

1.3.1 Eccrine Sweat Glands

There are two types of sweat glands: the apocrine glands which derive from the follicular epithelium of the hair and open into the follicular canal; and the eccrine glands which are true secretory glands. Both glands possess a single-layered secretory tubule and a double-celled excretory duct, the whole surrounded by a myoepithelial coat (Fig. 1.2). Whereas the apocrine glands perform no known useful function except for body odour, the eccrine glands are chiefly responsible for sweat secretion. Since sweat is a good electrolyte, it is expected that the eccrine glands must play an important role in the electrical properties of the skin.

The secretory coil of the eccrine glands is situated at the border of subdermis and dermis. Secretion is accomplished here by active solute transport. About one-third of the coil consists of excretory duct, which extends upwards through the dermis in the form of a straight tubule and opens to the surface of the epidermis as a pore. In the upper epidermis, however, the duct runs in a corkscrew pathway reminiscent of tubular nephrons in the kidney, thus increasing the diffusion rate of sweat into the corneum. The diameter of a sweat duct is approximately 5 - 10 µm.

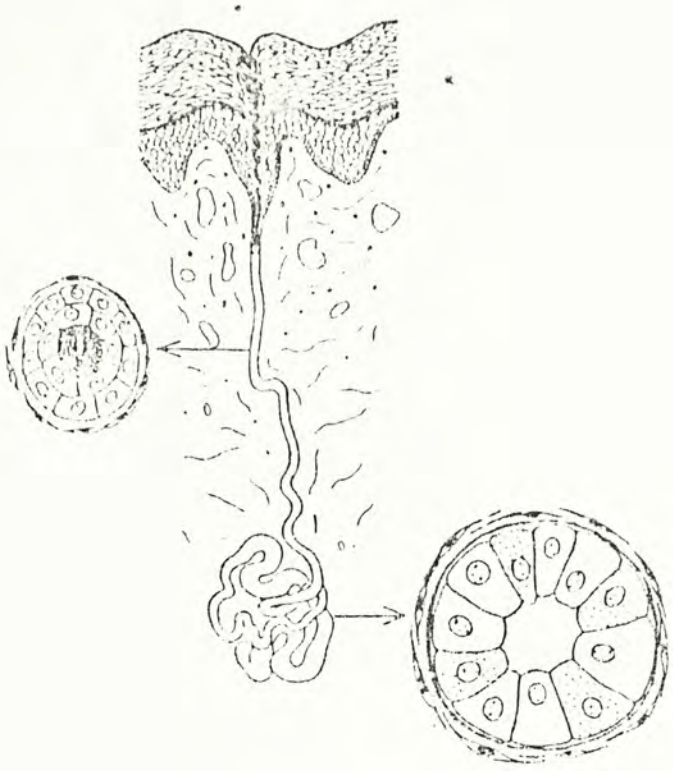

Fig. 1.2a Schematic diagram of the eccrine sweat gland showing the coil and duct in cross-section. (4)

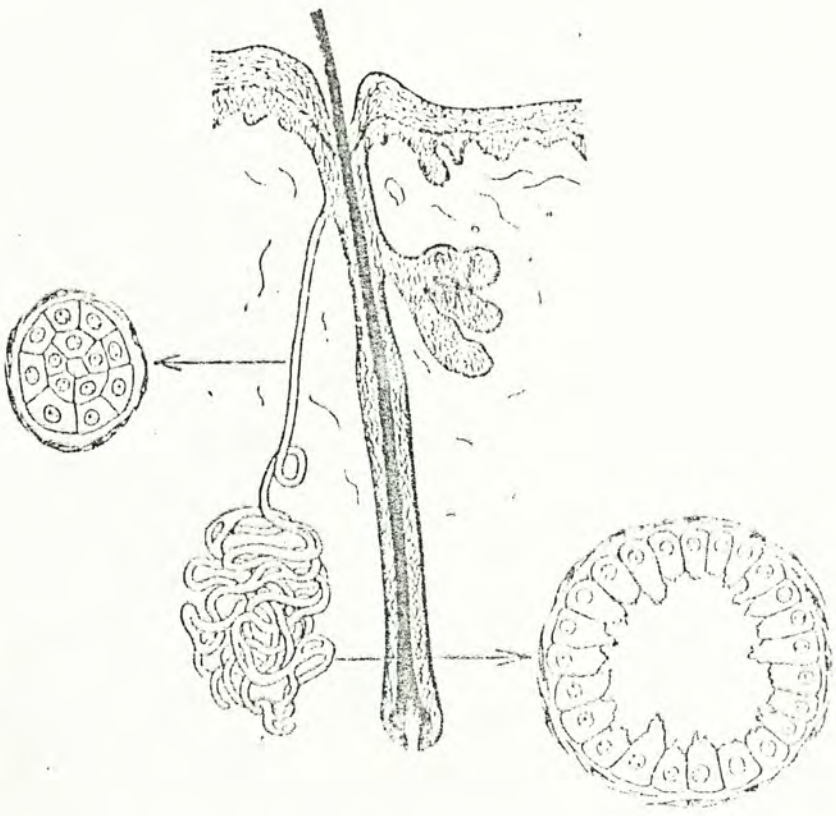

Fig.1.2b Schematic diagram of the apocrine sweat gland showing the coil and duct in cross-section. (4)

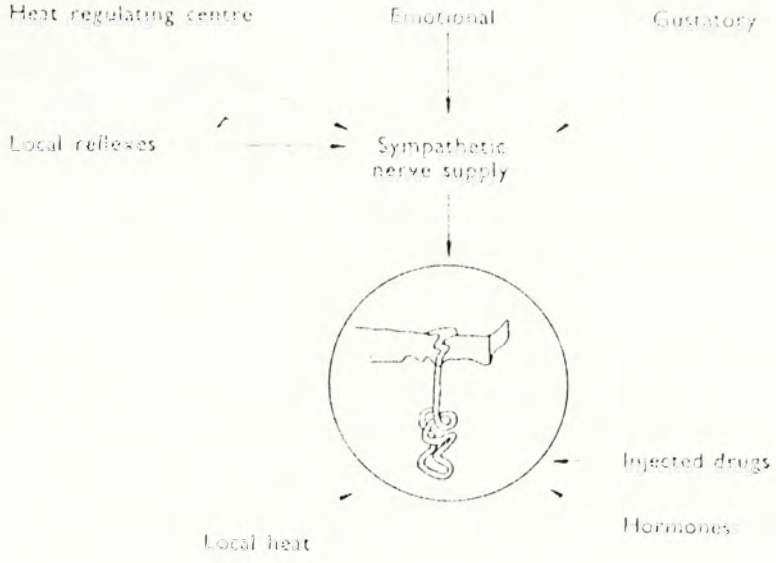

Fig. 1.3a The control of eccrine sweating. (2)

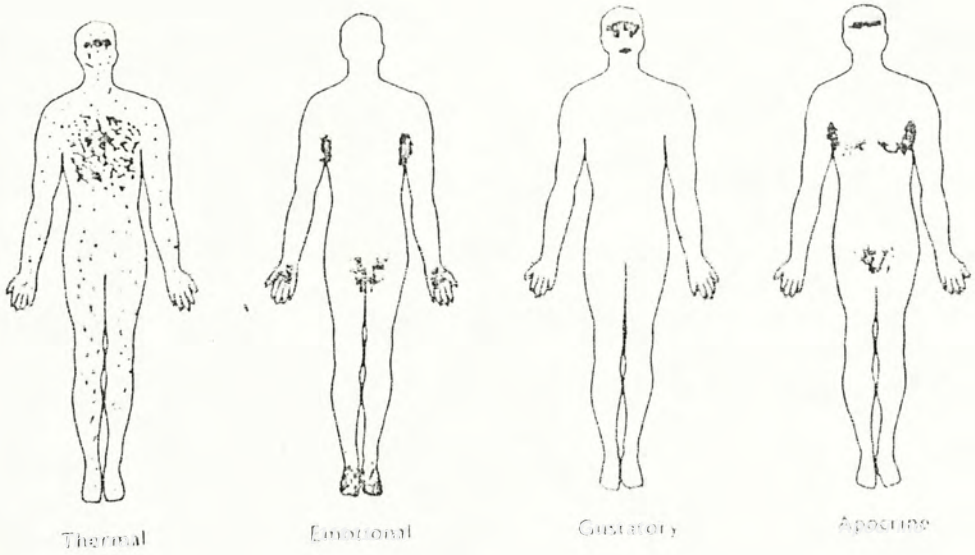

Fig. 1.3b Patterns of physiological sweating. (2)

In humans the eccrine sweat glands are distributed all over the skin surface. Local density of sweat pores may vary from 400 per cm^2 on the palms and soles to about 270 per cm^2 on the face and between 80 and 200 on other parts of the body.

The activity of the sweat glands depends on a number of stimuli, many of which execute direct control over the autonomic nervous system (Fig. 1.3a). The patterns of secretion resulted from different types of stimuli also differ markedly (Fig. 1.3b). Thermoregulatory sweating occurs especially on the trunk and face, and may occur over the body surface including the axillae, palms, and soles. Emotional sweating occurs especially on the palms and soles, and in the axillae. Physiological gustatory sweating is virtually restricted to the face, but may also occur elsewhere under pathological conditions.

1.3.2 Composition of sweat

Sweat is a dilute solution of a variety of substances (Table 1.1). Its actual composition varies among individuals, and even from time to time. When treated as an electrolyte for the passage of electric current, it may be considered as a weak saline solution with a concentration of about 0.3 % (or 0.05 M).

SUBSTANCE		AMOUNT (g%)
Water		99.742-99.221
Solids		0.258- 0.779
Organic solids		0.030- 0.290
Ash		0.144- 0.566
Chlorine (usually over 0.15%)		0.059- 0.346
Lactic acid	about	0.070
Sulphate	"	0.004
Sodium	"	0.150
Potassium	"	0.017
Urea	"	0.030
Sugar	"	0.004

Table 1.1 Composition of Human Sweat (6)

CHAPTER TWO REVIEW ON THE ELECTRICAL PROPERTIES OF SKIN

Skin is a mosaic in which layers of laminated structure pile up one on top of the other. These cell laminae are often perforated by appendages such as the sweat glands and hair follicles. The electrical properties of all these structures differ markedly, and very often they are subject to changes of the ambient and bodily conditions. Thus the skin appears to be an extremely inhomogeneous structure the electrical properties of which are largely influenced by spatial heterogenity on the body surface as well as temporal variability of the environment. This imposes some difficulties in describing the electrical properties of skin. Furthermore, since the passage of electrical currents is by means of ionic transfer, the electrical behaviour will depend somewhat on the electrode/electrolyte system employed for the measurement.

The electrical properties of skin include both its impedance characteristics and its potential. Since we are only concerned with the electrical impedance, the latter will not be discussed unless when appropriate.

2.1 SKIN RESISTANCE

Since the dermis is freely permeable to ionic movement, it is generally considered that the electrical resistance of skin is mainly due to the epidermis. There are two hypothesis to account for this epidermal resistance. In one hypothesis, the whole corneum is considered to be responsible for the observed resistance, with decreasing ionic permeability as one moves from the inner to the outer layers of the corneum. This is demonstrated by a skin-stripping procedure in which layers of corneum cells are removed by pressing an adhesive cellulose tape on the skin surface and pulling it away (7, 8). Alternatively, a microelectrode is inserted gradually into the skin (9). In either case, the resistance decreases progressively as the deeper part of the corneum is reached; the outermost keratin layers appear to have the highest resistance. Since the impedance of powdered keratin is found to be negligible unless it is kept absolutely dry (10), it is considered that the cellular structure of the corneum is essential for its impedance.

Another view of the epidermal resistance is the hypothesis that there exists a barrier layer within the corneum that is responsible to most of the resistive effects. This arises out of the fact that the horny cells are highly hydrophilic and thus it appears that they should not offer too much resistance to ionic current. This is supported by the experimental observation that many ions (e.g. thorium-X, and phosphate ions containing radioactive

Can penetrate readily most of the ...

phosphorus, Ref. 3). On the other hand, the epidermis is also known to play the role as a boundary for the regulation of body evaporation. Therefore it is reasonable to think that this function is achieved by placing a water-resistant barrier beneath the hydrophilic keratin layer. The exact location of this barrier is not known, but it is usually believed to lie in the stratum compactum (the more densely packed lower portion of the corneum), the stratum lucidum, or the granular layer (1, 3)

Whether the epidermal resistance is caused by the entire stratum corneum or only due to a specific barrier layer is still a point of argument. There is, however, an obvious pathway by which current can bypass. The eccrine sweat glands, when activated, deliver sweat onto the surface via the cockscrew sweat ducts which open to the skin surface. Since sweat is a good electrolyte, most of the current can pass along the duct down to the dermis. Suchi (9) showed that the resistance of a fine electrode placed on or near a sweat gland was much less than that between glands. Although the size of a sweat duct is quite small, the total current that can flow through all sweat ducts over a certain area may be quite larg- (compared with the corneum) if the density of sweat ducts is high. Besides, the sweat may have an effect on the corneum by hydrating it through the process of diffusion. This increases the ionic conductivity of the corneum, and hence the total resistance of the epidermis is reduced. In this way the sweat glands have a very important role in the apparent resistance of the epidermis. In

fact they have been identified to be a major mechanism responsible for electrodermal response phenomena occuring in the palms and soles (Sec. 2.3).

2.2 SKIN CAPACITANCE

Gildemeister (11) was among the first to measure skin impedance with alternating currents. In his experiment, he found that the impedance decreased at higher frequencies. He then attributed this to polarization effects which were usually found to occur in the phase boundaries of an electrode or a cell membrane. As such the apparent impedance of the skin would in fact be the result of a counter-EMF generated by the passage of electric current through a semi-permeable membrane. The setting up of this counter-EMF does not follow immediately after the start of current flow, but it is always some time after sufficient charges have been accumulated. This delay in time makes it very similar to the behaviour of a capacitor. Because of this, the polarization impedance can be viewed as consisting of a 'polarization capacitor' which in effect is similar to a lossy dielectric.

If polarization is the basic mechanism responsible for skin impedance, it is likely that the most probable contribution would be due to the epidermal cell membrane structure and the peripheral electrical path around the cell. The overall impedance

would then be that of a polarization capacitor in shunt with some resistive networks. However, this does not exclude the possible effects of some other processes. In an experiment to find the changes during an electrodermal response, Yokota and Fujimori (12) showed that the change in skin impedance during a response is due solely to a change in the parallel resistance, the polarization capacitance remaining unchanged. This would imply if polarization is a factor for the observed impedance, at least some static resistance paths exist across the skin sheath.

It is interesting to note that such a polarization effect, although so commonly recognised in so many occasions, has not received a satisfactory quantitative explanation. It is therefore quite doubtful if the use of it in explaning skin impedance is really appropriate. Perhaps a more convenient way to describe the capacitive effect in skin is to think in terms of a static capacitance or series of such capacitance arising out of the stratified structure of the epidermal cell laminae. However, no direct proof is available to show that this is more appropriate. Whatever its nature may be, it is almost certain that the capacitance must reside in the corneum, as demonstrated by the same skin-stripping experiment (Sec. 2.1) in which both the conductance and the capacitance were found to increase progressively as successive strips were removed (8). As stated by Lawler who carried out the above experiment, the increase in capacitance could have been caused either by decreasing the distance across the dielectric between the electrode

and the underlying conducting zone or by removing successive capacitors originally in a series arrangement. In either case, the corneum appeared to be the dielectric material of a capacitor or series of capacitors.

In accordance with this view, Tregear (7) then proposed a model which took into account both resistive and capacitive effects found in the corneum (Fig. 2.1). In this model, each cell lamina of the corneum is represented by a membrane capacitance C, intracellular resistance r, and a parallel extracellular resistance R_n (where n = 1, 2, 3, 4,..... and is the number of cell laminae measured from the skin surface). Each cellular model is then joined in series as in the corneum to give the total skin impedance. Since the outer laminae of the stratum corneum are usually drier than the inner ones, the resistance R_n decreases gradually downwards.

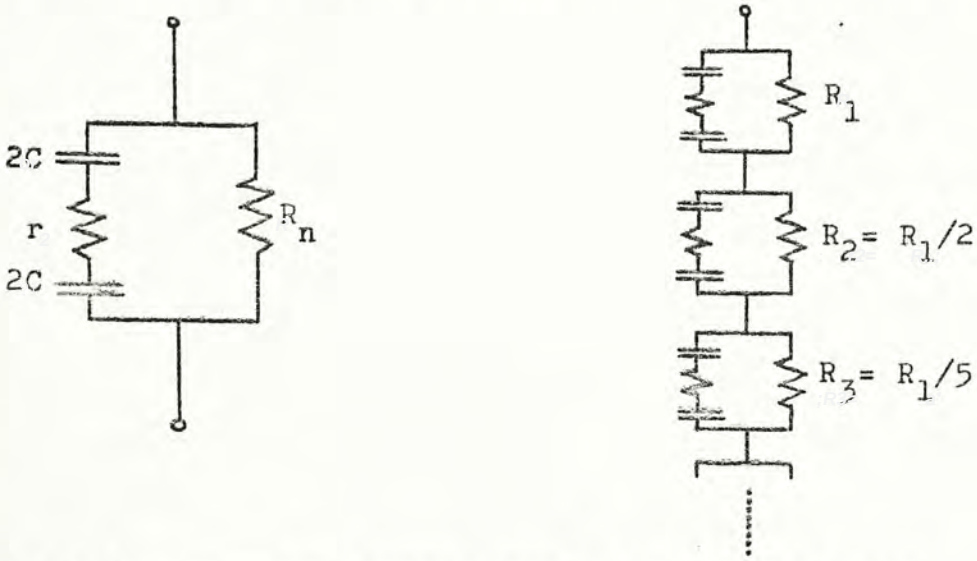

Fig. 2.1 Tregear's model for the skin impedance:
(a) Cellular model (single cell lamina)
(b) Complete model

2.3 ELECTRODERMAL RESPONSE (EDR)

2.3.1 What is EDR

Electrodermal response refers to the change in skin conductance and potential subsequent to an external stimulus. This phenomenon has been of interest to psychologists for many years as an indication of psychological activities. Recently more standard terminology has been used to classify each phenomenon. The following terms are more generally used:

SCL = Skin Conductance Level (base level)
SCR = Skin Conductance Response
SPL = Skin Potential Level (base level)
SPR = Skin Potential Response

Various types of EDRs are illustrated in Fig. 2.2. In most cases the sequence of events during an EDR may be described as follows. On exposure to an external stimulus (e.g. those causing pain, fear, shock etc.) strong enough to upset the psychological state of the subject, a sudden rise in skin conductance starts, usually one or two seconds after the point of stimulation. This reaches a peak in less than one second and may amount to a few percent to as much as 20 % of the base level. From this point conductance begins to recover slowly for some seconds to return to the base level. If the potential is simultaneously observed, one may find a monophasic change of potential having a similar but different time course.

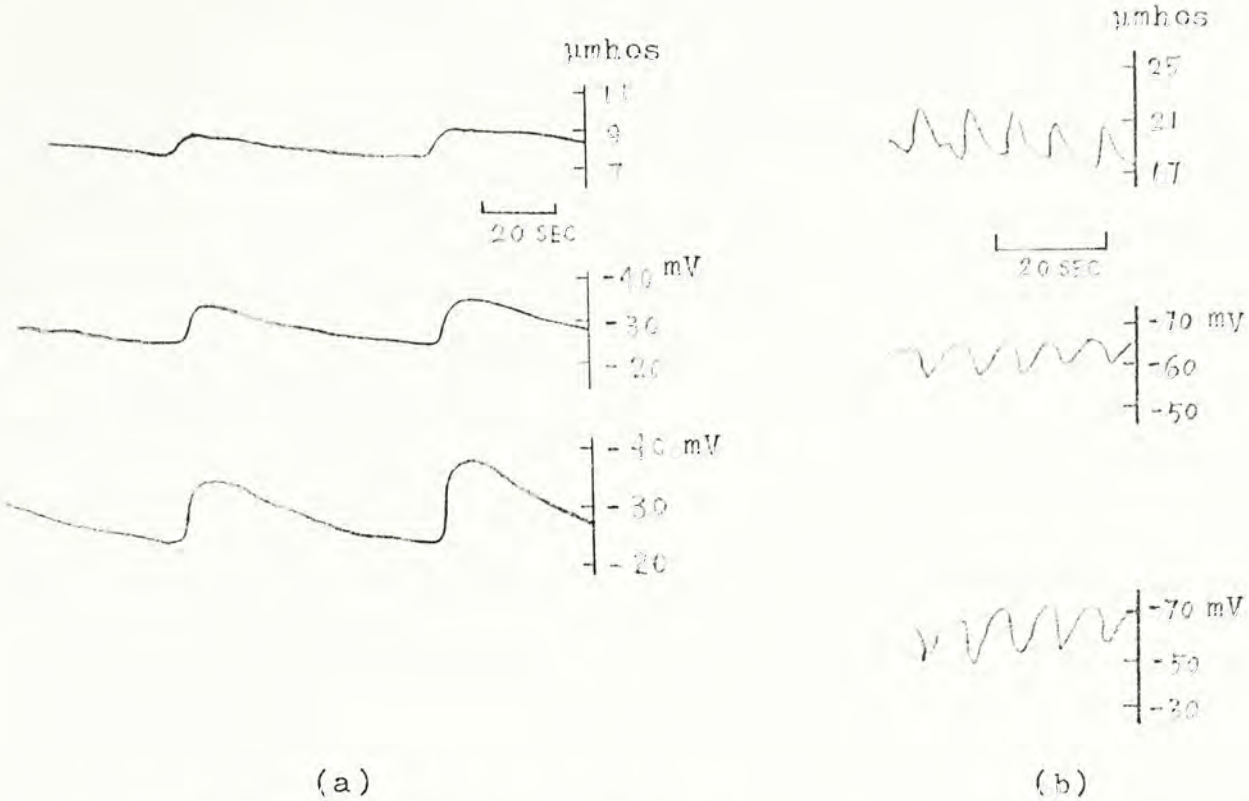

Fig. 2.2 (a) Slow recovery SCRs (upper tracing) and monophasic negative SPRs (middle and lower tracing); (b) Rapid recovery SCRs (upper tracing) and monophasic positive SPRs (middle and lower tracings). (13)

The most common response is a negative shift of potential at the active site. In some instances the SCRs may have a more rapid recovery limb, while the SPRs are monophasic positive, or else diphasic with a very small initial negative component. These responses can be elicited by asking the subject to take very fast, deep breaths just after the subject has blown up a balloon until it bursts. This association between positive SPRs and rapid recovery SCRs, on the one hand, and slow recovery, monophasic negative SPRs and slow recovery SCRs, on the other hand, is characteristic (13).

2.3.2 Mechanisms of EDR

Interesting enough EDRs are most easily observed in palm and sole areas where the population of sweat glands is densest. In spite of the much thicker epidermis found in these areas, the SCL is also found to be greater, suggesting that the sweat glands provide a better conductance pathway through the poorly conducting epidermis. In the light of this, much work has been done to identify any correlation between EDRs and sweat gland activities. Up to the present, numerous evidence has been found in support of this view (13, 14).

One basic mechanism by which the sweat glands can cause an instantaneous change in skin conductance is the secretion of sweat consequent upon sweat gland responses. This may follow from the stimulation of the nerves innervating the sweat glands. When the ducts are filled with sweat, they provide additional conductance pathways thereby producing an instantaneous increase in the overall conductance. If sweat is slowly reabsorbed from the ducts the increased conductance would decline slowly, completing the cycle of a slowly recovering SCR. At the same time, the conductance of the corneum may be gradually increased by sweat diffusing through the duct wall, but this action is too slow to accomplish an SCR. In the long run, however, the SCL may become higher.

In addition to the duct-filling mechanism outlined above

the skin possesses membrane-like properties which may also take part in the production of a response. One obvious evidence is the dependence of the amplitude of an EDR on the basis of electrolytes used to record the response. This can only be explained by the action of a semi-permeable membrane capable of offering selective permeabilities to different ions. During a response, however, the membrane becomes equally permeable to all ions, thus producing different fractional changes in each response. The exact location of such a membrane is still uncertain, but Edelberg (3) suggested that the most attractive site is the duct wall at the level of the germinating layer. At this point some salt is reabsorbed from the sweat to prevent excessive loss of it during sweating. Probably this salt reabsorption reflex can be triggered by a rise in either the sodium concentration in the sweat or the luminal hydrostatic pressure. In each case the permeability of the duct wall membrane is varied resulting in a change in the conductance and potential here. Unlike the duct-filling process this change in the membrane permeability can recover shortly to produce a rapid recovery SCR.

Although the duct-filling mechanism and the membrane mechanism may proceed independently, both of them originate from the presence of the sweat glands. In other words, the electrical properties of the skin can be greatly influenced by sweat gland activities. We shall have more discussions on this in Sec. 5.2.

CHAPTER THREE PRELIMINARY INVESTIGATION OF SKIN IMPEDANCE

In Chapter 2 we have seen that the impedance of the skin mainly resides in the epidermal stratum corneum which has a relatively higher resistivity. Associated with this resistive component is the capacitive effect originating from the cell laminae structure found in the corneum. Therefore, the impedance of the skin can be roughly viewed as similar to that of a lossy dielectric, or series of dielectrics.

Our primary objective is then to develop an electrical model to simulate the impedance characteristics of the skin in such a way that each component of the model corresponds to a structural unit of the epidermis. An important restriction on such a model is that the electrical properties of the skin as described by the model should be independent of the experimental method employed, i.e., no significant physiological changes should be induced during the course of any such measurement. This requires the applied voltage or current to be within physiological tolerable limits, otherwise non-linearity in the electrical parameters results. Throughout our following discussions, therefore, measurement

within the linear range is assumed unless otherwise stated. For instance, the voltage across the skin is well below order of a volt, and the current density is less than 5 $\mu A\ cm^{-2}$ (14).

3.1 EXPERIMENTAL METHOD

3.1.1 Experimental Set Up and Procedure

The set up for impedance measurement is as shown in Fig. 3.1. The FET OP AMP had a very high input impedance and served as a constant current source. For a given input signal, the current through the skin was determined by the input resistor R, and the output voltage was proportional to the impedance of the skin site connected across the electrode leads X_1, X_2. The phase of the

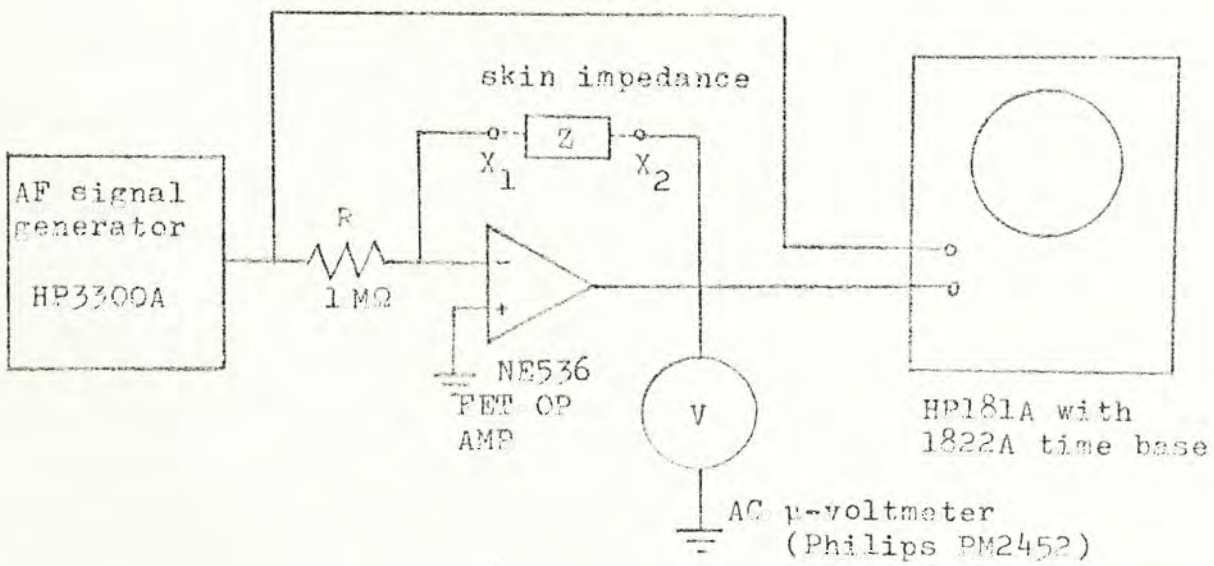

Fig. 3.1 Set-up for impedance measurement.

output relative to the input signal was measured using the storage scope with a delay time base. Both the impedance magnitude and phase were recorded at selected frequency settings.

Before electrode attachment was made the skin site was thoroughly cleaned with a piece of cotton ball soaked with rubbing alcohol, and let dry completely. This removed traces of surface grease and dirt on the skin and ensured a better contact. A Beckman Ag/AgCl electrode (9mm diameter) filled with electrode paste was applied to the 'active' skin site. The whole hand on the same side of the site was then immersed in a 0.05 M saline solution in a metallic container used as a reference eletrode. Because of the large surface area and the high conductivity of saline, the impedance of the reference electrode plus the reference skin site was always negligible. Also, the impedance of the Ag/AgCl electrode could be considered negligible under normal circumstances. Hence the measured impedance was mainly due to the 'active' skin site. After applying the electrodes to the skin, a stabilization period of about 30 minutes was allowed before measurement was taken (Sec. 5.3.1). The results were presented in frequency plots.

3.1.2 Noise Considerations

Since the measurement was made at a rather low signal level (about 0.1 μA), external interference constituted a major problem. The interference might be caused by external magnetic fields, electric

fields, or even electromagnetic fields. Most of these problems could be eliminated by the use of screened electrode leads and keeping away from possible sources of interference. Nevertheless this did not remove all the noise pick-up through the body because the latter was such a large volume conductor that even a small electric field from a power cable could give rise to appreciable interference. In order to minimize the noise, it was found that a simple arrangement of the electrode leads could help a great deal. To illustrate this, the equivalent circuit of Fig. 3.1 is redrawn omitting all signal sources except that due to interference which is in the form of a displacement current I_D coupled to the body through a hypothetical capacitor C_D (15). This is illustrated in Fig. 3.2 below.

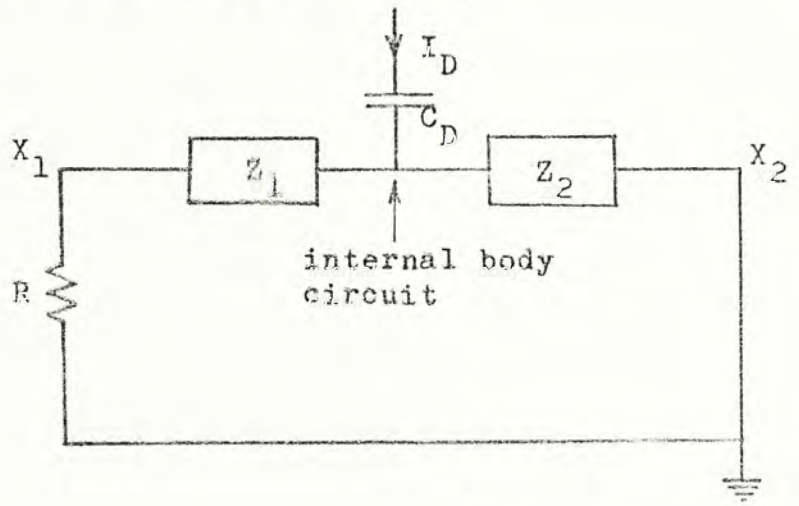

Fig. 3.2 Equivalent circuit of Fig. 3.1 as seen by the noise current I_D. Z_1,Z_2 represents skin-through-electrode impedance. The O/P resistance of the OP AMP and the resistance of the body internal are neglected.

Interference is measured as the noise potential generated across the electrodes, i.e. across points X_1, X_2. From the diagram it can be shown that this potential is given by

$$V_{12} = V_D - \left(I_D - \frac{V_D}{Z_2} \right) Z_1$$

where $V_D = I_D \left((R + Z_1) /\!/ Z_2 \right)$

If the reference electrode is connected to the output terminal of the OP AMP (i.e. X_2), then $Z_2 \ll Z_1$ and the noise potential $V_{12} \doteq I_D Z_2$. In the actual case this potential was rather low because the impedance at the reference site was negligibly small compared with the active-site impedance. On reversing the electrode arrangement, the noise potential would become much higher and affect the measurement seriously. Hence the first electrode arrangement was preferred.

3.2 IMPEDANCE-FREQUENCY PLOTS

As a first step to investigate the frequency characteristics of skin impedance, the magnitude of the impedance was plotted as a function of frequency. A typical impedance curve for the fingers is shown in Fig. 3.3. As seen from the graph, the impedance at low frequencies is large and close to the DC resistance; at high frequencies it is small and nearly the same as the resistance of

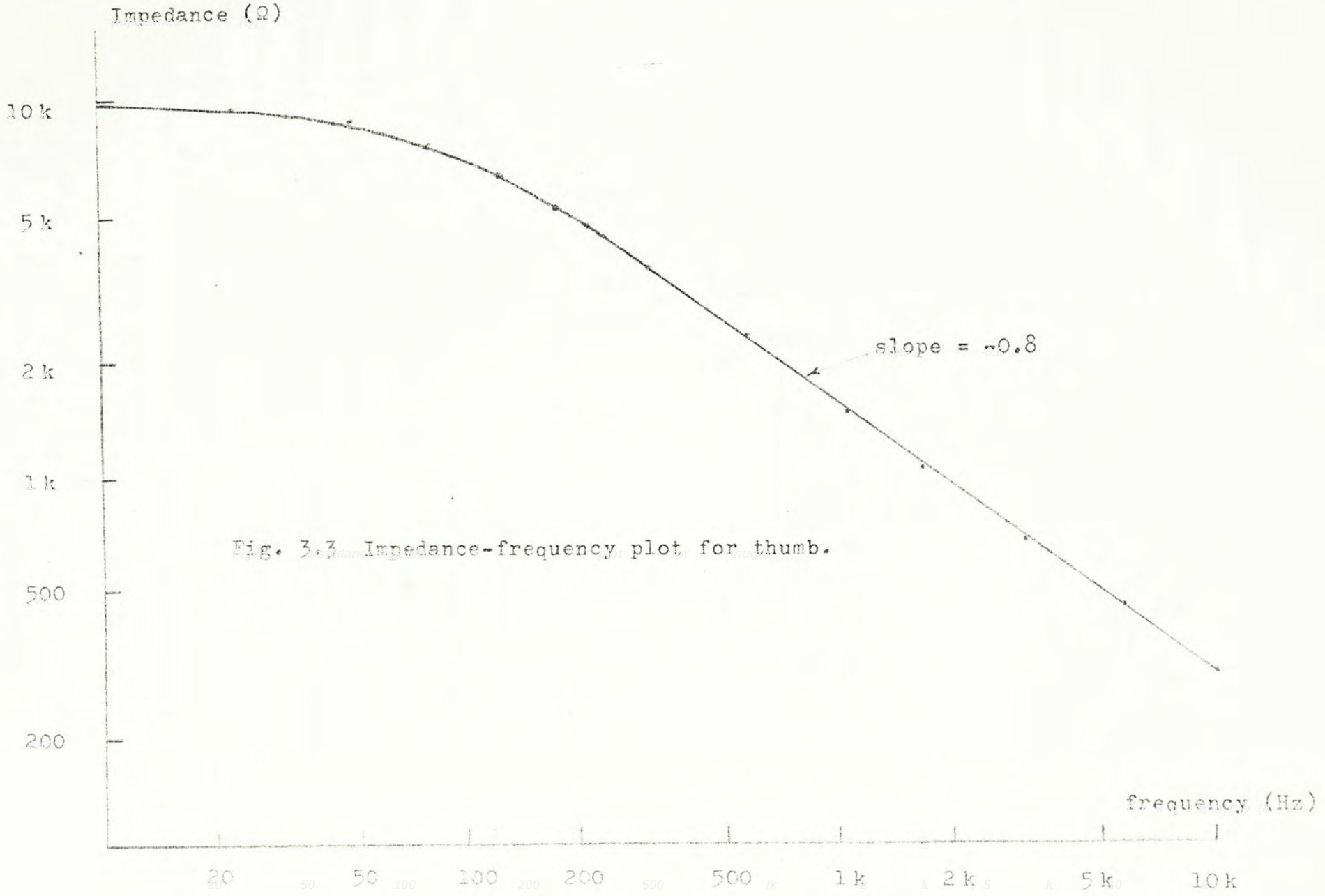

Fig. 3.3 Impedance-frequency plot for thumb.

the deep tissues. It is thus very similar to the frequency characteristic of a single pole impedance function. This result is similar to those of Swanson and Webster (16). Based upon the simple impedance curve they modelled the skin impedance as a parallel combination of a resistor and a capacitor, the two being in series with another resistor (Fig. 3.4).

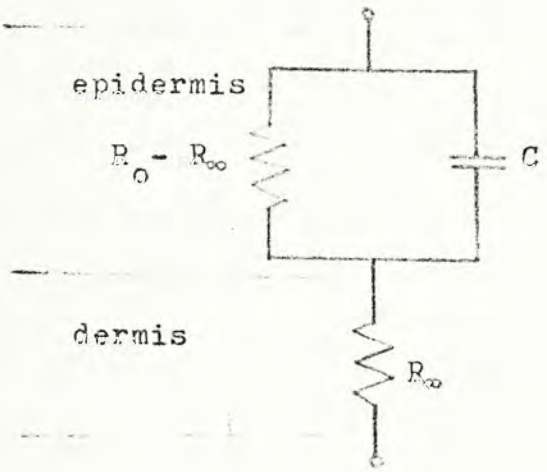

Fig. 3.4 Simple model for skin impedance by Swanson and Webster

Unfortunately this simple electrical model of the skin suffers from one serious drawback: the impedance curve at mid-frequencies departs significantly from the experimental curve, although the two bear similar shapes alongside. Such a discrepancy in the straight line slope is not usual in convential circuit analysis. It is well known from Bode that the frequency response of an impedance function far beyond its pole decays 20 dB/decade. In the log $|Z|$ vs log f plot they will give a straight line of slope equal to -1. But the straight line portion of the experimental curve always gives a slope less than unity, in our case it is in the range from -0.7 to -0.9 (for different skin sites). Clear enough this simple model of an RC combination would be quite

inadequate if a more rigorous representation of the skin impedance is desired.

The mid-frequencies straight line having a slope less than unity suggests some form of an electrical network other than the conventional pole-zero ~~analysis~~ type. Although it is possible to simulate a particular straight line response by adding more poles and zeros to the impedance function of the simple model, there is little justification as to the physiological significance of these added elements. Further, there are numerous electrical networks that can give the same impedance curve as the one obtained, and there seems to be no reason to choose one or the other. All these arguments disclose the inadequacies of the impedance plot as a basis for the analysis of skin impedance, and so a better form of data presentation is needed.

3.3 COMPLEX IMPEDANCE LOCI

If the simple model of Fig. 3.4 for skin impedance is assumed, the theoretical impedance function can be written as

$$Z = R_\infty + \frac{R_o - R_\infty}{1 + j\omega C(R_o - R_\infty)} \qquad (3.1)$$

The real and imaginary parts of the impedance are

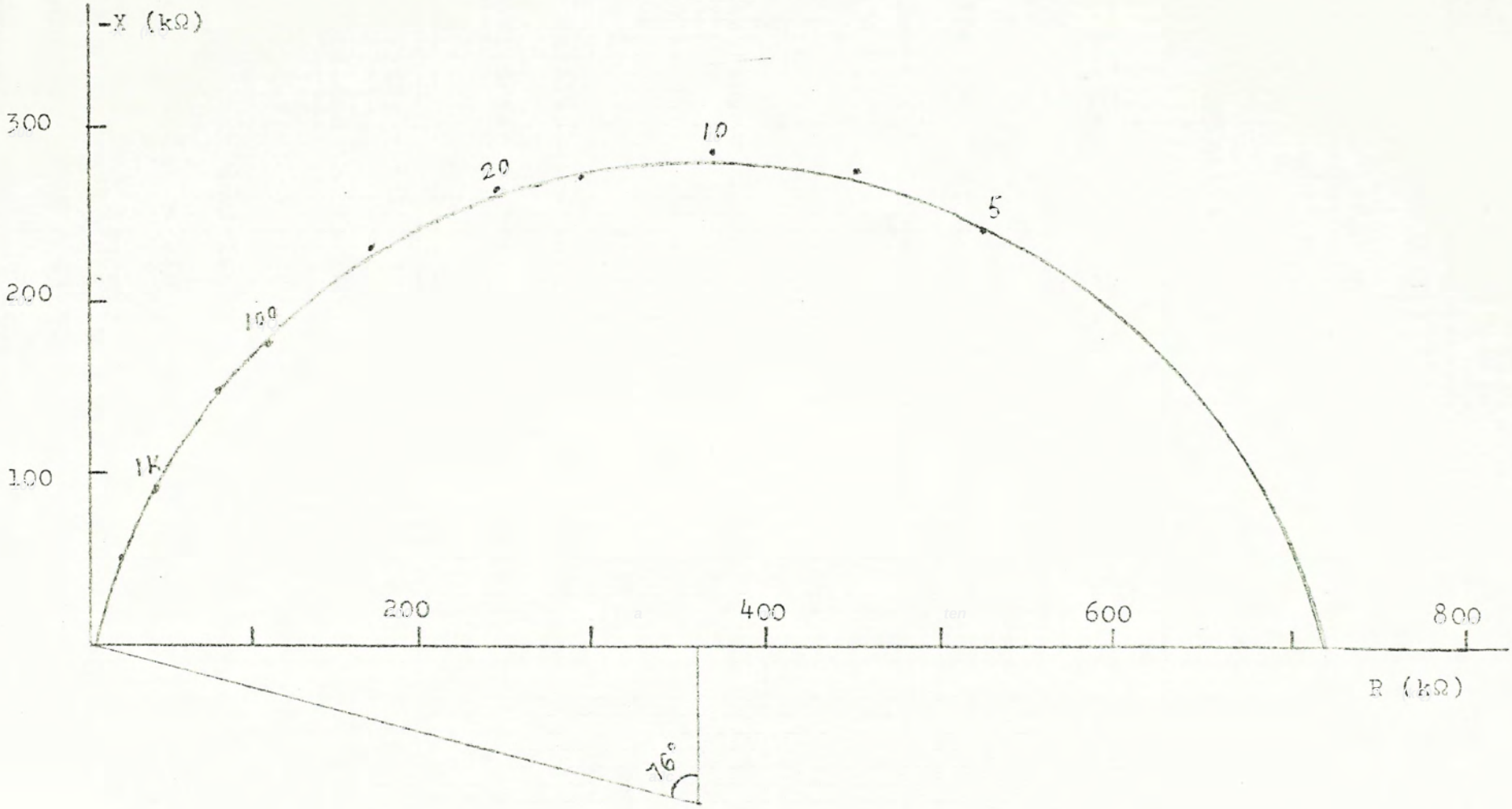

Fig. 3.5 Impedance locus from measurement on foot. Values shown are frequencies in Hz.

$$R = R_\infty + \frac{R_o - R_\infty}{1 + \omega^2 C^2 (R_o - R_\infty)^2}$$

$$X = - \frac{(R_o - R_\infty)^2 \omega C}{1 + \omega^2 C^2 (R_o - R_\infty)^2}$$

Combining and eliminating ω, we have

$$\left(R - (R_o + R_\infty)/2 \right)^2 + X^2 = \frac{(R_o - R_\infty)^2}{4}$$

A plot of the reactance against the resistance in the complex impedance plane gives a semicircle centred at $\left(\frac{R_o + R_\infty}{2}, 0 \right)$ and radius $\left(\frac{R_o - R_\infty}{2} \right)$.

An impedance locus obtained by measurements on the foot is as shown in Fig. 3.5. As predicted the impedance locus is found to be in the form of a semi-circular arc, but the centre of the arc is displaced downward from the real axis, the arc subtending an angle of about 152° at the centre.

Similar results were obtained by Khalafalla et al.(17) for human foot and the forearm. In order to explain the displaced circular-arc plot, they proposed an electrical model in which a frequency dependent resistance r is put in shunt with the capacitor C in the simple model of Fig. 3.4. A condition to be imposed on the resistor r is that its value is inversely proportional to the frequency such that $r = a/\omega$, where a is constant and ω is the angular frequency. This is illustrated in Fig. 3.6.

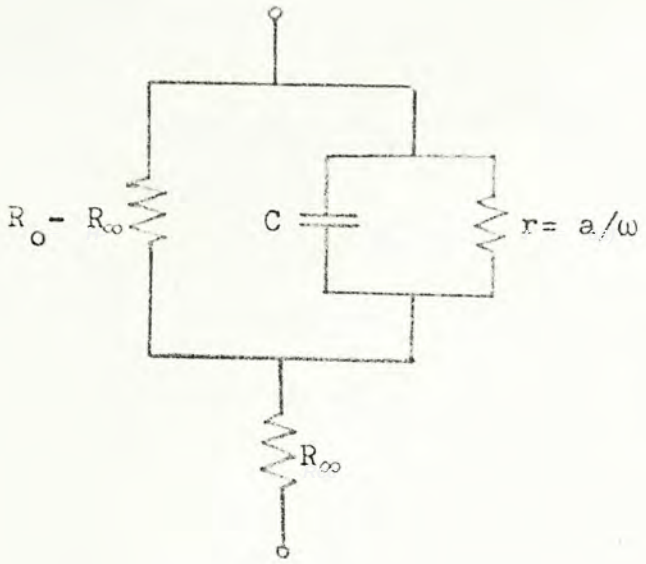

Fig. 3.6 Modified skin model by Khalafalla et al.

The impedance of this modified skin model is

$$Z = R_\infty + \frac{R_o - R_\infty}{1 + \omega R(1/a + jC)} \qquad \text{where} \quad R = R_o - R_\infty$$

The impedance locus of this electrical model of Khalafalla et al. also describes a circular arc in the complex impedance plane. However, if we go back to examine its impedance response, it is not difficult to find that the straight line portion of the curve also has a slope equal to -1. Such a discrepancy with the experimental result again makes it unacceptable as an equivalent model. Nevertheless this is already an improved version in that it conforms to the circular arc locus. In the next section we shall be able to develop a better electrical model which can take into account both the impedance plots and the impedance loci.

3.4 COMPLETE MODEL FOR SKIN IMPEDANCE

The introduction of a frequency dependent resistor r in shunt with a capacitor as in the modified skin model of Khalafalla et al. results in an admittance given by

$$Y = \omega\left(\frac{1}{a} + jC\right)$$

This admittance is characterised by having a constant phase angle, $\phi = \tan^{-1}(C/a)$ independent of the frequency. Also, the magnitude of this admittance varies as ω. This constant phase behaviour independent of the frequency results in the circular-arc locus in the complex impedance plane. On the other hand, the constant small slope in the impedance plot suggests that the impedance decreases according to certain power of the frequency. Combining these facts, we can write the impedance function as

$$Z = R_\infty + \frac{R_o - R_\infty}{1 + (j\omega C)^\alpha (R_o - R_\infty)} \qquad (3.2)$$

where $\alpha = \frac{\theta}{90^o}$; θ ($< 90^o$) being the constant phase angle;

and $(j\omega C)^\alpha = (\omega C)^\alpha(\cos\theta + j \sin\theta)$ is a constant phase admittance.

The corresponding equivalent circuit is illustrated in Fig. 3.7a.

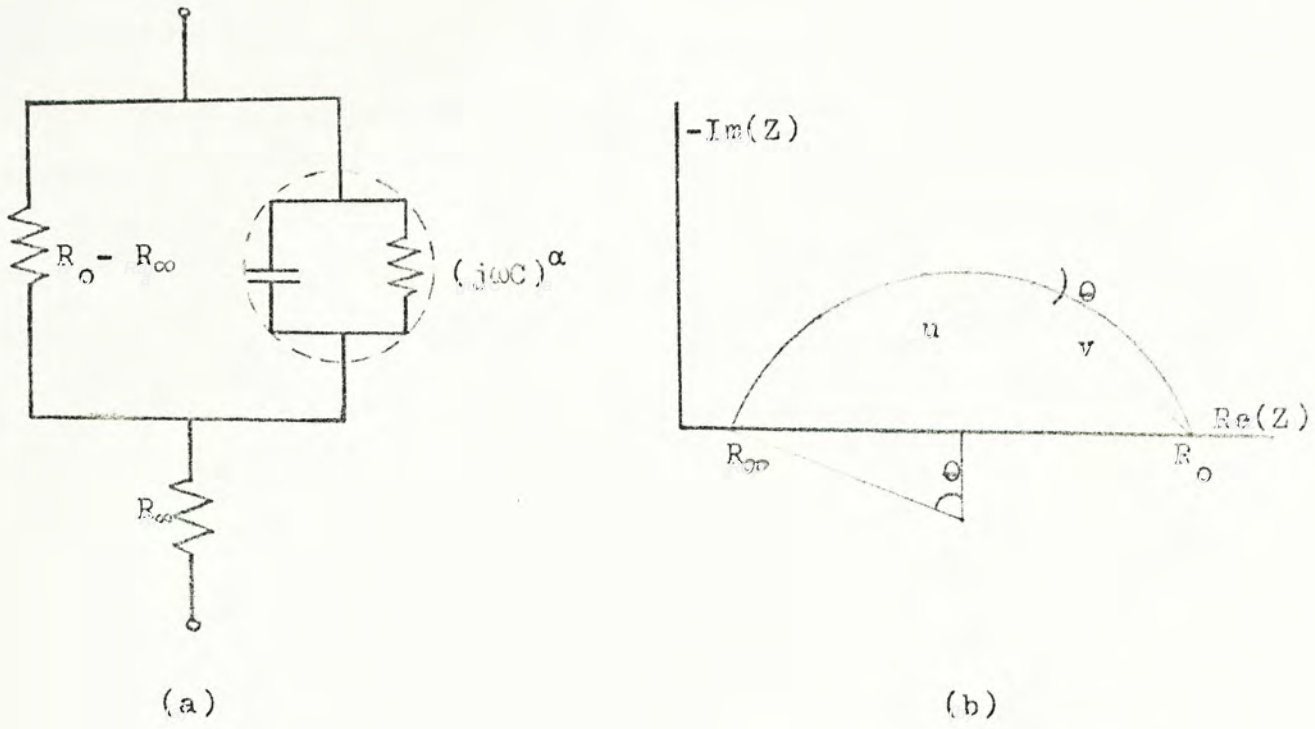

(a) (b)

Fig. 3.7 Complete model for skin impedance:
(a) equivalent circuit;
(b) impedance locus.

Writing $$u = Z^* - R_\infty = \frac{R_o - R_\infty}{1 + (-j\omega T)^\alpha} \qquad (3.3)$$

$$v = R_o - Z^* = (-j\omega T)^\alpha u \qquad (3.4)$$

where $T = (R_o - R_\infty)^{1/\alpha} C$,

and Z^* = complex conjugate of Z;

it can be seen that the angle between u and v is the constant Θ. It follows that the locus of Z is a circle and that the central angle subtended by $R_o - R_\infty$ is (2Θ) (Fig. 3.7b). The centre of the circle is at $(\frac{R_o + R_\infty}{2}, -\frac{R_o - R_\infty}{2} \cot \Theta)$ and the radius is $(R_o - R_\infty)/2$.

More important, this theoretical model can also explain the constant, non-unity slope behaviour of the impedance plots. Now at mid-frequencies,

$$R_\infty \ll \frac{1}{(j\omega C)^\alpha} \ll (R_o - R_\infty)$$

so that the impedance is approximately

$$Z = \frac{1}{(j\omega C)^\alpha} \quad .$$

A plot of $\log |Z|$ vs $\log \omega$ gives a straight line and the slope $-\alpha$ is always less than unity.

3.5 DISCUSSION

The empirical model for the epidermal impedance has been found to be consisting of a constant phase admittance shunted by a parallel resistance. Although no verification has been given to show that this model is a unique one for the skin, there are several advantages in using such a model. First, there is a striking simplexity in the mathematical representation. Besides, it will be shown that it is possible to identify a one-to-one correspondence between each component of the model and a particular physiological process.

The introduction of a constant phase admittance $(j\omega C)^\alpha$ in

the skin impedance model should not be too surprising because such an anomalous admittance is also found in other electrolytic processes involving ionic conduction. For instance, it was found that the polarization impedance of an electrode possesses a constant phase element varying as the square-root of the frequency (6). More appropriately perhaps, it was known that the impedance of a cell membrane exhibits similar circular-arc plots in the complex impedance plane (18). In fact, the equivalent circuit in Fig. 3.4 is also applicable to cell membranes.

The peculiar constant phase and frequency-dependent behaviour of this anomalous admittance incorporated in the model is an extremely interesting feature of a biological impedance. Not only is it so much different from ordinary passive circuit elements that the conventional method of circuit analysis fails to apply, there is also the important question of how such an admittance can originate in biological matter. Obviously this will lead to some clues regarding the fundamental mechanisms ocurring in living cells and, in particular, across the membranes of these cells. Despite the so many efforts invested, however, it seems that little progress has been made in explaining the physical nature of a constant phase, frequency dependent admittance. Abortive attempts had been focused on the theories of polar relaxation (19) first introduced by Debye and later modified by Cole (20, 21). These treatments often led to even more mathematical complexities which could be solved only with quite restrictive assumptions. These assumptions, of course, remained

to be explained and so in fact there would be little to be gained by this approach.

Another possibility is to think in terms of electrolytic polarization. It was found that electrodiffusion could be a possible mechanism responsible for the observed frequency characteristics (22-24). This approach, however, has encountered some difficulties in that the predictions do not correspond with experimental results. This, of course, may be due to undue simplifications in the basic assumptions involved, and on this a conclusion was made by Cole that without significant modification the electrodiffusion model was not adequate to explain observations on the squid-axon membrane (24).

We have attempted to derive the impedance characteristics for a cell membrane, using the electrodiffusion model but with some modifications. The result has turned out to be quite satisfactory (in a theoretical sense at least) and there is a good promise that some other membrane properties may be explained as well. Since this part of the work can stand in its own right, it has been included in this report as Part II of the project.

CHAPTER FOUR TRANSIENT RESPONSE STUDIES

From the impedance locus of the skin we have already obtained the equivalent model representing skin impedance. Before going into more experimental explorations concerning this model, we digress at this point and introduce another approach for data presentation -- the transient response plots.

First it should be noted that whereas the circular-arc plot has thrown much light on the form of the impedance, it is not entirely without disadvantages. As pointed out by Schwan (19), the circular plot may sometimes be misleading as definite but slight deviations from the circle may not be easily noticeable. The arc then appears rather like a round-out locus approximating to the experimental points. Furthermore, in the low frequency end of the locus where the magnitude is relatively larger, accuracy requirements will be increasingly more important because even slight errors (of 1-2 %) in the measurement will result in significant deviation in the arc. In some applications (as in our case which will be discussed in Sec. 5.1.1) where the low frequency end extends to order of several Hertz or lower, measurements will be difficult without significant errors (25).

There is yet another problem which makes the frequency domain method unfavourable for experimental purpose. During an experiment, a definite amount of time is required for the determination of the impedance at different frequencies covering a wide range, and in an event that is slowly time-varying the accuracy will be much impaired. Unfortunately many biological systems are never in an absolute steady state. For example, in our experiments with the skin the impedance was found to be slowly changing with time (Sec. 5.1.1).

It is recognised that most of these problems can be at least alleviated by using computer on-line processing[26]. An alternative way is to present the data in the time domain, i.e., to study the transient behaviour of the skin impedance following a given excitation. Partly for the lack of equipment for computer on-line measurement, and partly for the need for analytical purpose, the transient response method was developed and employed in our measurements.

Conventionally the study of transient behaviour of the skin has been limited to the approximation by a simple exponential curve. Lane(27) applied a step voltage to the skin and measured the current strength during the initial transient and subsequent steady-state period, and from this they estimated the value of the shunt capacitance. This method is based on the simplified model of Fig. 3.4 in which a single time constant is involved. In this

Chapter we shall assume that the impedance is of the form specified by equation (3.2) and we shall endeavour to study its voltage transient response following the application of a step current.

4.1 CHARACTERIZATION OF THE IMPEDANCE FUNCTION

The impedance function of equation (3.2) can be written as

$$Z(\omega) = R_\infty + \frac{R_o - R_\infty}{1 + (j\omega/\omega_o)^\alpha} \qquad (4.1)$$

where $\omega_o = 2\pi f_o = (R_o - R_\infty)^{-\alpha} . C^{-1}$.

We note that ω_o is the corner (angular) frequency of the impedance function when presented in the Bode plot. By separating equation (4.1) into real and imaginary parts and differentiating the latter with respect to ω, we may find that maximum reactance occurs at $\omega = \omega_o$. Hence ω_o is a characteristic frequency of the impedance function.

Given a circular plot, the impedance function $Z(\omega)$ is completely characterized by the parameters R_∞, R_o, α, and ω_o. We shall prove that the transient response of $Z(\omega)$ is a well-defined function and that a close estimation of these parameters can be obtained from the measurement of the transient response.

4.2 LAPLACE TRANSFORM OF THE IMPEDANCE FUNCTION

The transfer function corresponding to an impedance function of equation (4.1) is

$$Z(s) = R_\infty + \frac{A}{k + s^\alpha} \qquad (4.2)$$

where $k = \omega_o^{\alpha} = (2\pi f_o)^\alpha$

$A = (R_o - R_\infty)k = (R_o - R_\infty).\omega_o^{\alpha}$.

If a unit step current is applied, the voltage response can be found by means of the inverse Laplace transform. Thus,

$$Z(t) = \frac{1}{2\pi j}\int_{\sigma - j\omega}^{\sigma + j\omega} (R_\infty + \frac{A}{k + s^\alpha}).\frac{e^{st}}{s}.\, ds$$

$$= R_\infty + \frac{A}{2\pi j}\int_{\sigma - j\omega}^{\sigma + j\omega} \frac{e^{st}}{(k + s^\alpha)\, s}\, ds \qquad \omega \to \infty \qquad (4.3)$$

This complex integral cannot be evaluated by ordinary methods because the term s^α is in general a multi-valued function. Since this function has a branch point at s= 0, a path is chosen as indicated in Fig. 4.1 so as to eliminate the branch point from the integral.

It can be seen that as $R \to \infty$ integration along AB is the same as the integral in equation (4.3), and the line integral along the entire closed path gives the sum of the residues at each singular

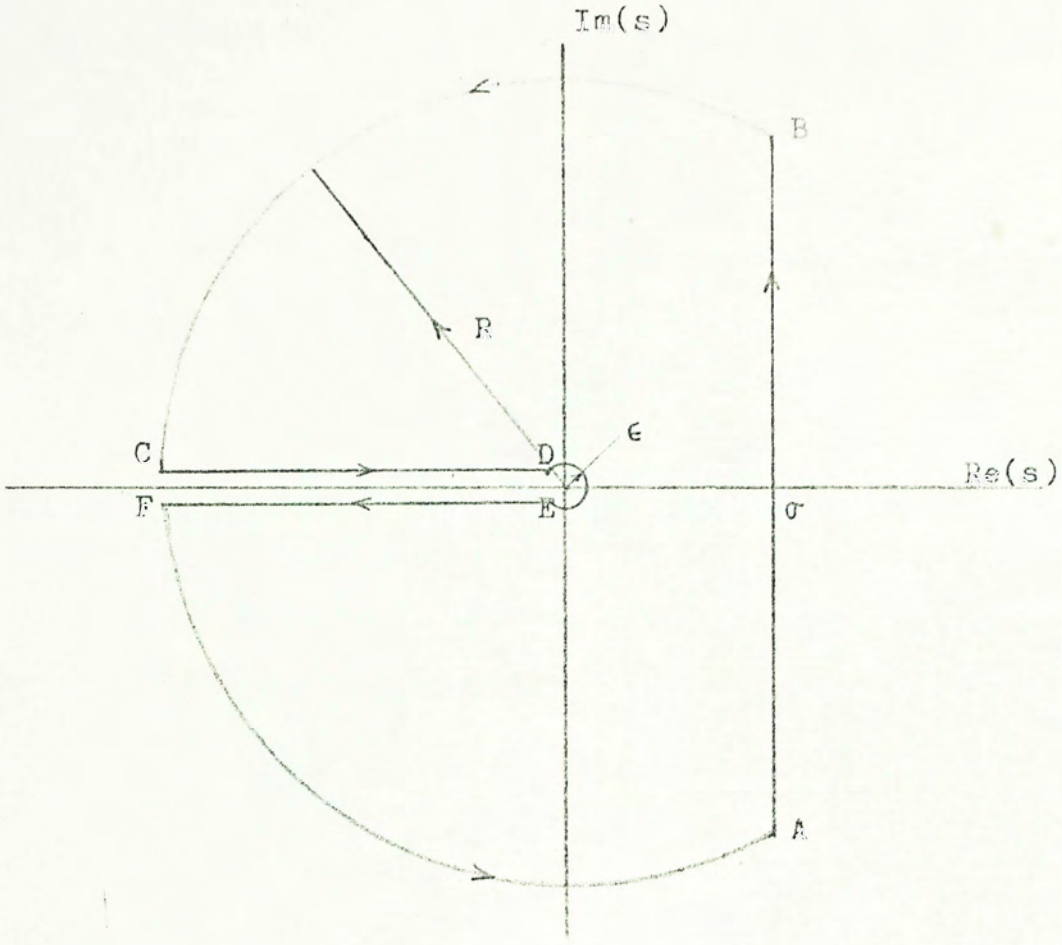

Fig. 4.1 Integral path in the complex plane. σ is arbitrarily chosen so that all singularities are enclosed by the path. ($R \to \infty$, $\epsilon \to 0$).

point within the bounded region. Therefore,

$$\frac{A}{2\pi j} \oint \frac{e^{st}}{s(k + s^{\alpha})} ds = \sum_{i=1}^{n} \text{Res} \left(\frac{A e^{st}}{s(k + s^{\alpha})} \right)_{s=s_i} \qquad (4.4)$$

where s_i represents a singular point and n is the number of such points enclosed. Note that the complete line integral is made up of integral paths along AB, BC, CD, DE, EF, and FA.

We can now evaluate the integral by considering individual sections of the path.

(1) We note that as $R \to \infty$, $|s| \to \infty$ and $\mathrm{Re}\, s < \infty$ so that the integrand will tend to zero. Hence

$$\frac{A}{2\pi j} \int_{BC} \frac{e^{st}}{s(k + s^{\alpha})}\, ds = \frac{A}{2\pi j} \int_{FA} \frac{e^{st}}{s(k + s^{\alpha})}\, ds = 0 \qquad (4.5)$$

(2) The integral along small circular path DE can be evaluated by using the following theorem (28):

$$\lim_{\epsilon \to 0} \int_{\odot DE} f(s)\, ds = -2\pi j \lim_{s \to 0} s\, f(s)$$

Since in our case $\lim_{s \to 0} s\, f(s) = \frac{1}{k}$, it follows that as $\epsilon \to 0$

$$\frac{A}{2\pi j} \int_{\odot DE} \frac{e^{st}}{s(k + s^{\alpha})}\, ds = \frac{-A}{k} \qquad (4.6)$$

(3) Since s^{α} is in general a multi-valued function, we let

$$s = r^{\frac{1}{\alpha}} e^{j\phi} \qquad (4.7)$$

where r is real and $-\pi < \phi \leq \pi$ (i.e. only the principal values of s are considered). Hence we have

$$s^{\alpha} = r\, e^{j\alpha\phi} \qquad (4.8)$$

Since we are only interested in those values of α given by

$0 \leq \alpha < 1$, it follows that $-\pi < \alpha\phi < \pi$ and s^{α} cannot be a negative real quantity. Consequently,

$$\sum_{i=1}^{n} \text{Res} \left(\frac{A e^{st}}{s(k + s^{\alpha})} \right)_{s=s_i} = 0 \qquad (4.9)$$

(4) To evaluate the line integral along CD, we first note that as far as this integral is concerned s can be written as

$$s = x^{\frac{1}{\alpha}} e^{j\pi} \qquad (4.10)$$

$$ds = \frac{1}{\alpha} . x^{\frac{1-\alpha}{\alpha}} . e^{j\pi} . dx$$

where x is real variable. Hence we have

$$\frac{A}{2\pi j} \int_{CD} \frac{e^{st}}{s(k + s^{\alpha})} ds = \frac{A}{2\pi j} \int_{R}^{\varepsilon \to 0} \frac{e^{-x^{\frac{1}{\alpha}} t} . x^{\frac{1-\alpha}{\alpha}}}{(k + x e^{j\pi\alpha}) x^{1/\alpha}} dx$$

$$= \frac{-A}{2\pi j \alpha} \int_{0}^{\infty} \frac{e^{-x^{1/\alpha} t}}{x(k + x e^{j\pi\alpha})} dx \qquad (4.11)$$

Similarly,

$$\frac{A}{2\pi j} \int_{EF} \frac{e^{st}}{s(k + s^{\alpha})} ds = \frac{A}{2\pi j \alpha} \int_{0}^{\infty} \frac{e^{-x^{1/\alpha} t}}{x(k + x e^{-j\pi\alpha})} dx \qquad (4.12)$$

Finally, combining (4.11) and (4.12), we have

$$\frac{A}{2\pi j} \int_{CD+EF} \frac{e^{st}}{s(k + s^{\alpha})} ds = \frac{A}{2\pi j \alpha} \int_{0}^{\infty} \frac{e^{-x^{1/\alpha} t}}{x} \left(\frac{1}{k + x e^{-j\pi\alpha}} - \frac{1}{k + x e^{j\pi\alpha}} \right) dx$$

$$= \frac{A \sin \pi\alpha}{\pi j \alpha} \int_{0}^{\infty} \frac{e^{-x^{1/\alpha} t}}{k^2 + x^2 + 2kx \cos \pi\alpha} dx \qquad (4.13)$$

From the above derivations, we may now obtain an expression for the time function Z(t). Substituting equations (4.5), (4.6), (4.9), (4.13) into equation (4.4), we have

$$\frac{A}{2\pi j}\int_{AB} \frac{e^{st}}{s(k+s^{\alpha})}\,ds = \frac{A}{k} - \frac{A \sin \pi\alpha}{\pi\alpha}\int_{o}^{\infty} \frac{e^{-x^{1/\alpha}t}}{k^2 + x^2 + 2kx \cos \pi\alpha}\,dx \qquad (4.14)$$

Substituting (4.14) into (4.3) and noting that $A/k = (R_o - R_\infty)$, the transient response becomes

$$Z(t) = R_o - \frac{A \sin \pi\alpha}{\pi\alpha}\int_{o}^{\infty} \frac{e^{-x^{1/\alpha}t}}{k^2 + x^2 + 2kx \cos \pi\alpha}\,dx \qquad (4.15)$$

Equation (4.15) is a general form for the transient response with $0 \leq \alpha < 1$. In case $\alpha = 1$, the residue in equation (4.4) must be evaluated and the solution for Z(t) will be a simple exponential.

It can be shown easily that the integral in (4.15) is bounded and well defined. For a given value for α, this integral can always be evaluated numerically or by simple approximation methods. In particular, we consider the case where $\alpha = 1/2$, corresponding to Warburg's polarization impedance for electrodes (6). In this case a closed form for Z(t) can be obtained. Putting $\alpha = 1/2$ in equation (4.15), we get

$$Z(t) = R_o - \frac{A \sin(\pi/2)}{\pi/2}\int_{o}^{\infty} \frac{e^{-x^2 t}}{k^2 + x^2 + 2kx \cos(\pi/2)}\,dx$$

$$= R_o - \frac{A\, e^{k^2 t}}{k}\, Erf_c(k\sqrt{t}) \qquad (4.16)$$

where the last integral is evaluated using integral tables (29)

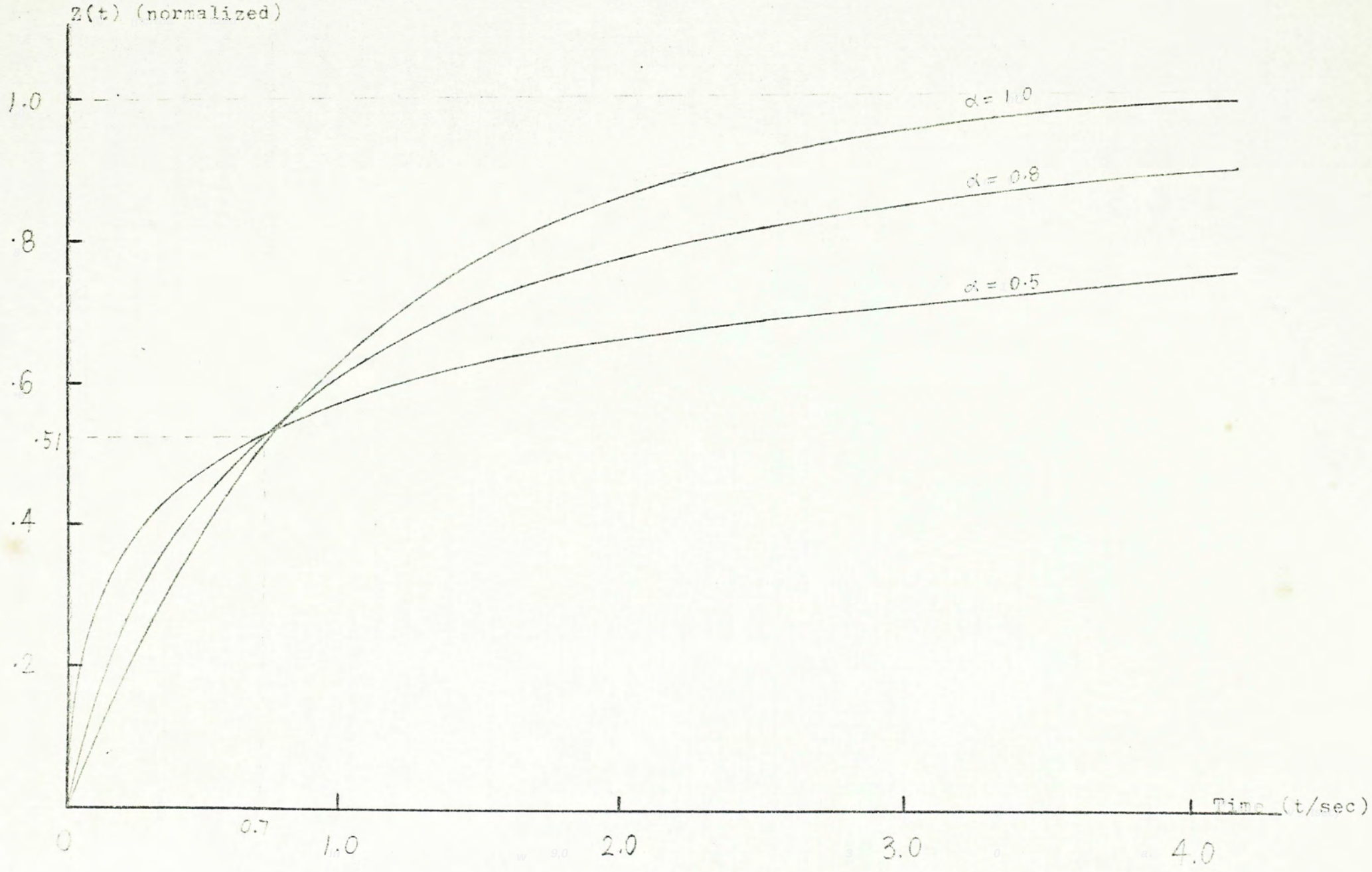

Fig. 4.2 Theoretical response curves for 3 different values of α (k=1, R_{ss}=0).
Note that the curves are closest to one another at approximately (0.70, 0.51).

A plot of (4.16) is as shown in Fig. 4.2. Also shown are the curves corresponding to $\alpha=1$, 0.8 for comparison. It can be seen that for a smaller α the curve rises more steeply at first but approaches the final steady-state value more slowly. The point at which the three curves are closest to one another is approximately at $t=0.7$ (for $k=1$).

4.3 ESTIMATING FUNCTION PARAMETERS FROM THE TRANSIENT RESPONSE

Given the parameters R_o, R_∞, α, and ω_o we can compute numerically the magnitude of the voltage response at discrete time intervals. by use of equation (4.15). In practice, however, the transient response curve is plotted experimentally and we seek to estimate from it the corresponding parameters.

Suppose now an experimental response curve is given. The values of R_o and R_∞ can be obtained by noting the initial step and the final steady-state response respectively. Owing to the implicit nature of the integral in (4.15) the other two parameters (α and ω_o) are more difficult to determine; a direct estimation of one parameter from the given response curve is almost impossible without knowledge of the other. To overcome this difficulty, let us first rewrite equation (4,3) for the time function as

$$Z(t) = R_\infty + \frac{1}{2\pi j}\int_{\sigma-j\infty}^{\sigma+j\infty} \frac{(R_o - R_\infty)\, e^{st}}{s(1 + (s/\omega_o)^\alpha)}\, ds$$

Introducing a new variable $p=s/\omega_o$, we have

$$Z(t) = R_\infty + \frac{(R_o - R_\infty)}{2\pi j}\int_{\sigma'-j\infty}^{\sigma'+j\infty} \frac{e^{p(\omega_o t)}}{p(1 + p^\alpha)}\, dp$$

where $\sigma' = \sigma/\omega_o$.

For simplicity we shall assume $R_\infty=0$ in our following discussions. This assumption is justified for most biological materials as is the case in our study with skin impedance (Sec. 3.1.1). If R_∞ is not small enough, the result is a constant offset voltage in the response and can easily be subtracted to give the actual transient response voltage. Thus the assumption does not affect generality in our discussion. With this assumption and putting

$$t' = \omega_o t \qquad (4.17)$$

$$\bar{Z}(t') = Z(t)/R_o \qquad (4.18)$$

we have

$$\bar{Z}(t') = \frac{1}{2\pi j}\int_{\sigma'-j\infty}^{\sigma'+j\infty} \frac{e^{pt'}}{p(1 + p^\alpha)}\, dp$$

$$= \mathcal{L}^{-1}\left(\frac{1}{p(1 + p^\alpha)}\right) \qquad (4.19)$$

Equation (4.19) represents the theoretical transient response of the given impedance function (4.1) normalized both in magnitude and time scale. This normalization process enables comparison between the theoretical response curves and experimental curves of varying parameter values. A set of theoretical, normalized response curves can then be tabulated in discrete time intervals

using equation (4.15). Since we have proved that the function is well-behaved we chose the more convenient way of using the computer subroutine to perform the inverse transform (ICL Scientific Subroutine FPLAPI9).

To compare the experimental response curve with the set of theoretical curves, it is noticed that for a considerable range of α values the theoretical curves are fairly clusted together at approximately t'=0.7, where an average value of 0.51 can be assigned to any curve with deviations of within3% (Fig. 4.2). This condition holds for $0.5 < \alpha < 0.9$. To show this more explicitly $\bar{Z}(t')$ is differentiated with respect to α to give

$$\frac{\partial Z(t')}{\partial \alpha} = \mathcal{L}^{-1}\left(\frac{\partial}{\partial \alpha} \frac{1}{p(1+p^{\alpha})} \right) = \mathcal{L}^{-1}\left(\frac{-\log p}{p^{1-\alpha}(1+p^{\alpha})^2} \right) \qquad (4.20)$$

The value of $\frac{\partial Z(t')}{\partial \alpha}$ is evaluated by the same inverse transform method and the results are plotted in Fig. 4.3. It can be seen that $\frac{\partial Z(t')}{\partial \alpha} \doteq 0$, for most values of α, at a time approximately t'=0.7, the maximum deviation from zero being not more than $\pm$ 0.05. Hence the response curves have minimum dependence of α at this point. Because of this, the point (0.70, 0.51) can be taken as a reference point for the comparison between experimental and theoretical curves.

To a first approximation, therefore, the point in the experimental curve at which the response is just 51% of the final

$\frac{\partial}{\partial\alpha}\left\{\mathcal{L}^{-1}\frac{1}{p(1+p^{\alpha})}\right\}$

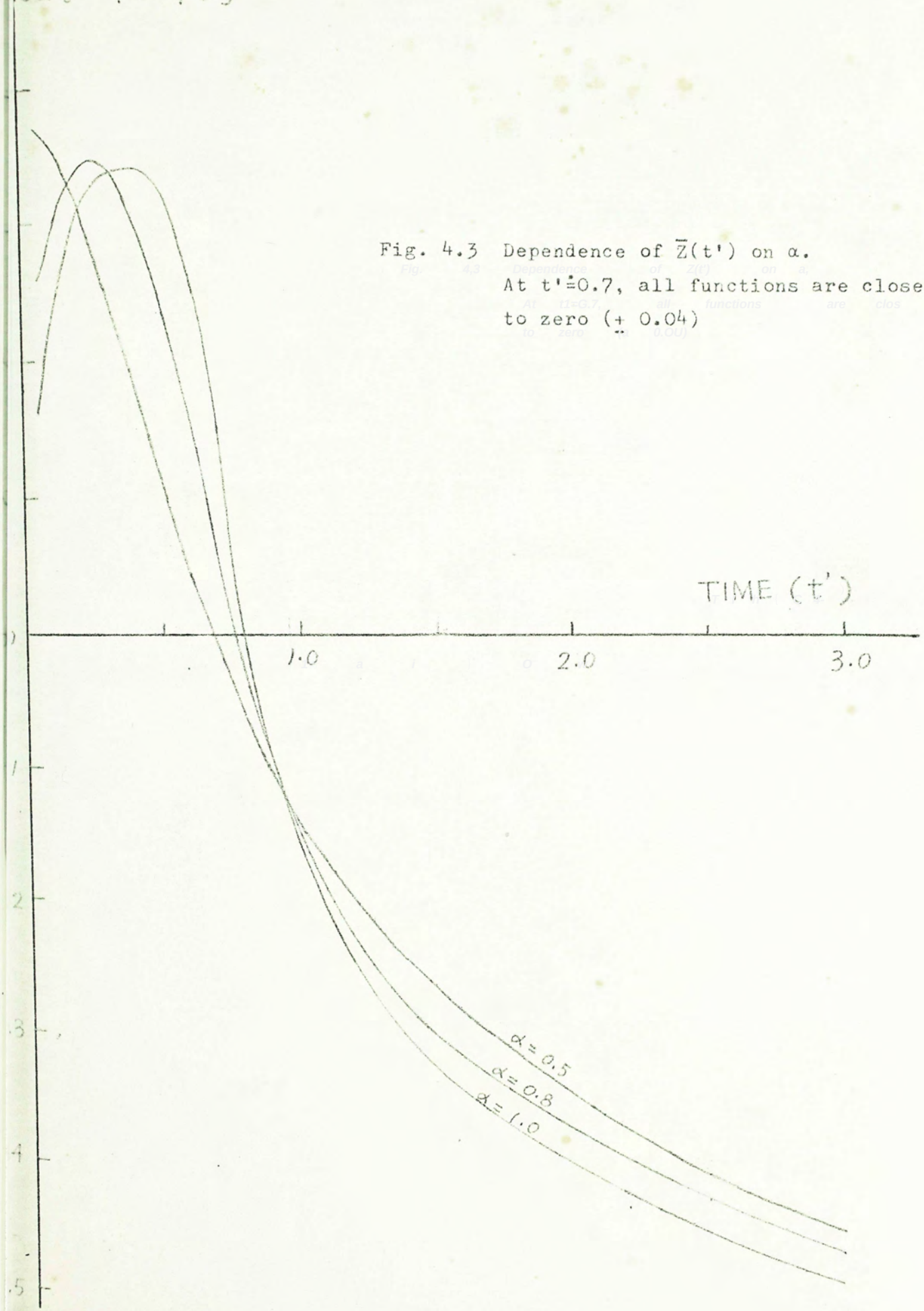

Fig. 4.3 Dependence of $\bar{Z}(t')$ on α.
At $t' \doteq 0.7$, all functions are close to zero ($\pm$ 0.04)

value is noted. Let the time be t_o. Other points in the curve can be compared to the set of theoretical curves at the corresponding time intervals by multiplying with the time scale factor $0.7/t_o$. Thus the phase constant, α, of the experimental curve is given by the theoretical curve closest to it (when appropriately scaled in time). This curve fitting process can be refined iteratively by adjusting the time scale slightly each time when the closest theoretical curve is specified and its time value at 51% response noted. However, the approximation happens to be so close that usually one or two iterations are enough.

Once the optimised value for α is determined, the characteristic frequency can be calculated from the time scale factor. From equation (4.17),

$$\omega_o = t'/t \qquad (4.21)$$

so that the characteristic frequency is

$$f_o = t'/2\pi t \qquad (4.22)$$

4.4 TRANSIENT RESPONSE MEASUREMENTS

4.4.1 Method

The transient response of forearm skin impedance was studied. The

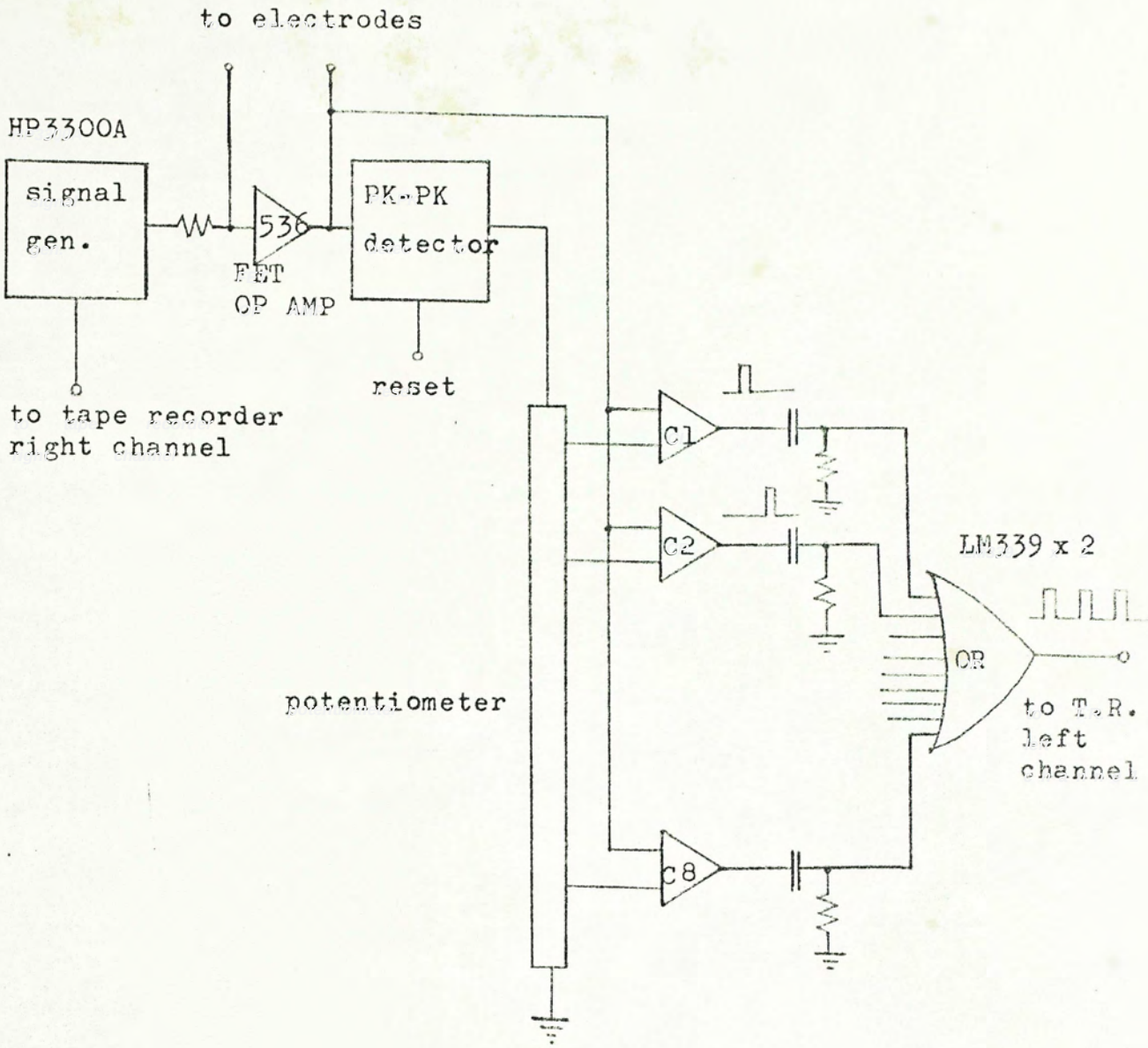

C1 to C8 are voltage discriminators LM339 (NS).

Fig. 4.4 Circuit for voltage transient measurement.

procedure and preparation were the same as described in Sec.3.1.1, but the input signal was a bipolar square wave of about 0.1 Hz. The frequency of the square wave was low enough to allow the response to attain steady state in each half cycle. The current density was about 0.1 μA cm^{-2}. The output response was fed to some level discriminator circuits (Fig. 4.4) which were set to change state about some fractional parts of the peak-to-peak level of the voltage response. The whole recording process would take only one and a half cycle of the input square wave. During the first cycle, the peak-to-peak level of the output response was detected and held as a reference to the level discriminators. Since the peak-to-peak detector circuit had a very large hold time (> 100 sec) this reference level was practically constant during the next half cycle, during which time the response was to be determined. The cross-over level of each discriminator was set to be some fractional parts of the peak reference by means of a potentiometer circuit. As the response signal dropped from its peak, each discriminator would trigger in turn giving rise to a series of 8 pulses at the outputs. The transient response curve could be plotted from the measured time between each pulse and the start of the excitation. In practice a permanent record was obtained by joining the outputs of all discriminators through an OR gate to form a serial output which was then fed to a tape recorder for later read-out. From the time measurements obtained from the tape recorder replay output the timing at any other point could be interpolated (Lagrange interpolation, ICL subroutine F4LAGRNG). In this way the entire transient response curve could be reproduced.

After the transient response was recorded, the signal was changed to a sine wave and the impedance locus was determined. The results from the transient response and the impedance locus were compared. In another series of measurements the Ag/AgCl electrode was replaced by a dry brass electrode (15 mm Ø) and similar procedures were followed.

4.4.2 Results

The impedance loci for the two series of measurements are plotted as in Fig. 4.5. Both loci conform to circular plots closely. To further show that the results are consistent with the form of impedance function (4.1) let us first rearrange the equation to give

$$\frac{R_o}{Z(\omega)} - 1 = (j\omega/\omega_o)^{\alpha}$$

Simplifying terms and taking logarithm on both sides, we have

$$\log\left|\frac{Z(\omega)}{R_o - Z(\omega)}\right| = -\alpha \log \omega + \alpha \log \omega_o$$

$$= \alpha \log T' - \alpha \log(2\pi/\omega_o) \qquad (4.23)$$

where $T' = 2\pi/\omega_o$ is the period.

This gives a straight line graph in the log-log scale with slope equal to α and the characteristic frequency given by the intercept.

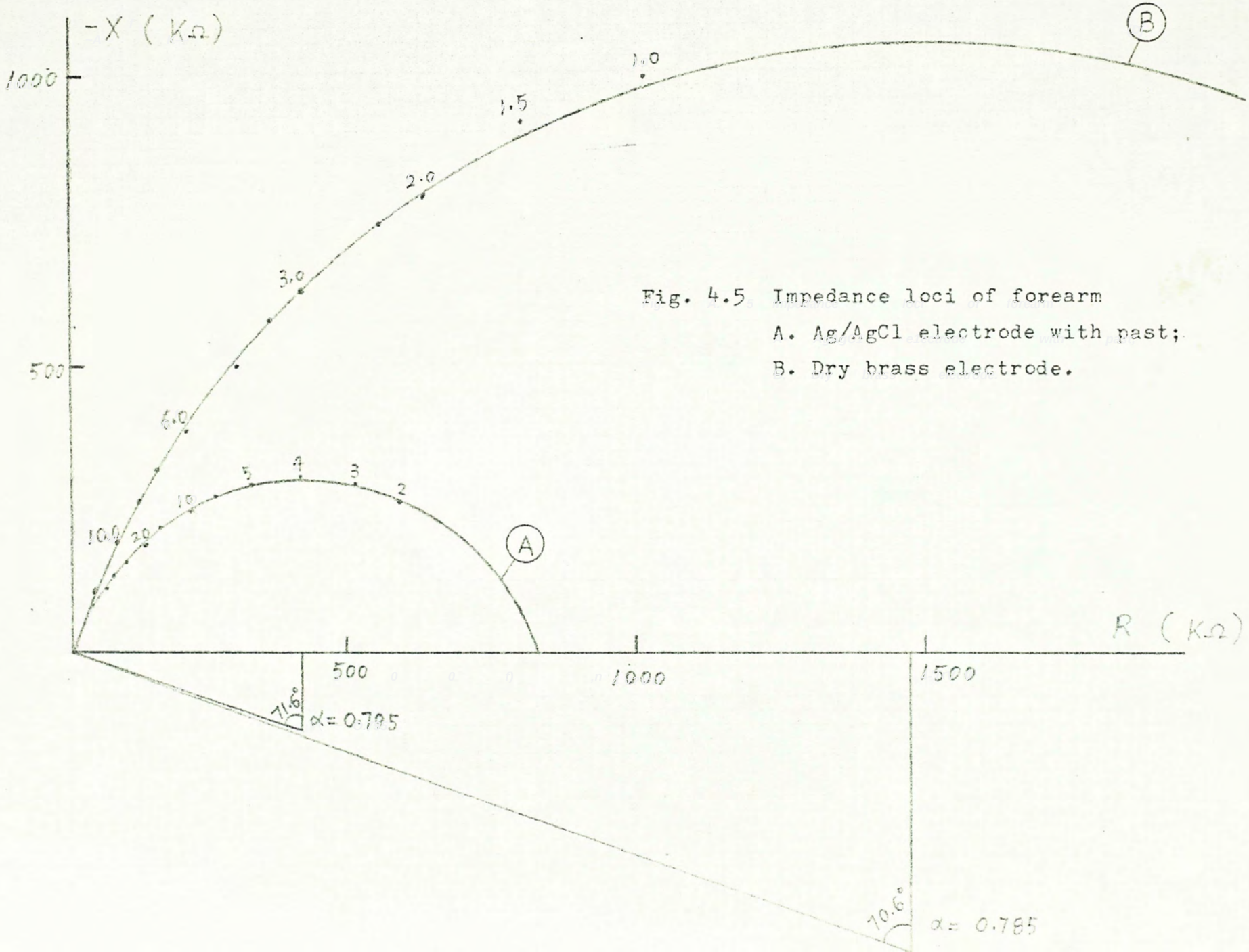

Fig. 4.5 Impedance loci of forearm
A. Ag/AgCl electrode with past;
B. Dry brass electrode.

Fig. 4.6 Plot of $\left|\frac{Z}{R_o - Z}\right|$ with period.

A. Ag/AgCl electrode with paste;

B. Dry brass electrode.

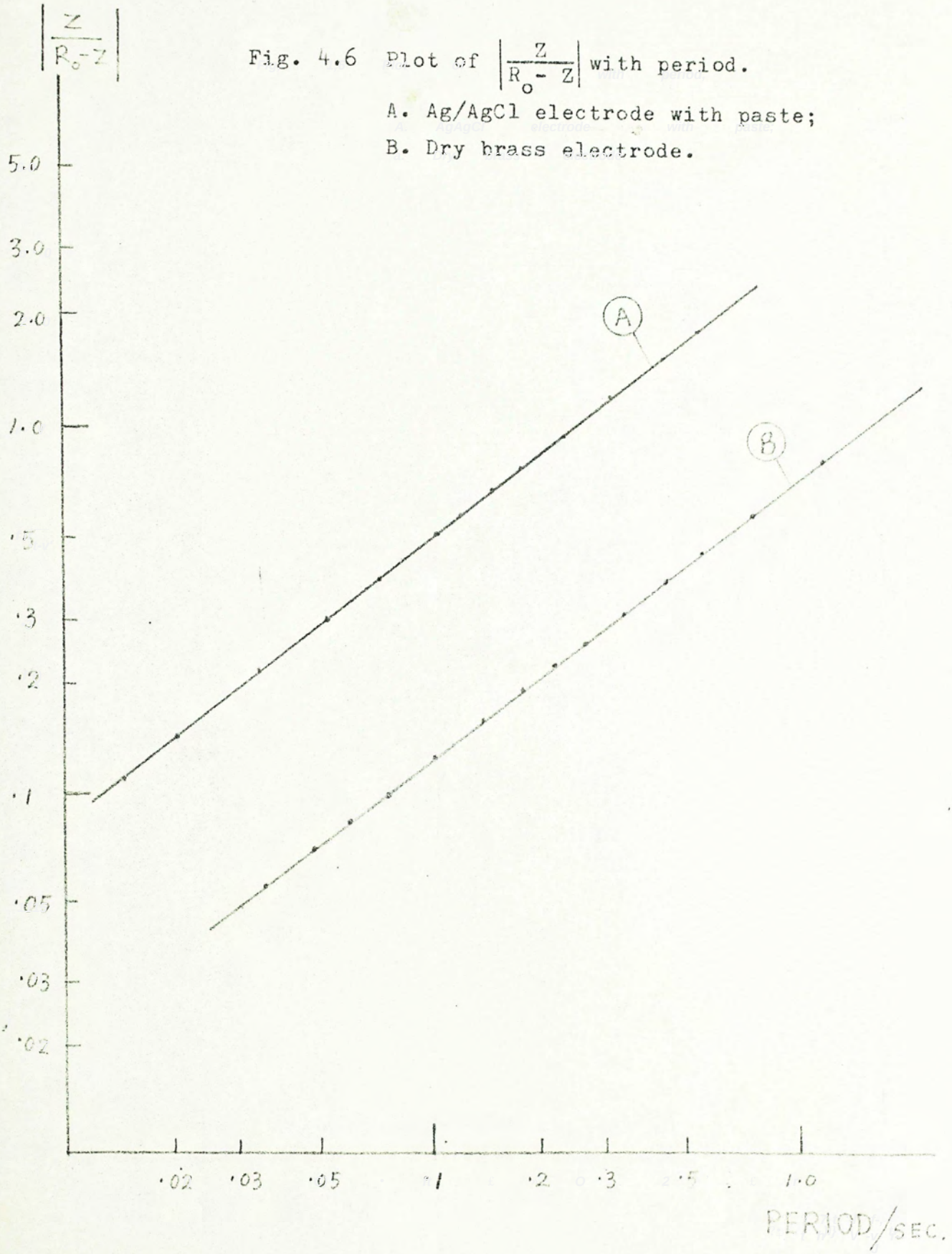

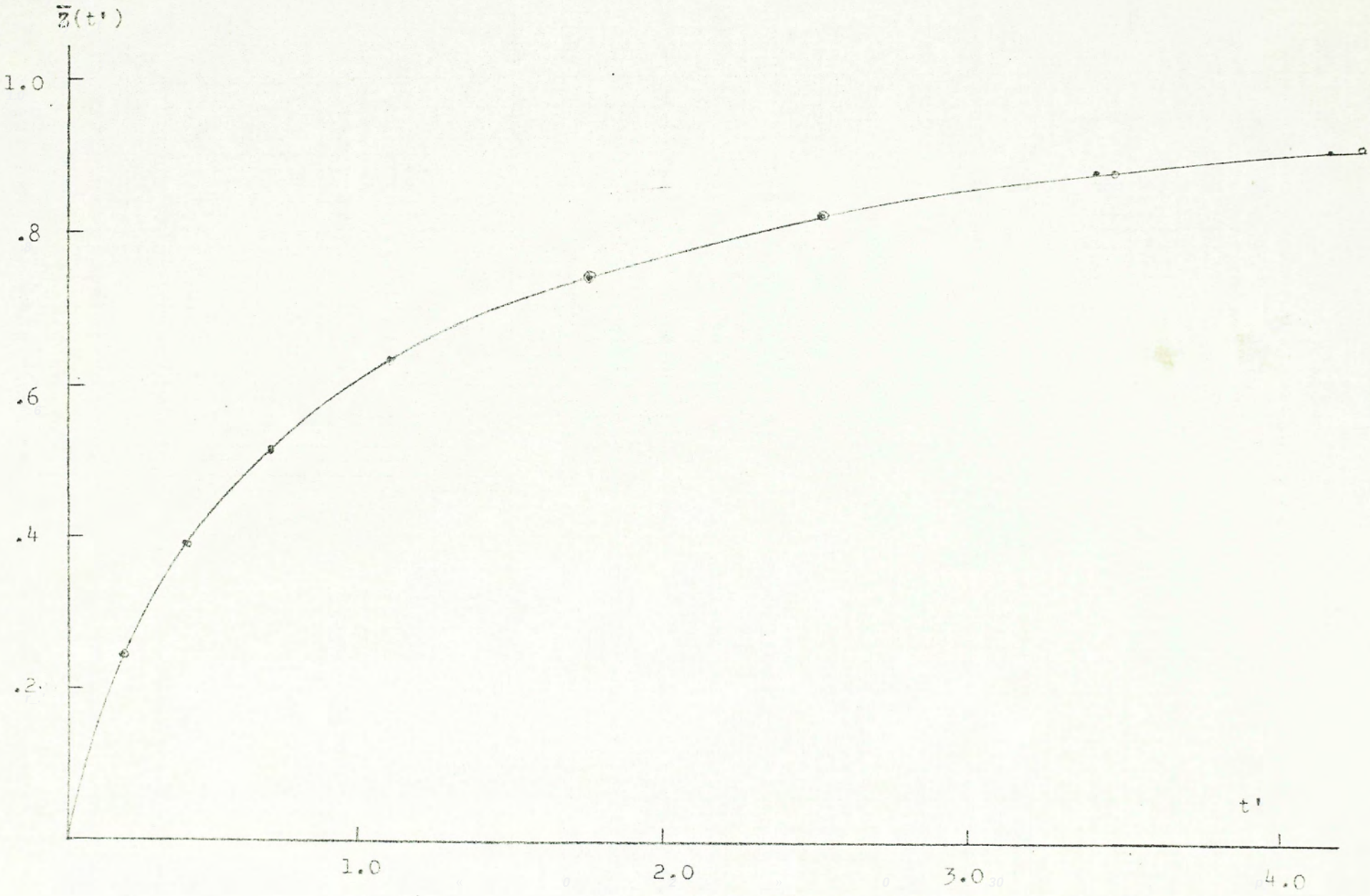

Fig. 4.7 Voltage transient response plots. Solid curve: computed response curve corresponding to α=0.79. Experimental results are shown in dots for Ag/AgCl electrode and circles for brass electrode (normalized in magnitudes and time scales).

The experimental results are plotted as in Fig. 4.6. Two straight line graphs are obtained, justifying the use of the impedance function (4.1). Furthermore, the values for α and ω_o can readily be obtained.

Next, the theoretical response curve closest to each experimental response curve was selected by iterative fitting. The results are plotted as in Fig. 4.7. The maximum deviation of the experimental points from the theoretical curves are within 1%.

Table 4.1 compares the parameter values as obtained from the frequency plots and the transient response plots. The results are in good agreement with each other. However, owing to the difficulty in extending the measurement frequency to lower than 1 Hz, the frequency method is bound to have a greater degree of uncertainty.

	Dry brass electrode		Ag/AgCl electrode with paste	
	Trans. Resp.	Z-locus	Trans. Resp.	Z-locus
R_o	2.9 MΩ	2.9 MΩ	830 kΩ	840 kΩ
α*	0.790	0.785	0.795	0.795
f_o	0.70 Hz	0.68 Hz	4.25 Hz	4.20 Hz

Table 4.1 Parameters as determined by transient response measurement and Z-locus.
(* the value for α is within $\pm$0.005)

4.5 DISCUSSION

The transient method, like most time-domain methods in general, offers a fast and sufficiently accurate means for the determination of a biological impedance. This is especially of advantage when the impedance to be determined is slowly time-varying or if it has a low characteristic frequency. The main disadvantage of this method is that slight deviations from the ideal circular-arc behaviour is not readily recognisable. For example, if the series resistance R_∞ is replaced by another impedance (not purely resistive), the method will fail to apply. This may sometimes happen if the polarization impedance of the electrode is not negligible compared with the impedance to be measured. But in this case even the impedance locus will not give ideal circular arcs. For our purpose, therefore, both methods will be used whenever appropriate.

It must be emphasized that the voltage transient method developed in this Chapter is applicable to all biological impedances given by the same circular-arc function. In fact, it has been noted that this method may find application in the well-known voltage clamp experiments with the squid-axon (30). In the early voltage clamp series, the initial capacity transient was usually approximated by a simple exponential. However, this approximation method was criticized for giving a higher value for R_∞ (31) and an appreciable error in the capacitance (32).

A similar transient method was introduced by Fitzhugh and Cole (30). In their treatment, the inverse transform was approximated by two infinite series each corresponding to short time and large time respectively. For intermediate values of t their method became less satisfactory. Unfortunately, they were unable to provide a handy way to compare the experimental curves with computed results. The voltage transient method developed in this Chapter is obviously more useful than theirs in that (1) a better mathematical form for the time function is obtained; (2) a simple scheme is provided for direct parameter estimation from experimental curves.

CHAPTER FIVE FURTHER EXPERIMENTAL INVESTIGATIONS

In view of the similarity between our empirical model for skin impedance and the membrane model, we may assert that the apparent skin impedance must be of a membrane origin. Now the epidermal stratum corneum, which is a major site for the impedance, is composed of some 40 to 400 laminae of more living cells deep within and extinct horny cells towards the surface, it is of some interest to understand how each lamina contribute towards the overall membrane-like impedance. According to the 'barrier layer' hypothesis, the impedance of most cell layers would be negligible except for a few layers forming a barrier somewhere within the stratum corneum. On the contrary, there is also the possibility that the whole stratum corneum makes up the impedance.

Our next step was then to locate this membrane-like impedance within the corneum. For this purpose the skin-stripping experiment appeared to be a powerful method and will be discussed in the next section. It was intended that not only the individual resistance and capacitance values down to each level be determined, but the form of the impedance in relation to the ideal circular-arc

behaviour was also investigated. Furthermore, the impedance in the palmar region was also investigated. On account of the prominent sweat gland activities remarkable of this region, the role of the sweat glands could be clearly revealed. Throughout these experiments we would seek to construct a complete skin impedance model which corresponded to all prominent phsiological processes found in the skin. Next we would like to scrutinize the relative importance of these processes and the effects of some external factors influencing them.

5.1 SKIN STRIPPING EXPERIMENT

As discussed in Chapter 2 skin-stripping experiments had been conducted by several investigators to determine the effect of the epidermis on the overall impedance. Most of these experiments, however, were concerned with the measurement of either the resistance or the resistance and capacitance, at each level of strip and at a particular frequency only. This procedure, although illuminating, was obviously incomplete especially when one took into account the frequency-dependent nature of the impedance we justified. In view of this, we wished to investigate the frequency characteristics of the impedance down to each level of the skin and from these measurements infer the changes in the parameters of the model as given in Fig. 3.4, or any deviations therefrom.

5.1.1 Method

The impedance of two skin sites on the ventral side of the forearm were separately investigated. The forearm was representative of the general body surface devoide of sweat gland activities (under normal conditions), and was convenient for the operation of skin-stripping. Two electrodes were employed: a 9 mm Ø Ag/AgCl electrode (with paste) and a 15 mm Ø brass-plate electrode. The dry brass-plate electrode was used because it had a minimum effect on hydrating the skin and would not vary the impedance by the process of electrolyte diffusion down the skin. Both hydration and electrolyte diffusion might affect the original state of the skin especially when successive strippings/measurements were made in which case the effect would become accumulative. However, the impedance of the dry electrode was relatively uncertain and might become a source of error when the skin impedance was reduced after several strippings. Hence the simultaneous use of both electrodes would compensate the shortcomings of each other. The brass-plate electrode was polished to shinness each time before application so as to eliminate surface dirt andirregularity, thus facilitating better electrode contact. The electrodes were applied with rubber straps as used in electrcardiography allowing application with about the same pressure each time. The arrangement for the reference site was the same as before.

The experiment was carried out in a quiet room where the

temperature was fairly steady and was around 22°C. The RH was about 80%. Before the normal procedures started the subject was allowed to stay in the room for about 30 minutes to acclimitize to the room conditions. The skin site was cleaned with rubbing alcohol and let dry completely. After electrode attachment a stabilization period was allowed until the readings became steady and measurement started (at deeper strip levels the stabilization period might be shorter or exempted). The impedance of each active skin site was determined in turn. Following each measurement the skin was stripped with cellulose tape. This procedure removed some cell layers of the corneum and thus reduced its thickness (33). No further cleaning was necessary. Measurements were made at each stripping level until nearly all the keratin layers were removed, at which time little difference in the impedance was observed by further stripping.

For the initial few strippings, measurements in the time domain were used because the characteristic frequency of the impedance at this stage was quite low (about 1 Hz). Measurement speed and accuracy could then be considerably increased using the voltage transient method. The basic setup was as illustrated in Fig. 4.4 before. As the stripping proceeded it was found that the characteristic frequency increased progressively, so that after several strippings it might be as high as 10 Hz or more. The time constant of the circuit, so to speak, would then be on the order of 10 ms or less. As the tape recorder and the measuring system

were both band-limited, accuracy would be quite impaired. Furthermore, as the impedance of the skin was gradually reduced, effects due to other processes including the polarization impedance of the electrode became more important. These would appear as a low-frequency, series component in the overall impedance, and in the transient response would result in a slowly rising component following the initial transient. In this case the voltage transient method would fail to apply, and it would then be better to follow the frequency domain method. In order to minimize the effect due to electrode impedance the Ag/AgCl electrode was treated with Kodak D-19 photographic developer (stock solution, full strength), a method described by Getzel and Webster (34). The impedance of the developed Ag/AgCl electrode was found to be 280 Ω at 2 Hz and less than 100 Ω at 20 Hz. For a skin impedance of 10 kΩ at 2 Hz this would result in an error of less than 3%. This error was further reduced by subtracting the measured impedance of the electrode at each corresponding frequency from the skin-electrode impedance.

There was yet another consideration that encouraged the use of voltage transient method to all possible extent, notwithstanding the errors caused by electrode polarization at deeper strip levels. This is because, after some strippings, the impedance of the skin was found to increase with time. The change took place slowly (about 3% per minute), but in the time course of the measuremennt the total change might be quite appreciable. This result was contradictory to the observation on unstripped skin, in which case the impedance decreased with time (Sec. 5.3.1). It

was thought that the gradual increase in impedance was due to reformation and drying out of the newly exposed keratin cells subsequent to each stripping. As pointed out by Hunter and Williams (35), the stripping technique inevitably causes erythema and a definite recovery cycle, so that the changes brought about is in fact deeper than the mere removal of the skin material. If so the finding of impedance variation down to each level of strip would in deed be a rough estimation of the true state of the skin only. Nevertheless this estimation might be acceptable if the time of measurement could be kept to a minimum, as provided by the voltage transient method.

5.1.2 Results and Discussions

A total of 11 strippings were performed. For strip no. 0 to 5, the transient response of each skin site was determined and for the rest the frequency method was used. The results were found to obey the circular-arc law or its time-domain equivalent. The impedance loci corresponding to strippings nos. 5 to 11 were plotted as in Fig. 5.1 and 5.2. From the expanded graphs the 3 parameters (α, f_o, R_o) characterising the circular-arc function were determined. Those parameters from the transient measurement were obtained using the method described in Sec. 4.3. All three parameters were plotted against the number of strippings and the results are shown in Fig. 5.3 - 5.5. From these plots the following observations can be made:

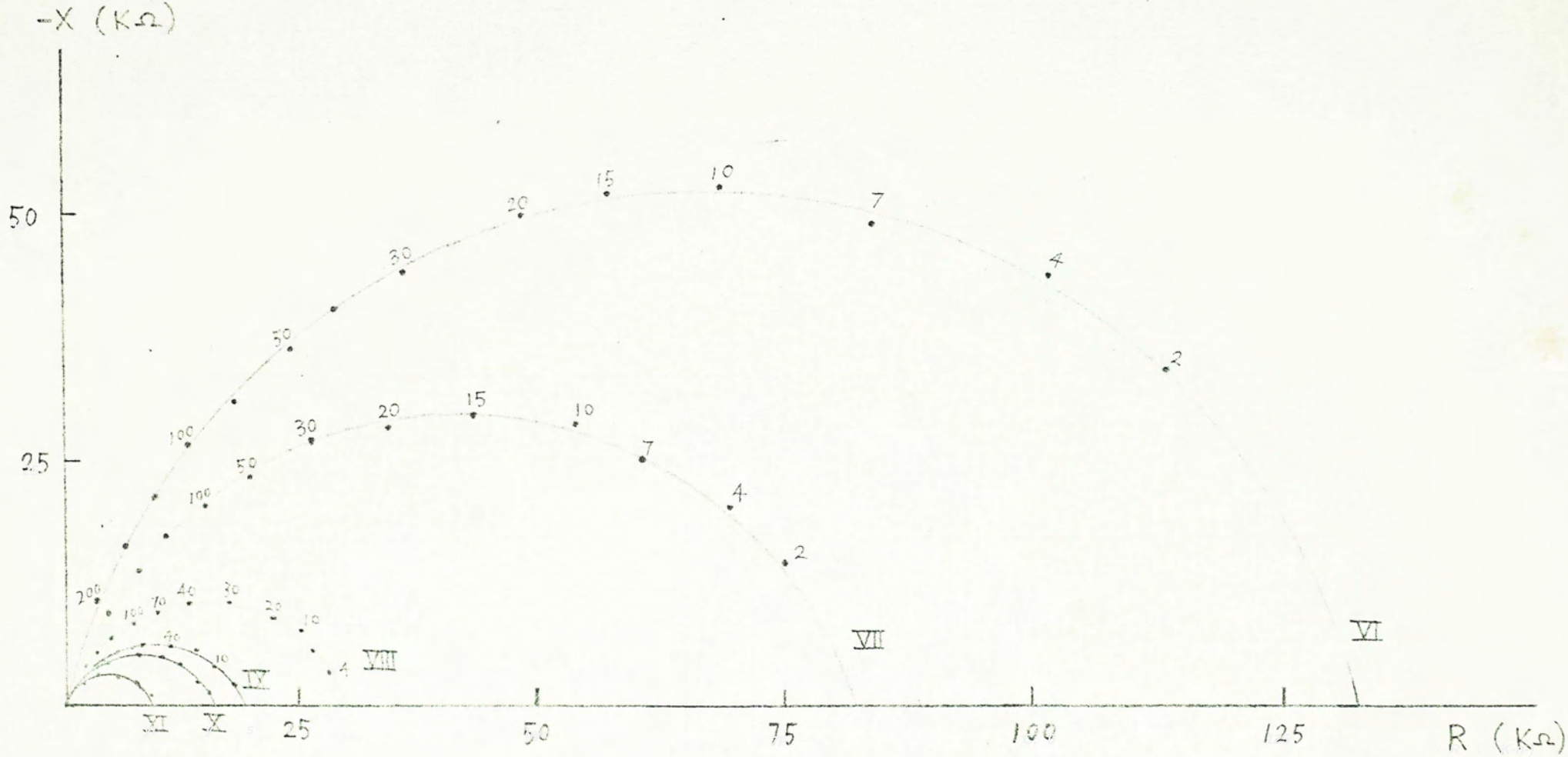

Fig. 5.1 Impedance loci of skin using paste electrode (Ag/AgCl).
Roman numerals shown represent no. of strippings. Frequencies are shown in Arabic no.

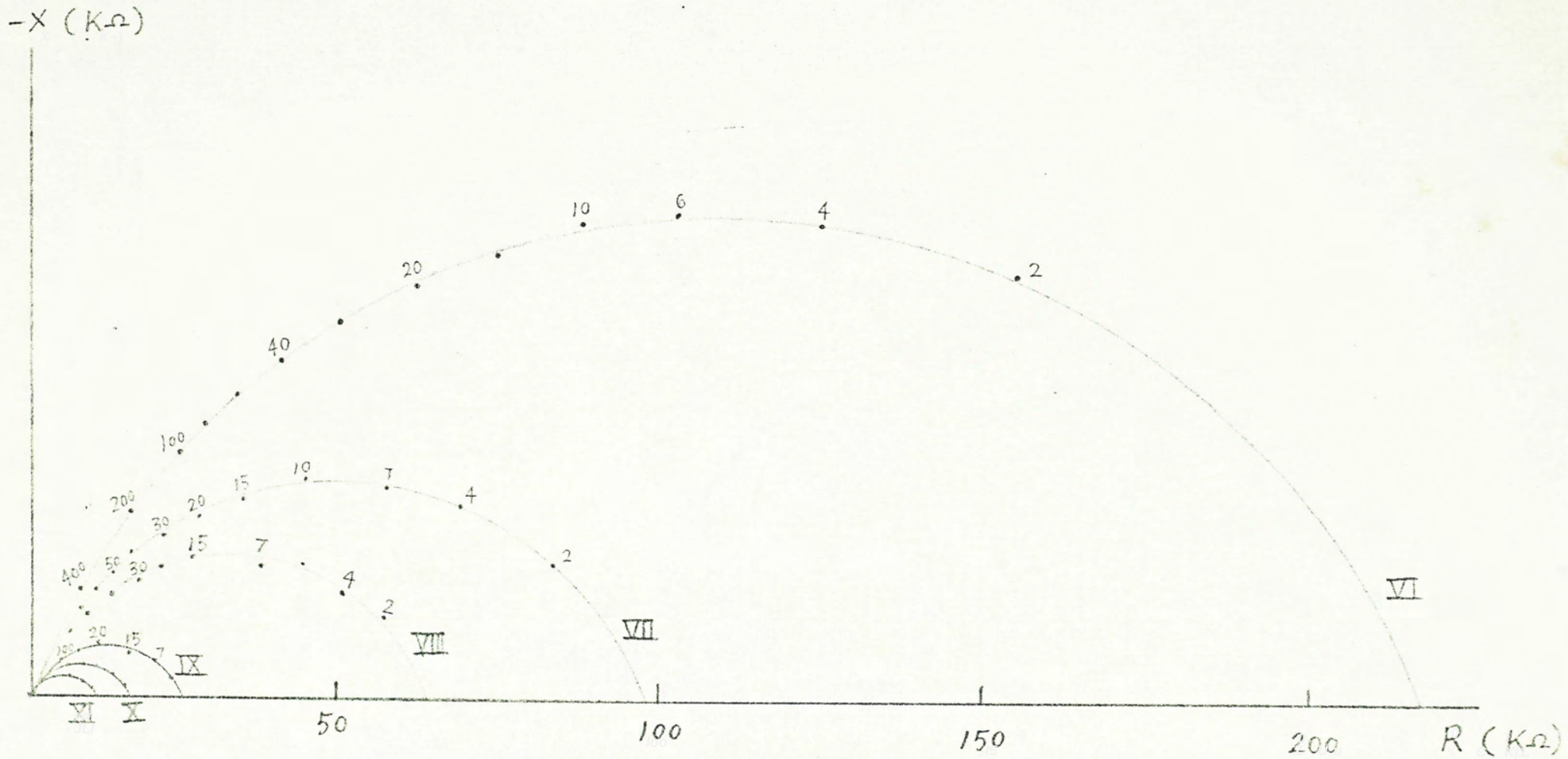

Fig. 5.2 Impedance loci of skin using dry electrode (brass plate).

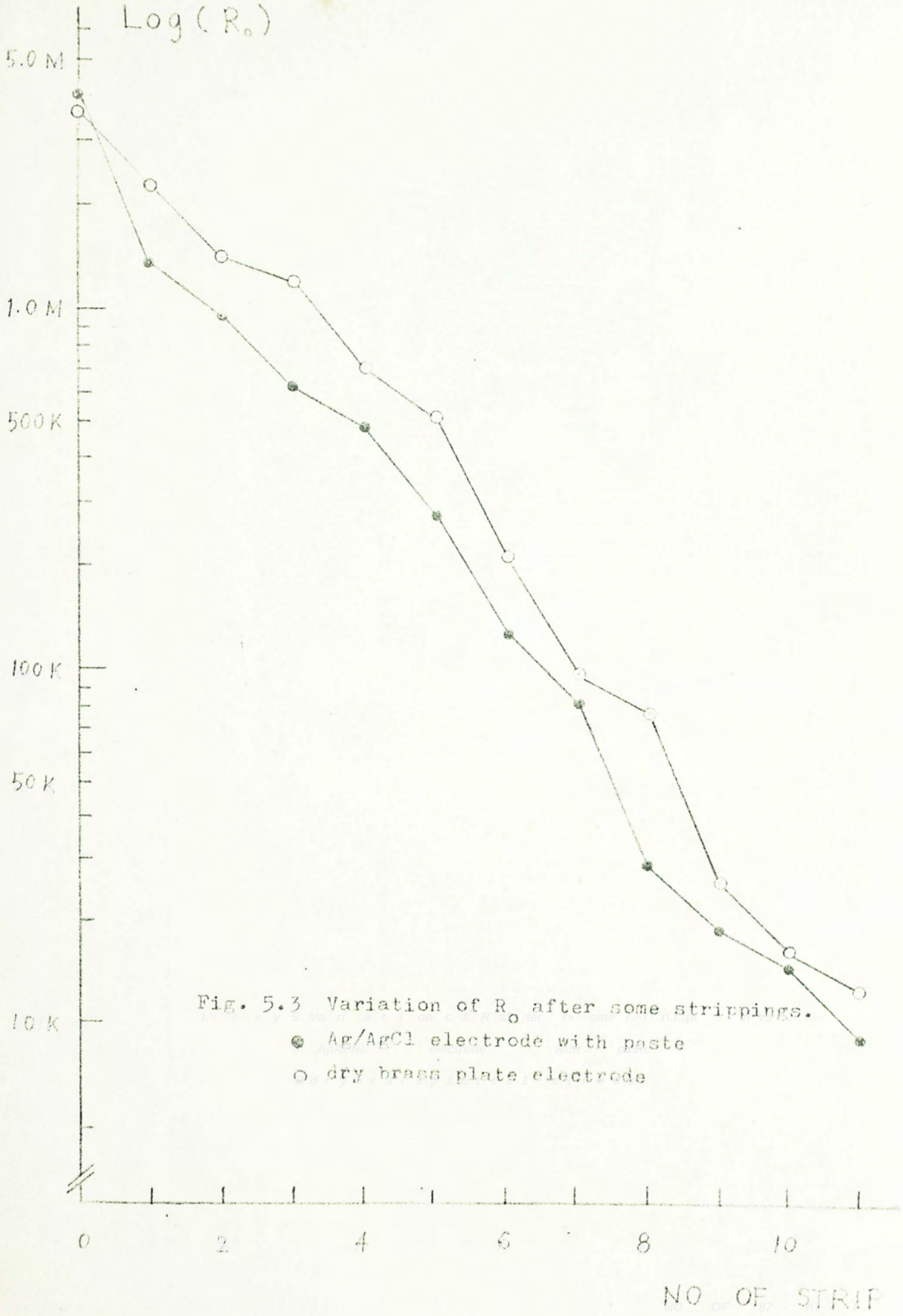

Fig. 5.3 Variation of R_o after some strippings.
● Ag/AgCl electrode with paste
○ dry brass plate electrode

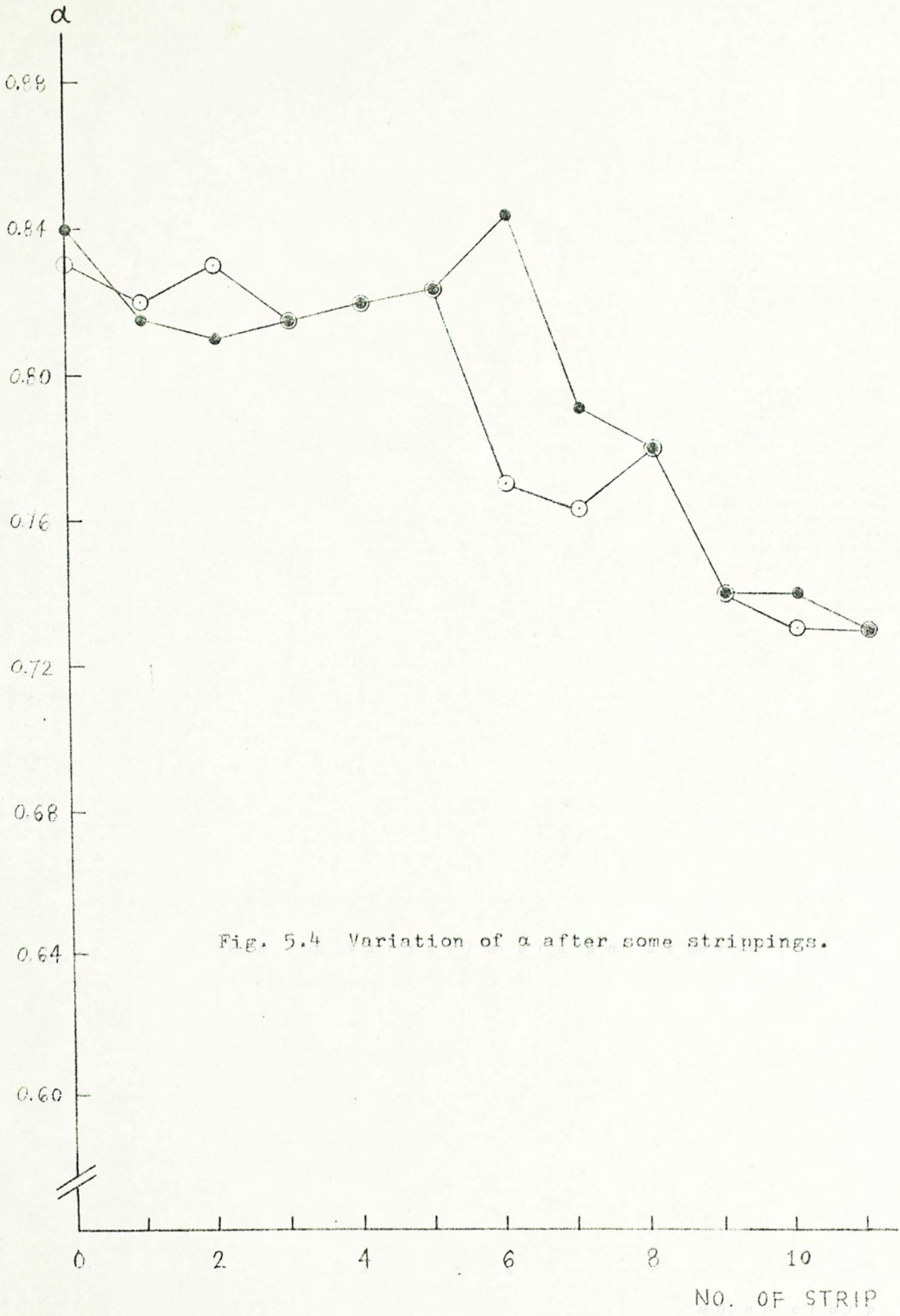

Fig. 5.4 Variation of α after some strippings.

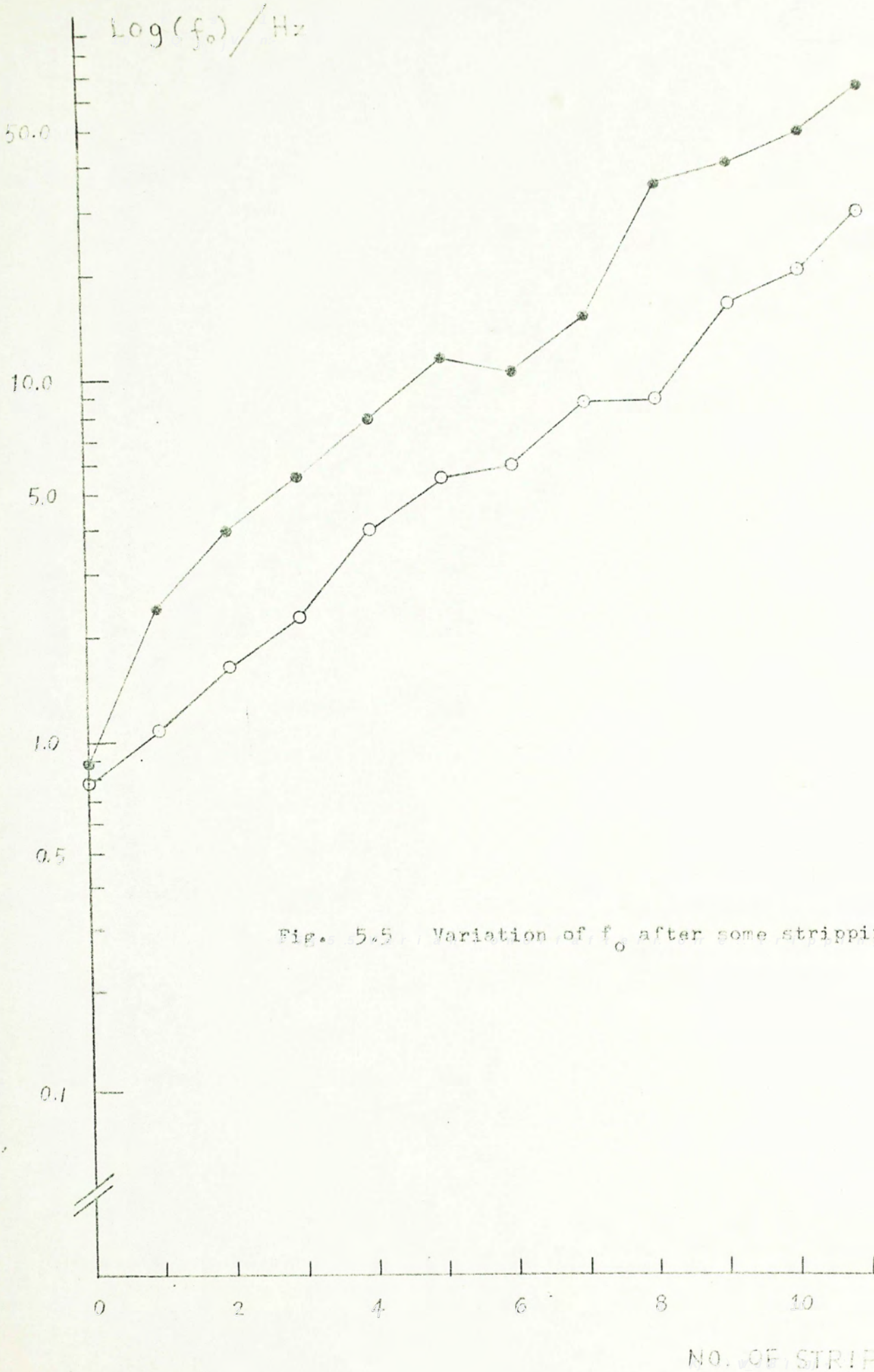

Fig. 5.5 Variation of f_o after some strippings.

(1) The DC resistance, R_o, drops almost exponentially with the number of strippings n. This does not necessarily imply that the resistance bears an exponential relationship with the depth of the skin, because the depth may not be simply proportional to n. As a matter of fact, the upper layers of keratinous cells are more easily removed by adhesive tape than the lower layers (33). Nevertheless each strip brings off only a small fraction of the total keratin (36), and thus can serve as a rough estimation of the thickness. Consequently it may be concluded that most of the resistive effect resided in the uppermost part of the corneum.

(2) From the progressive decrease in R_o for successive strippings, the existence of a 'barrier layer' seemed quite unlikely. It was claimed by Tregear (7) that a discontinuity in R_o was observed at approximately 20 μm down from the skin surface. But even in his case the total change was much smaller than the initial resistance drop in the uppermost cell laminae.

(3) The phase constant, α, changes little at first but gradually decreases as the deeper tissue of the corneum is reached. Therefore α was dependent upon the morphological state of the underlying cells.

(4) As R_o decreases exponentially down the skin, the characteristic frequency f_o increases in a similar manner. It is thus apparent that there will be little change in the polarization capacitance.

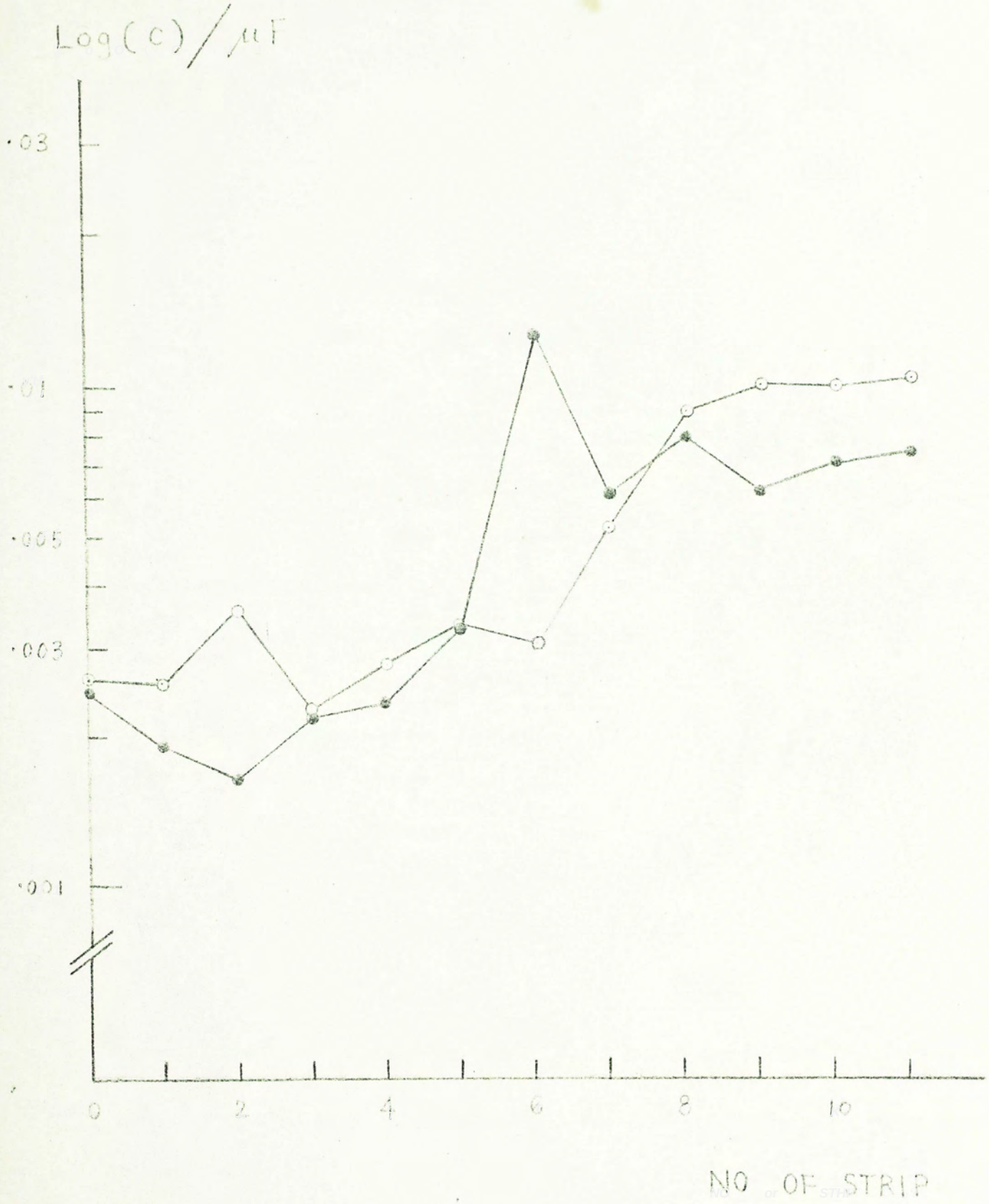

Fig. 5.6 Variation of polarization capacitance after some strippings.

To show this, we note from equation (4.1) that the polarization capacitance is given by

$$C = \frac{1}{2\pi f_o (R_o)^{1/\alpha}}$$

The value of C at each stripping level is obtained by the above equation and the results are plotted as in Fig. 5.6. It can be seen that while R_o has dropped by more than two orders of magnitude, the change in C is hardly more than 5 times. Assuming that the capacitance per cell layer was fairly uniform throughout the whole stratum, one may conclude that the resistivity must be higher in the upper part than in the lower. At each stripping level, therefore, the resistance (and hence the impedance) was mainly attributed to the uppermost few cell layers having highest resistivity; the result is that the capacitive effect was also due to these layers only. The actual thickness of these layers might vary, but it could not be the whole remaining stratum. This would explain why the measured capacitance was relatively independent of the total thickness of the stratum corneum remaining after stripping.

5.1.3 Conclusion

The impedance of the skin was found to be mainly due to the uppermost few cell layers of the stratum corneum. This applied to the skin in its original state or after a number of strippings. This

was a manifestation of the non-uniformity in the electrical properties of the corneum. The existence of a 'water barrier' was not evident, but rather the impearmeability was caused by the entire corneal layer with more effects from the surface laminae.

With reference to the equivalent model of Fig. 3.7 one may wonder how this highly non-uniform horny cell structure can account for the observed impedance-frequency characteristics. Yamamoto and Yamamoto (37, 38) related this to a distribution of relaxation times which over a large range may give the same frequency dispersion characteristics. We reject this approach as a sole explanation because of two reasons. First, the condition of a circular plot can be satisfied only with a particular form of distribution function (19), and it is doubtful if it can be applicable at all times. Secondly, each cell alone is known to have similar frequency characteristics. Following these arguments, we conclude that each cell laminae of the corneum could be represented by the equivalent circuit of Fig. 3.7a. It is noted that in general the series combination of many such equivalent circuits does not give the same form of equivalent circuit unless all component circuits are identical. In view of the non-uniform structure of the corneum this seems quite unlikely. However, if the impedance can be thought to be mainly constituted by the few cell laminae close to the surface, this condition can be established provided that the electrical properties of these layers are fairly uniform among themselves. The effect of distribution of relaxation times will take care of slight local

variations within these laminae. As a result, the form of the overall impedance can be quite similar to the individual cell lamina impedance.

In summary we may include the effect of the morphological variations in the corneum by separating the original model into two parts, as illustrated in Fig. 5.7. The first parallel circuit (subscript 1) represents the surface cell layers of higher electrical resistivity. The rest of the corneum is represented by the second parallel circuit (subscript 2) and is considered to be of negligible effect compared with the above. In practice, therefore, this model conforms to the original model as in Fig. 3.7.

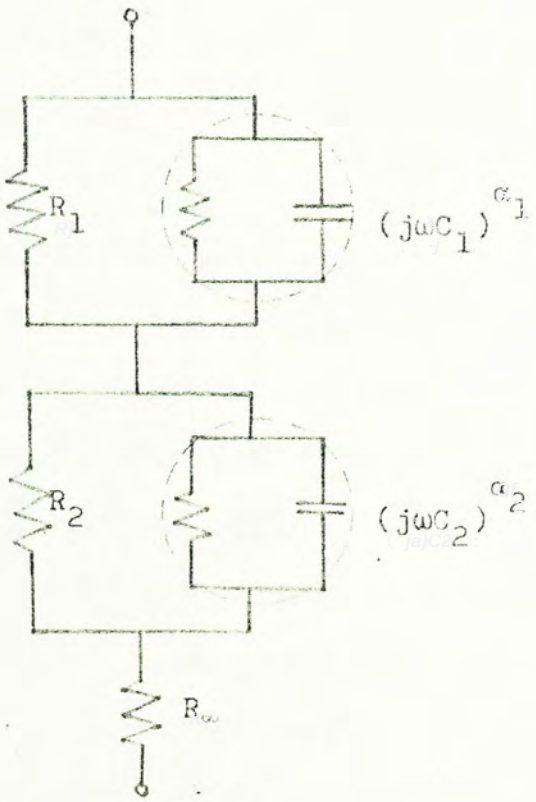

Fig. 5.7
Equivalent skin model taking into account the effect of structural variations in the corneum. ($R_2 \ll R_1$)

5.2 IMPEDANCE AT PALMAR SITES

The impedance at palmar sites is of interest to our study because this region is well-known for sweat gland activities. This effect is demonstrated by the prominent EDRs observed when the subject is in a state of psychological activities. It is therefore helpful to compare the impedance in this region with those on other parts of the body.

Paradoxically, the measurement of palmar impedance happens to be much more difficult, if not impossible, as there is always an incessant fluctuation in the impedance level to be recorded. This is due to the fact that even in a state of complete relaxation the subject is unavoidably under some stress during the experiment, so that EDRs are intermittently elicited. On account of this we resolved to use the voltage transient method since this would require shorter time and might even serve to trace the changes during an EDR. However, this attempt turned out to be unsuccessful. From the transient response of the thumb it was discovered that following the initial transient there was a slowly rising period (about 10% per second) before the final steady-state value was attained. This showed the form of the palmar impedance was different from our model either due to the inclusion of some additional elements to the basic model or a fundamental change in the circuit model. Evidently a low frequency process must be present. In order to understand this better, we resorted to using frequency measurements.

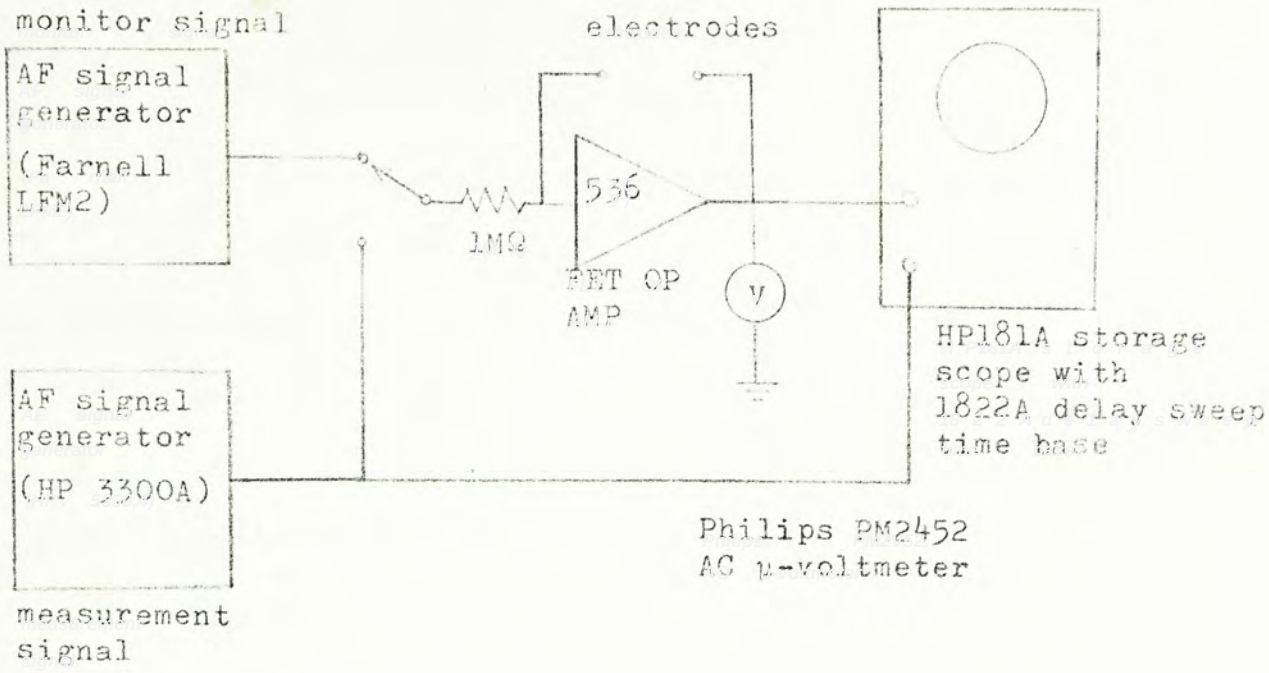

Fig. 5.8 Set up for measurement of thumb impedance

5.2.1 Method

The impedance of the left thumb was investigated. The basic set up was essentially the same as before but in order that the EDR did not affect our measurement a special monitoring signal was connected to the input as shown in Fig. 5.8. The monitoring signal had a constant frequency of 2 Hz and a constant amplitude the same as the actual signal for measurement. Before each measurement, the input to the OP AMP was switched to the monitoring signal generator and the output magnitude was observed. While EDR was active the output would be fluctuating all the time. To compare the impedance at different frequencies measured at different time, a particular

monitor output level was selected as reference. This corresponded to a certain impedance level of the skin. Each time when this reference monitor level was attained at the output the actual measurement signal generator was switched into circuit (to replace the monitor signal generator) and the output magnitude and phase were quickly recorded. After this, the switch was reversed again to check that no significant change in the monitor level took place. The same procedure was taken for other measurement frequencies and in this way all readings could be compared with reference to the same DC (low frequency impedance level. This method avoided the use of frequency filters for monitoring purpose making possible the extension of the measurement range to very low frequencies. This was of great advantage because from the transient response study of the thumb impedance described a low-frequency process in the skin was clearly evident.

5.2.2 Results and further Work

5.2.2.1 Discrepancy in low frequency range

The impedance locus for thumb was obtained and plotted (Fig. 5.9). It can be seen that the impedance locus at high frequencies can be described by a circular arc as before, but the low frequency branch deviates remarkably from the same arc. From the magnitude plot (Fig. 3.3) it was noted that a constant slope at mid-frequency range was obtained. Hence it was thought that the impedance model

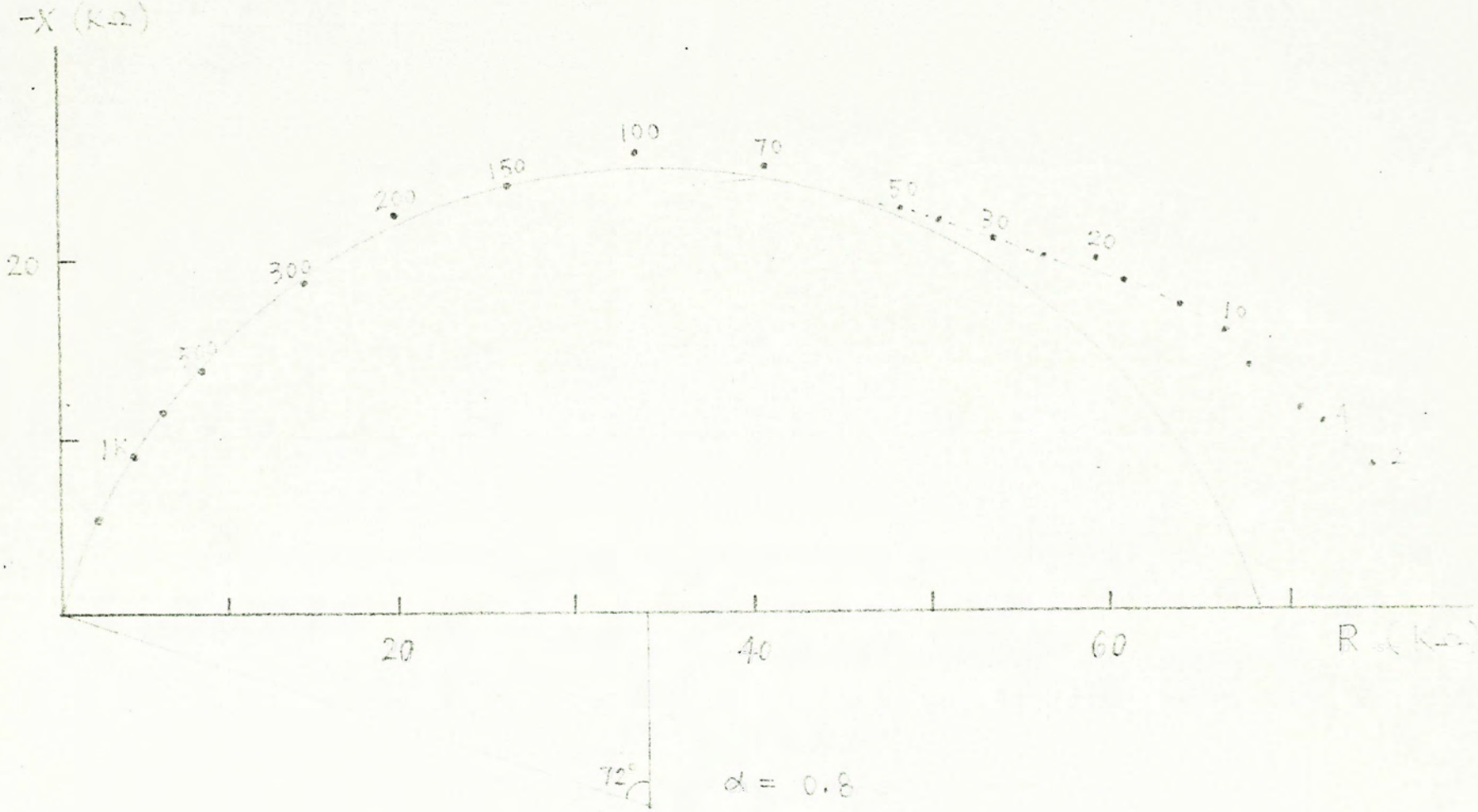

Fig. 5.9 Impedance of thumb showing a low frequency departure. Broken line shows actual locus at low frequencies.

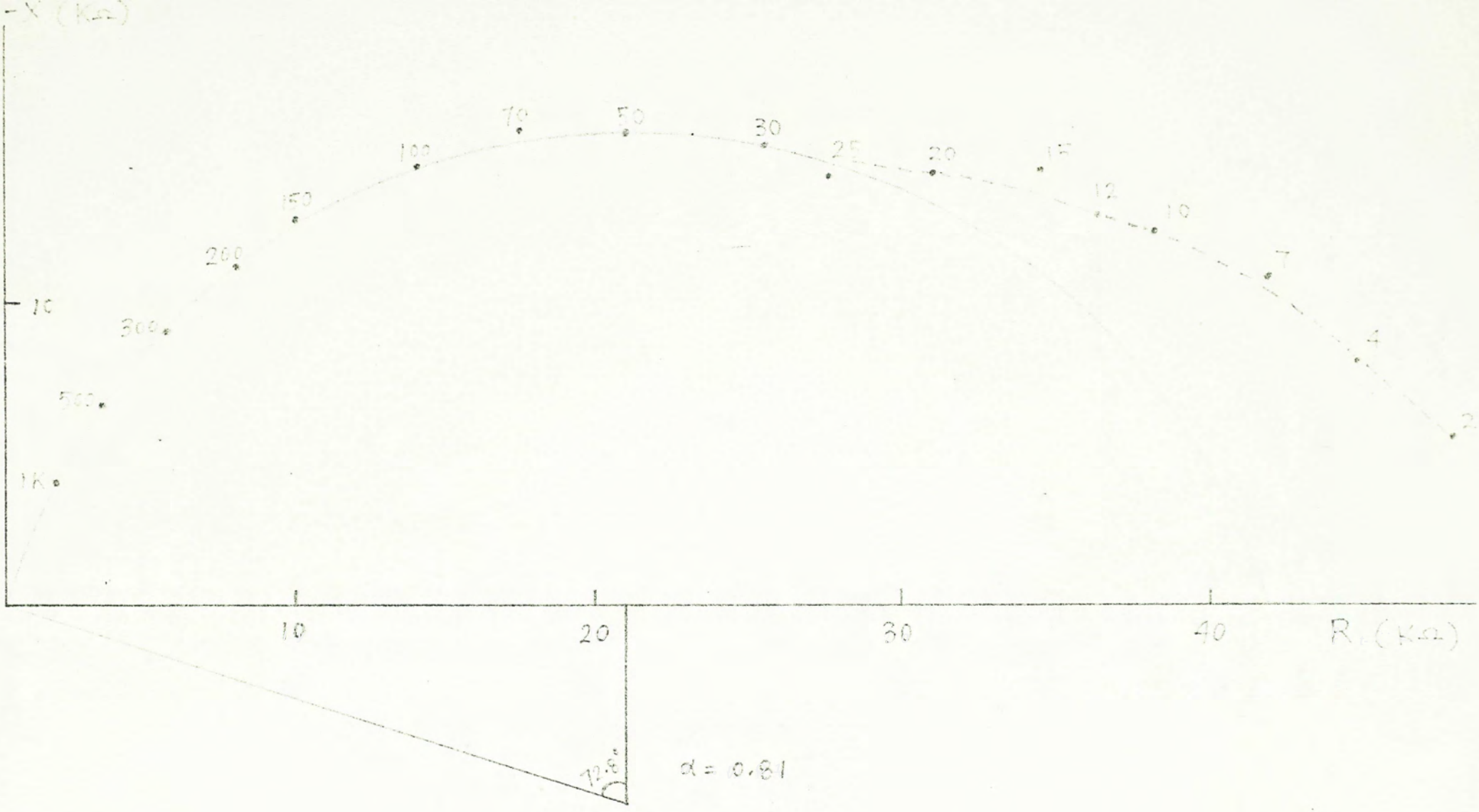

Fig. 5.10 Impedance locus of forearm after sweating. Broken line shows actual locus at low frequencies.

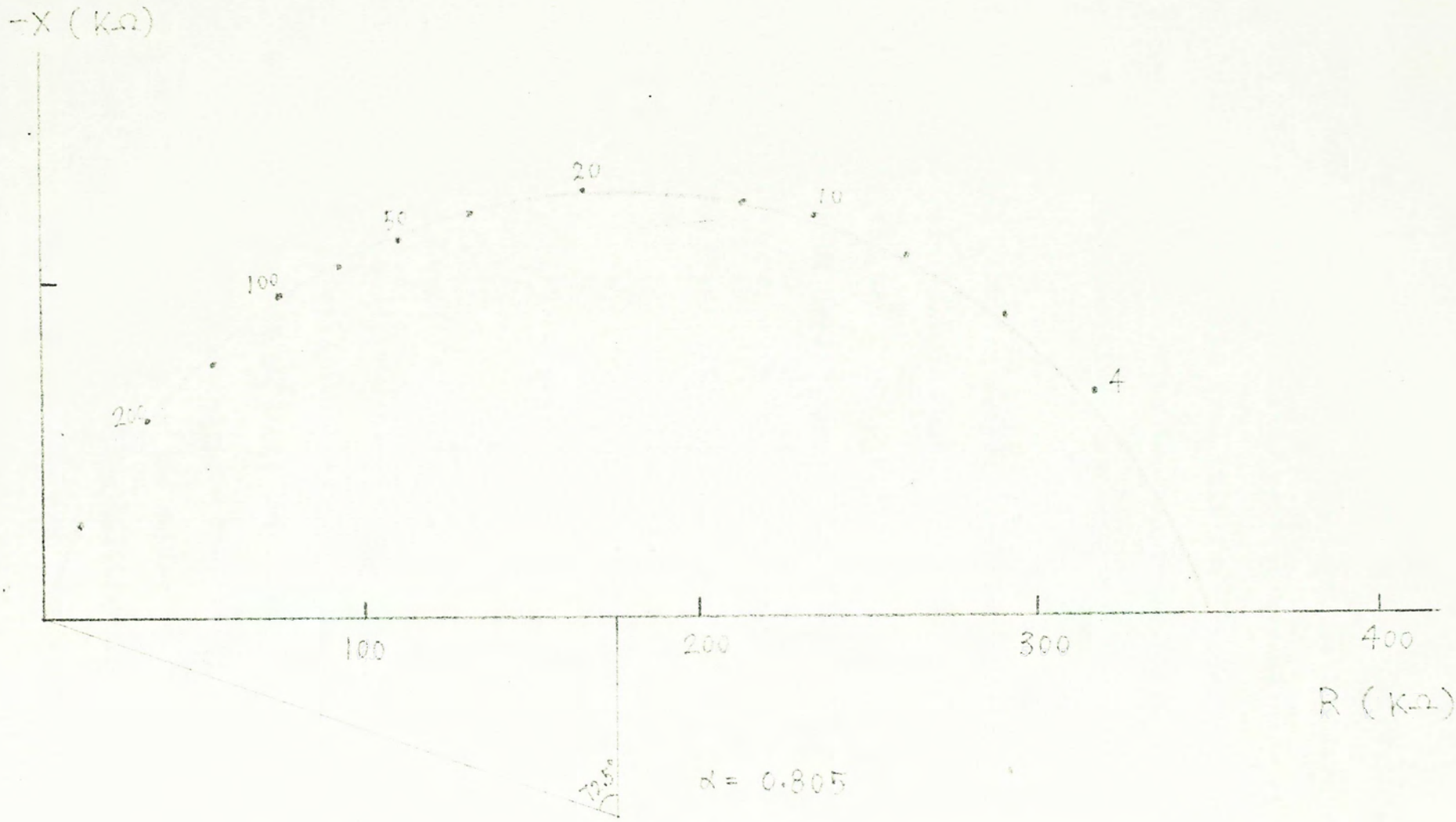

Fig. 5.11 Impedance locus of thumb after administration of atropine

for thumb was essentially the same as that in Fig. 3.7 at intermediate and higher frequencies, but in the low frequency branch (order of several Hz) another process became more significant and seriously distorted the arc. This low frequency process could be in series or in shunt with the original model, but it was almost certain that a capacitive component must be involved.

This peculiar feature was also observed for other fingers and for the palm. Now the major morphological difference between palmar sites and the forearm was that palmar sites possessed a higher density of sweat glands (Sec. 1.3) which, even under thermoneutral conditions, were fairly active. It was thus reasonable to think that the sweat glands were the main cause for such discrepancy.

5.2.2.2 The role of sweat glands

To support this view two further experiments were carried out. In the first experiment, the subject was allowed to undergo vigorous sweating by doing mild exercise in bright sunlight. The degree of sweating was observed by doing the iodine-starch test (39) on the right forearm. When a sweat pore was secreting sweat a tiny bluish-black spot could be seen on the surface. After most sweat glands had been activated, the subject was kept in a warm room to maintain rigorous sweating. The impedance on the left forearm was then observed, and the impedance locus plotted. It was found that under

this condition the impedance dropped by more than an order of magnitude, and EDRs were observed as in the palmar sites. More important, both the transient response and the impedance locus were distorted in a similar manner as in the thumb (Fig. 5.10).

Next, the impedance of the thumb was observed again with the sweat glands being inhibited. This was achieved by topical administration of atropine, a cholinergic blocking agent which prevented the excitation of sweat glands, by the method of iontophoresis (i.e. driving the drug down the sweat glands by passing a steady current, see Ref. 40). The thumb impedance was observed 15 minutes after the iontophoresis process. The result was that the basal impedance level was increased, and EDRs were totally eliminated. In addition, circular arc impedance locus was obtained without any departure at low frequencies (Fig. 5.11).

From these observations it is clear that the low-frequency effect was due to the presence of the filled sweat ducts. But how did they function to bring about such an effect? In the first place it is recognized that the full length of the filled sweat duct behaves like a conductance pathway. We now want to calculate the resistance of a sweat duct in the length of the corneum. The following approximate values are assumed (Sec. 1.3):

average duct diameter, $d = 8\ \mu m$

approximate thickness of thumb corneum, $t = 700\ \mu m$

resistivity of sweat (0.3% NaCl), $\rho = 120\ \Omega cm$
(by measurement)

where an upper limit for the corneum thickness has been used on account of the cockscrew pathway of the sweat duct here. From these values the resistance of a sweat duct across the corneum can be calculated as

$$R_s = \rho \frac{t}{\pi d^2/4} = 16.7 \text{ M}\Omega$$

For a 9 mm Ø electrode and for a sweat gland density of 400 per cm^2 (Sec. 1.3) there will be approximately 250 sweat glands under the electrode. Assuming that all of them are activated the total resistance due to sweat glands alone is

$$R_o = R_s/250 = 67 \text{ k}\Omega$$

This compares well with the extrapolated value of 68 kΩ from the circular arc (Fig. 5.9). Hence we may conclude that the parallel resistance is almost solely due to the sweat glands.

5.2.2.3 Effect of duct wall and partially filled ducts

In the above calculations two assumptions have been made: (1) the electrolytes in the dermis are in good electrical contact with the duct lumen and hence the resistance is mainly due to the epidermal portion of the duct; (2) all ducts are fully filled and are in good contact with the electrode.

In practice the duct wall has a finite resistance and the total ductal resistance should also include this component.

Also, although most palmar sweat glands are active to some extent at all times, not all of them participate in surface sweating. In fact this has been the basis of the duct-filling hypothesis for EDRs. Due to these two factors, the actual resistance due to sweat glands should be higher than expected.

We shall now show that by inference from the experimental data the first assumption is acceptable. Assuming that the conductance across the duct wall is G_m and the ductal capacitance is C_m (per unit length units), the situation is similar to a lossy cable having finite internal resistance (Fig. 5.12). The cable equation is given by

$$\frac{\partial^2 V}{\partial x^2} = G_m R_i V + C_m R_i \frac{\partial V}{\partial t}$$

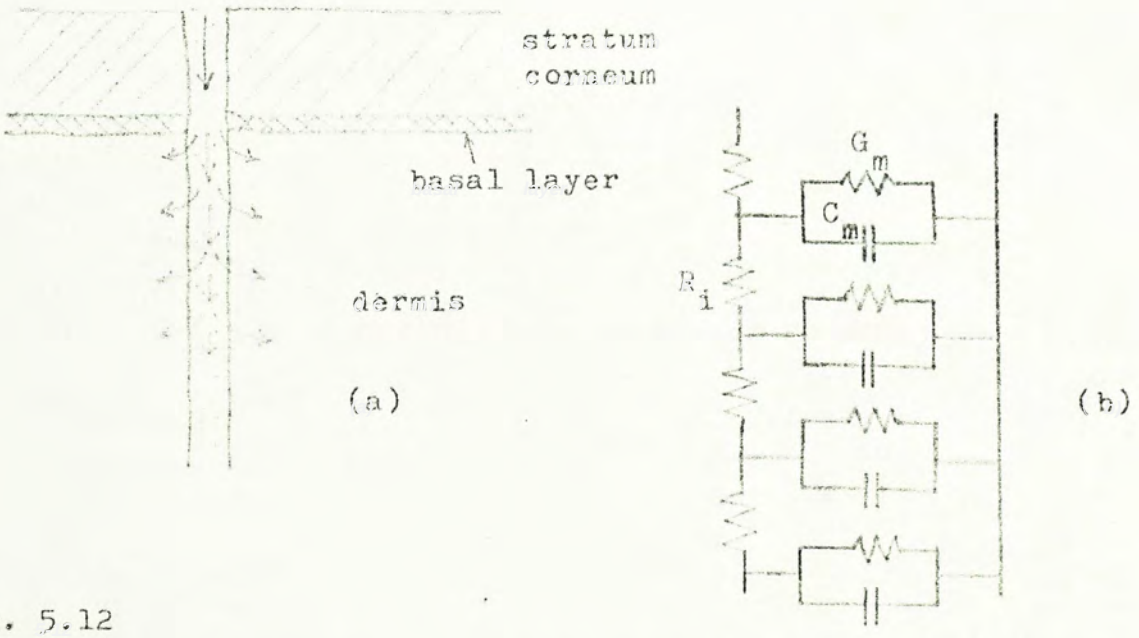

Fig. 5.12
(a) Current pathway along sweat duct at dermal level (indicated by arrows)
(b) Cable analog assuming infinite conductivity in the external fluid.

where V is the potential difference between the duct lumen at distance x measured from the junction between the dermis and the basal cell layer of the epidermis; R_i is the resistance per unit length of the sweat in the duct lumen. From above, the value of R_i is

$$R_i = \rho/A = 240\ M\Omega\ cm^{-1}$$

Under steady state condition we have

$$\frac{\partial^2 V}{\partial x^2} = G_m R_i V$$

Substituting the boundary conditions $V(0) = V_o$, $V(\infty) = 0$, the solution becomes

$$V = V_o e^{-x\sqrt{G_m R_i}}$$

The resistance of the cable is obtained by summing the transverse current components. Therefore

$$R_c = \frac{V_o}{\int_o^\infty G_m V\, dx} = \frac{\sqrt{G_m R_i}}{G_m} = \sqrt{\frac{R_i}{G_m}}$$

From Fig. 5.9 the actual ductal resistance is about 80 kΩ (estimated). Subtracting the extrapolated value of 68 kΩ, and multiplying with the number of sweat ducts, we have

$$R_c = (80 - 68) \times 400\ k\Omega = 4.8 M\Omega$$

Substituting this value into the above equation for R_c, we have

$$\sqrt{R_i/G_m} = 4.8 \text{ M}\Omega$$

from which

$$G_m = \frac{240 \times 10^6}{(4.8 \times 10^6)^2} = 1.04 \times 10^{-5} \text{ mho cm}^{-1}$$

At higher frequencies the transverse current density will be considerably increased by capacitive effect, and hence the cable impedance will be much reduced. The characteristic frequency at which capacitive currents become significant is

$$f_o' = \frac{1}{2\pi C_m/G_m}$$

Since the sweat duct wall is composed of two cell layers and an epithelial coat (Sec. 1.3), the capacitance is at most equal to that of four membranes in series. Taking a membrane capacitance of 1.0 μF cm^{-2} (18), we have

$$C_m = \pi d \times (10^{-6}/4) = 6.25 \times 10^{-10} \text{ F cm}^{-1}$$

From the values of C_m and G_m obtained above we may now find a value for f_o'. Substituting these values into the equation for f_o', one gets

$$f_o' = \frac{1.04 \times 10^{-5}}{2\pi \times 6.25 \times 10^{-10}} = 2.6 \text{ kHz}$$

This value of the characteristic frequency f_o' is many orders higher than the frequency range (about 1 Hz) at which the the departure in the impedance locus is observable. Consequently, if the duct wall impedance is to be considered, its contribution to the total impedance should be very small, and in the frequency range of interest (1 Hz to 1 kHz) it remains essentially as a pure resistance. As seen in the impedance locus, this effect is negligible. What is more, it can by no means be the cause for the low frequency departure in the impedance locus.

Having eliminated the possibility of the duct wall effect, we are only left with the probable effect of incomplete filling of some sweat ducts. In this case the DC current pathway is mainly via those sweat ducts that are fully filled only. If an AC current is applied, more sweat ducts can participate even if they are not in direct contact with the electrode surface. We now show that this event always takes place at a frequency lower than the characteristic frequency of the extrapolated circular arc. Near the surface only a portion of the total number of sweat glands are in contact with the electrode. Let the resultant resistivity at this level be ρ_1, and below this the resistivity due to all sweat ducts be ρ_2. Since $\rho_2 < \rho_1$, it follows that the sweat duct portion near the surface can be bypassed by the polarization capacitance of the corneum at a lower frequency than in the lower part. This will be seen in the impedance locus as a departure from circular-arc plot in the low frequency branch of the locus.

5.2.3 Conclusion

When sweat ducts are filled, they form a DC bypass through the relatively more resistive corneal layer. The electrical model is therefore similar to the basic model we derived before ; the only differnence is that the DC resistance across the corneum is replaced by the total resistance of the filled sweat ducts.

Current passing down the sweat ducts may enter the body internal circuit through the duct wall at the level of the dermis, the resistance of the duct wall being negligible compared with the length of the duct. This is consistent with the finding that this part of the duct is ion-permeable as demonstrated by the observation of movement of methylene blue from the duct into the connective tissue (3).

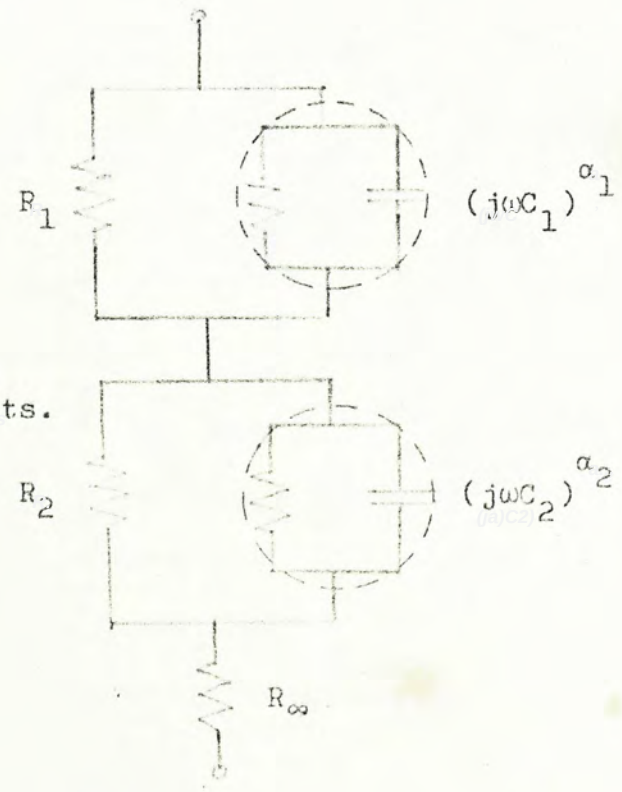

Fig. 5.13
Equivalent skin model of palmar sites. R_2 is the resistance of all sweat ducts. R_1 is the resistance of the surface portion of those fully-filled ducts.

On the other hand, the process of duct-filling, under normal conditions, may not be complete in all the sweat glands. In this case a low-frequency departure in the impedance locus can be observed. The complete electrical model for palmar sites is represented by the equivalent circuit of Fig. 5.13. In this model the total resistance of all sweat ducts in the lower portion of the corneum is represented by R_2. The extrapolated value of the DC resistance from the ideal circular-arc plot is then equal to $(R_2 + R_\infty)$. The actual value of the DC resistance should also include R_1, corresponding to the resistance of the fully-filled ducts in the upper portion the corneum, which is seen in the impedance diagram as a departure from circular-arc locus at lower frequencies.

5.3 FACTORS AFFECTING SKIN IMPEDANCE

In the above we have deduced equivalent models representing skin impedance at two difference sites that are typical of the general body surface and where there is a high density of sweat glands respectively. These model adequately describe the characteristics of the skin impedance as a function of the morphological structure and physiological state of the skin. In reality, the physiological state of the body is ever-changing, subject to the temporal variations in the physical factors of the environment and the body itself. As a consequence, each component of the models may be quite different at different times, even for the same

location. From a practical point of view, therefore, it is necessary to understand how the skin impedance is affected by these factors.

Here we shall point out the effects of some common physical factors known to affect the skin. The discussion presented, of course, is not meant to be exhaustive. As a matter of fact, any physical changes in the environment may have direct of indirect influence on the skin impedance. What we are concerned with, however, are those that may create problems in normal practice.

5.3.1 Time

In general, the impedance immediately after electrode attachment was rather high but then it decreased almost exponentially with time. The time constant for the drop was about 6 minutes, and a final quasi-steady value was attained in about 20 - 30 minutes. The stabilization time required by a dry electrode was a little longer than the electrode used with paste, and the fractional change was also greater. These results had been thoroughly studied by Almasi and Schmitt (41).

With our voltage transient set up it was possible to trace the sequence of changes during the stabilization period. It was because the temporal variations in the skin impedance was rather slow compared with our measurement time with voltage

transient method. From these observations we noticed that during stabilization only the resistive component (R_o) decreased with time, the polarization component remaining essentially the same throughout. This suggested that the temporal changes were mainly caused by increased current pathways under the electrode, probably a result of increased perspirations trapped within the area or by slight hydration effect if electrode paste was applied.

5.3.2 Pressure

5.3.2.1 Method

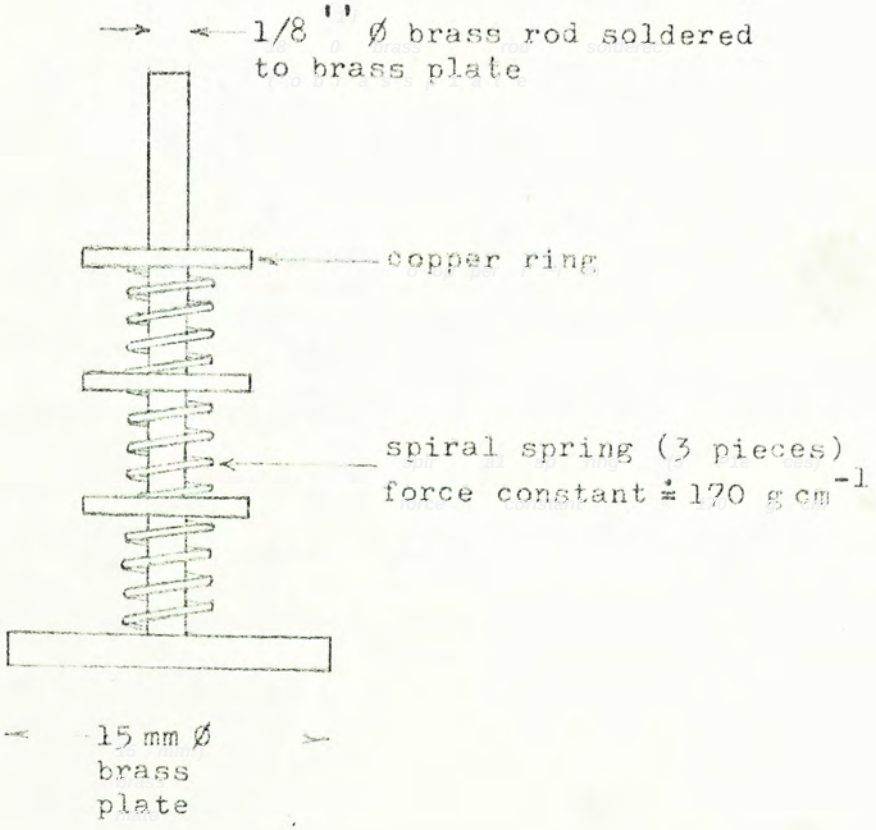

Fig. 5.14 Spiral spring system for pressure setting

A dry, polished brass plate electrode 15 mm Ø was placed on the ventral side of the forearm. The site had been thoroughly cleaned with alcohol followed by stripping with adhesive tape for 2 times. These procedures ensured that the exposed surface was ideally clean. The brass plate had a central stem on which a spiral spring system was mounted (Fig. 5.14). The electrode was held in position on top of the skin by means of a holder clamp. By screwing the clamp, the spiral springs were tightened, producing a pressure on the skin. The central stem was graduated in 5 mm intervals. As the copper ring on top was displaced in position, the pressure set up could be estimated by noting the total displacement of the springs. With a force constant of 170 g cm^{-1} the pressure set up would be about 50 g cm^{-2} (0.5 N cm^{-2}) for each 5 mm increment.

Similar procedures were followed as previously described with the voltage transient method. A stabilization period of about 20 minutes was allowed until the readings became steady. The pressure was increased from 50 g cm^{-2} to 250 g cm^{-2} in steps of 50 g cm^{-2}, after which it was decreased in similar steps to the original value. The maximum and minimum pressure were considered limiting values to produce discomfort or to maintain satisfactory contact, respectively. For each pressure setting, the voltage transient response was determined immediately after application of the new pressure, repeated by the same after about 3 minutes. Little difference in the two was noticed.

After that, the polished brass electrode was replaced by a similar one, but this time the electrode surface had been ground with woodwork sand paper. This produced a rough and irregular electrode surface. Exactly the same procedures were repeated as in the above over the same skin site. The results of the two electrodes were compared.

5.3.2.2 Results

For the smooth electrode, increased pressure had very little effects on the parameters (α, ω_o, R_o) of the impedance. Increasing the pressure from the lower to the upper limiting value reduced R_o by less than 2% with a corresponding slight increase in f_o (negligibly small), whereas the value of α was virtually unaltered. The results are illustrated in Fig. 5.15.

On the contrary, the rough electrode showed marked changes with the application of different pressure. The value of α, as before, was fairly indifferent to pressure changes, but R_o decreased drastically following an increased pressure. At the outset, i.e. when the pressure was minimum, the value of R_o was found to be higher than in the previous case with the smooth electroce. Following an increased pressure, R_o decreased progressively until the upper limit for pressure was reached, at which time R_o became close to the value as with the smooth electrode. As the pressure was gradually removed, the impedance returned to a lower value than the original one at the start. Along with the changes in R_o, the

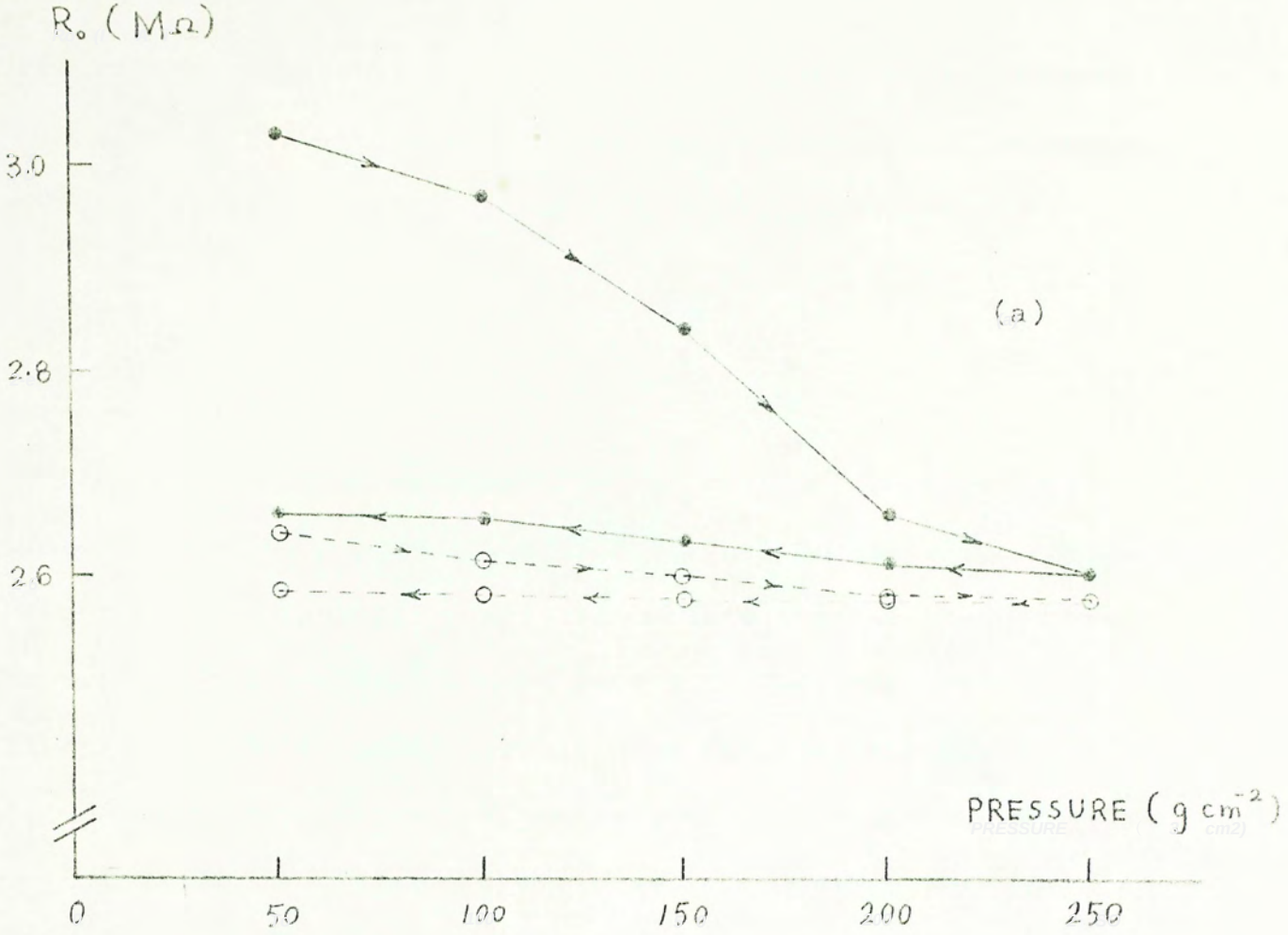

Fig. 5.15 Variation of (a) DC resistance, and (b) characteristic frequency, with pressure.
broken line: smooth surface electrode
solid line : rough surface electrode

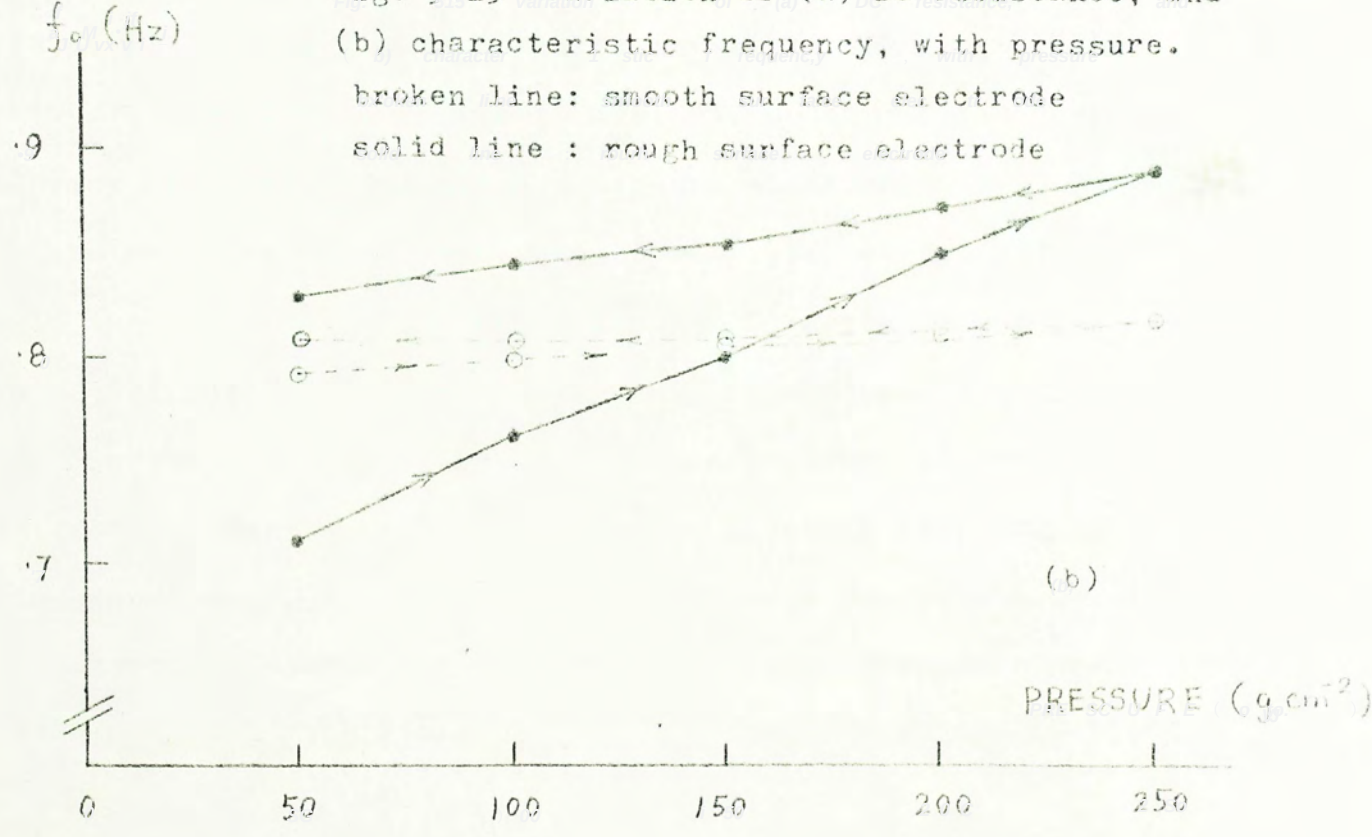

characteristic frequency (ω_o) was found to change in accordance to equation (4.1) in such a way that the polarization impedance, $(j\omega C)^{\alpha}$, appeared to be fairly constant (Fig. 5.15).

5.3.2.3 Discussion

This simple experiment demonstrated the role of the electrode surface in producing pressure artifact. This could be explained in terms of the change in effective surface area of the electrode with different pressure. For the smooth surface electrode, contact with the skin was almostly perfect even for moderate pressure settings so that an increased pressure did not improve any further. For the rough electrode, however, the electrode surface was interlaced with grooves and ridges, and with a small applied pressure only the outstanding part of the surface was in contact with the skin. This resulted in a higher resistance value. With an increased pressure, the effective contact area was considerably increased, allowing more resistive paths under the electrode. The lower limit for the resistance was then that of complete electrical contact, as in the case of the smooth electrode. Once the electrical contact was established, only part of it would separate as a result of reducing the pressure, because the skin appeared to 'stick on' the electrode surface after the passage of electric current. Throughout all these changes, the polarization impedance was relatively unaffected because it was essentially a 'displacement current' effect and would therefore be quite independent of the available conduction paths.

When using the dry electrode (e.g. as clinical monitoring electrode) two important factors must be considered if a stable and satisfactory record is desired. Here below is a brief discussion on both.

Electrode size and shape

The electrode surface must have a definite shape, preferably flat or slightly curved. If the electrode has a round tip (as in the search electrodes of some commercial instrment for electo-acupuncture), the actual surface area in contact with skin well be uncertain. The effective electrode area will then be determined by the pressure applied to the electrode, and to the contour of the skin surface. The result, of course, will be unreliable.

On the other hand, the skin surface, if examined on a semi-microscopic scale, is fairly irregular in nature. This irregularity becomes more significant when a small surface electrode is used, the contact surface becoming less controlable. The situation is not much improved if a greater pressure is applied as this very ofter leads to local deformation over the small area on which the electrode is pressed. More than that, the sharp edge of a small electrode may indent or even puncture the skin surface and quickly lowers the skin impedance (42). This is the problem generally encountered in practising electroacupuncture. No wonder Noordergraaf and Silage (43) could have found a variability in the skin resistance in excess of 300% when a force of 10.5 N was applied on the small electrode tip (unspecified size) !

Preparation of skin and electrode surfaces

If the skin is not clean enough, part of the surface will be covered by a thin layer of dirt preventing current flow. This effect is highly sensitive to the application of increased pressure as this will definitely promote better contact. Before a dry electrode is applied, therefore, it is helpful to strip the skin surface with adhesive tape for a number of times. This simple procedure will remove aggregates of dirt and ruptured keratin cells on the surface, providing an ideal electrical contact with the electrode and as a result eliminating the problem of pressure artifact in the recorded signal. In such considerations, a stabilization period is also important for the dry electrode to develop complete contact with skin through the accumulated perspiration within the enclosed area.

With a moist electrode the effective area is almost that of the entire electrode surface, so that pressure artifact can be minimized. Lawler (8) observed that the application of pressure up to 300 $g\,cm^{-2}$ had no effect on the values of resistance and capacitance recorded. It was expected that the use of electrode paste should have the same effect, but the result of Swanson and Webster (16) showed that a slight reduction in the impedance was observed with increased pressure. In this case, the change should not be a result of changes in effective area, but it was likely that the application of pressure promoted the permeation of electrolytes through the corneum, and hence reduced the impedance. The fractional change in this case is not so annoying as for dry electrodes.

5.3.3 Hydration

5.3.3.1 Hydration of forearm

The forearm was hydrated by running water over it for about 15 minutes. The voltage transient response before and immediately after hydration were recorded using the dry brass electrode.

It was found that the effect of hydration was to decrease the DC resistance R_o. Nevertheless the change was not so remarkable as expected (only about 40% decrease was observed) showing that the laminae structure of the corneum over the forearm was fairly impermeable to water. This explained why the successive application of electrolytes on the skin surface during the skin-stripping experiment had so little effect on the measured impedance. Furthermore, it was found that a shorter stabilization period (only 3 minutes as compared to 20 minutes as mentioned above) was necessary for the hydrated skin. This is a reasonable result as the moisture remaining on the skin surface would fascilitate electrode contact in a shorter time than the simple process of perspiration.

5.3.3.2 Hydration of the fingers

The left thumb was immersed in water for about 20 minutes. The impedance locus was determined before and immediately after

immersion using the Ag/AgCl electrode as before.

The impedance of thumb after immersing in water was found to be larger than its original value (Fig. 5.16). This result at first sight seemed unreasonable and contradictory to our result with the forearm. However, it was noticed that hydration of the corneum, other than to fascilitate current flow directly through the horny cells, had another important effect on the palmar surface. When the corneum was hydrated, swelling of the horny cells forming the laminae structure resulted, produding

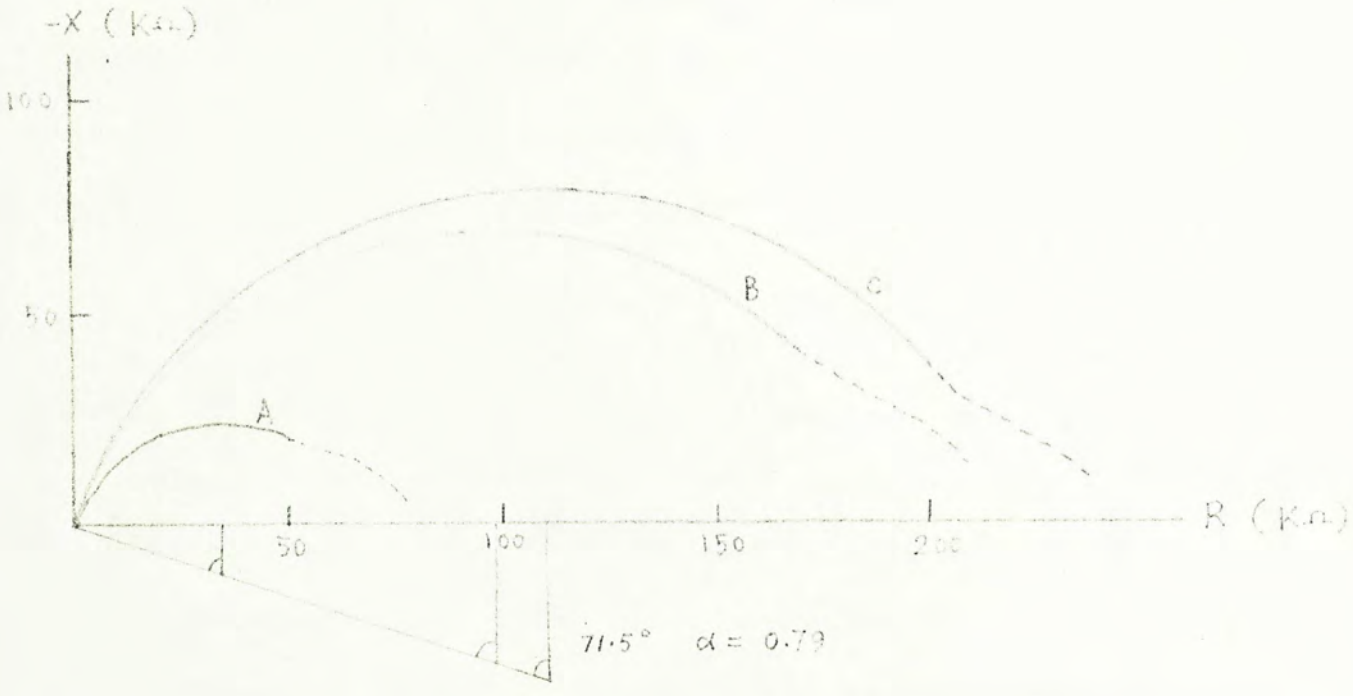

Fig. 5.16 Impedance locus of thumb: (a) normal conditions; (b) after immersion in water; and (c) after sweating.

a simple mechanical pressure which blocked up the sweat ducts. This duct-blocking mechanism due to hydration had been confirmed by microscopic observation of the sweat pores (44). In the palmar areas where the conduction of current is mainly via the ducts, this would produce significant changes in the measured impedance. Moreover, the corneum in these areas are usually much thicker, so that the total pressure exerted on the duct walls would be quite large.

5.3.4 Sweating

The effect of sweating on the forearm has been described in Sec. 5.2.2.2. In general, this results in marked decrease in DC resistance, obvious EDRs, and a low frequency departure in the impedance locus. All these are characteristic of palmar areas .

The effect of sweating on the impedance of thumb was observed. To increase the rate of sweating, the subject was allowed to do mild exercise in a warm room. The result was similar to that of simple hydration (Fig. 5.16). It was thought that prolonged surface sweating on the palmar surface resulted in hydration of the corneum, stimulating the duct-blocking mechanism which in turn affected the impedance. In this way the duct-blocking mechanism functions as an 'automatic shut-off' system which can close up some ducts when the sweating rate becomes too excessive. This may

be the reason why the palmar areas, in spite of their high density of sweat glands, are seldom identified with rigorous surface sweating to such an extent as observed on the chest, forehead, and the back of the body.

The effect of inhibiting sweat gland activities by means of iontophoretical application of atropine was observed and the results have been noted in Sec. 5.2.2.2. In brief, this increases the DC resistance, eliminating EDR completely and results in an ideal circular-arc impedance locus.

5.3.5 Temperature

The effect of temperature on skin impedance was investigated. The left hand and forearm was placed in a constant-temperature enclosure in which the temperature could be controlled from 0°C to 50°C to any desired value and maintained steady by circulating water in the outer jacket and nitrogen gas inside the enclosure. The circulating water and nitrogen were both maintained at the desired temperature by a constant temperature bath and circulator (Forma Scientific 2095), as shown in Fig.5.17.

As expected, change in temperature affected the sweating rate which was a major cause for changes in skin impedance. The effect was more remarkable in the palmar areas then on the forearm

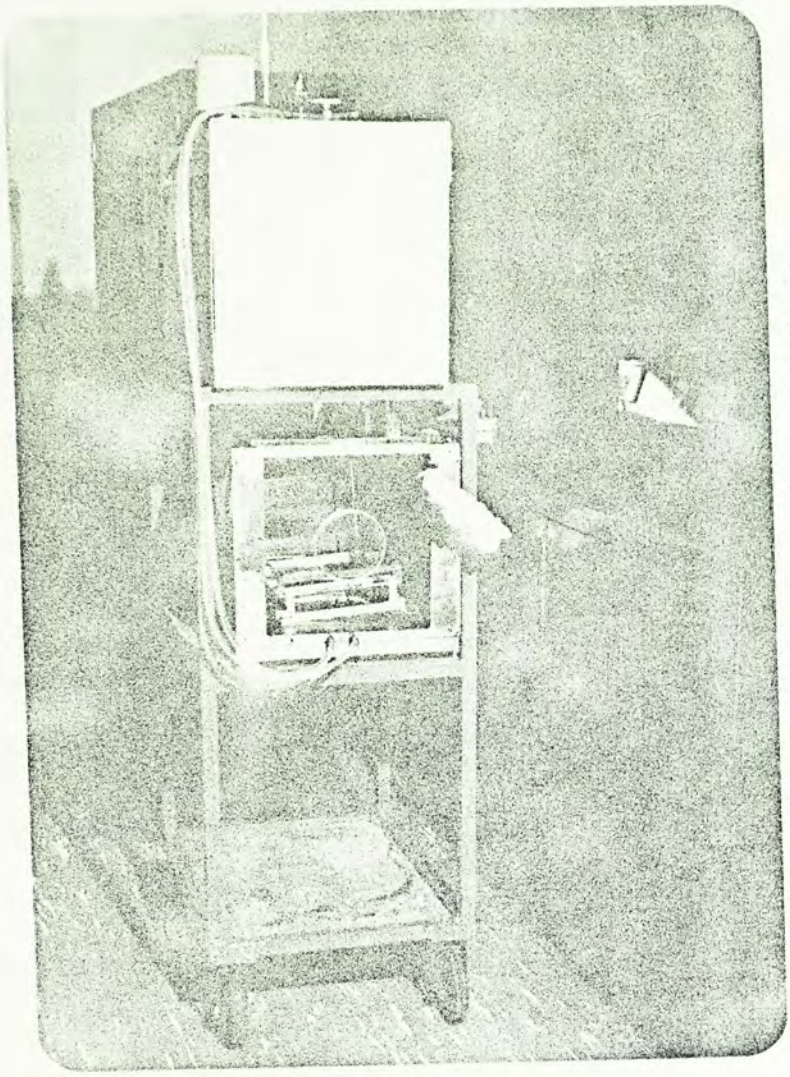

Fig. 5.18
Constant temperature system
Upper: constant temp. bath & circulator
Lower: constant temperature enclosure

5.3.6 Conclusion

Of the several factors affecting skin impedance, two can be considered to be of fundamental importance: the effects of electrode area and sweating. Both have an effect on the DC resistance pathway. In palms and fingers surface sweating can be limited by swelled corneal cells which block the ducts. In using a dry electrode, pressure artifacts can be minimized by (1) skin stripping; (2) a polished electrode surface; and (3) moistening or simple perspiration.

CHAPTER SIX RYODORAKU AND ELECTROACUPUNCTURE

6.1 INTRODUCTION

One modern approach to unveil the myth of the ancient Chinese Acupuncture methodology is the study of electrophysiological phenomena on the body surface. Lavier (45) postulated a flow of 'Galvanic current' induced by stimulation at the acupuncture point; this current being transmitted via a meridian to bring about regulation of the abnormalities occuring in the related body organ. Kim Bong Han (46), a Korean biologist, observed that the peristaltic movement of the large intestine was reflected in a corresponding fluctuation of skin potential at (足 三 里). ST-36 In China, similar investigation have been reported (47 - 49).

The hypothesis of electro-physiological interplay in Acupuncture would imply that the electrical properties of the acupuncture points and meridians should be in some way different from other parts of the body. In 1950, Nakatani (50), a Japanese medical doctor, conducted an extensive survey on the electrical conductance over the entire body surface, and claimed that the

skin surfaces over most acupuncture points were more conductive. He called these points Ryodo points, meaning good conductive or electropermeable points; the patterns or meridians joining them was named Ryodoraku. He related these to the activities of the autonomic nervous system which were known to be closely concerned with the regulation of some body functions. He then developed a method to adjust the malfunctions of the internal organs by regulating the autonomic nerves. The treatment was known as Reactive Electropermeable Point Treatment (REPP), and was performed by applying electrical stimulation at the related electropermeable points located by conductance measurements.

Following the report of Nakatani much work had been done to verify the existence of electropermeable points, but the results turned out to be controversial. Some asserted that electropermeable points were observable in the vicinity of some acupuncture loci (42, 46, 51 - 56). Others held that the electrical conductance at the acupuncture points were not necessarily higher; the locations of the observed electrpermeable points were indefinite and unrelated to the established acupuncture loci (57). Up to the present, no consensus has yet been reached.

6.2 POSING THE PROBLEMS

One disputable factor in the study of skin conductance is the reliability of the method adopted. Indeed this is the basis on which comparison of different results would be of significance. The general problems inherent in measurements of this kind are those discussed in Sec. 5.3.3; the more important ones include pressure, current density, electrode and electrode preparation, and sweating. Unfortunately many of the methods currently practised by most investigators seemed to have little control of all these factors. Noordergraaf and Silage (43) challenged that the conductance could be largely affected by deliberate or unintentional manipulation of the search electrode, and concluded that the observations could be explained within the framework of biomechanical properties of the skin-electrode system. In other words, the subjective conviction of the investigator may have a strong influence on the outcome, making it even more unreliable.

Another difficulty arises from the diversity of the approaches adopted for the investigation. In summary, there are three different ways to investigate the point-to-point conductance on the skin surface. The first is the original method used by Nakatani and some others, in which a DC voltage of 12 to 21 volts is applied to the skin by means of a dry electrode (1 cm diameter). At a point where the conductance is thought to be higher a sudden flow of current occurs, and the subject can feel a stinging sensation (42, 50). In another method, the excitation voltage is

only 1 - 2 volts or smaller; the conductance is indicated by the amount of current that can flow. In this case no sensation can be experienced by the subject (53 - 55). While the first method can always locate the electropermeable points having absolute conductance maxima, this method at best indicates local maxima only, and the result has to be tested by statistical and stochastic methods. The third one is basically an endogenous method in which certain body signal is measured on the skin surface. The signal can be an ECG potential (58), or even simply the line frequency pickup (42). The main criticism on the last method are the instability of the signal source and the capacitive effect of the epidermis.

It should be noted that the last two methods differ from the original method of Nakatani in one important aspect: they operate within the linearity limit of skin conductance. This criterion, though likely to be a more reasonable one to make, marks the departure from the original conception. There is no point whatsoever to follow a different approach to tackle the same problem while the original idea still remains untested. Further, it is often with this latter approach that disputes stand up high (43, 53, 57), showing that a greater degree of uncertainty also ensues. Based on a series of preliminary investigations we found that while the excitation (measurement signal) was small enough to maintain linearity, no significant local variations in conductance could readily be observed on the forearm. Therefore

we shall rule out this approach and concentrate upon the original method. We shall however modify this method to eliminate, as far as possible, all physical and human factors that can cause unreliable results.

6.3 TOWARDS A SOLUTION

6.3.1 Pain sensation in Ryodoraku

The stinging sensation characteristic of the Ryodoraku or similar methods was of great interest. It had been noted earlier that the resistance of the skin was caused by the upper layers of the epidermal stratum corneum. The structure here was mainly composed of extinct horny cells, and certainly was devoid of sensory fibers. Why then was there the sensation of pain? Was it that the epidermal resistance at these points (average specific resistance about 1 $M\Omega\,cm^2$) was so low as the dermal resistance ($\sim$ 1 $k\Omega\,cm^2$) where the nerve fibers were embedded? If so the variation of resistance over these areas must be very distinct and should be easily identified by any methods. But it was not the case.

Obviously this fact was not seriously taken by many investigators, including those who practised Ryodoraku therapy. We decided that this would lead to some clues concerning the nature of Ryodoraku.

6.3.2 The Epiductive Tape electrode

To begin with, it was found that the use of a solvent-activated tape electrode, known as 'Epiductive Tape Electrode' (electrode model 3850, Medtronic, Inc.) was of great advantage (59). The electrode was in the form of a tape with a conductive silver microparticle paint on one side. When activated by acetone the paint could stick onto the skin surface firmly, seeping into the keratin layer of the skin. After a few minutes the solvent dried out completely, and a firm electrical contact with the skin surface was obtained. This contact could be removed by simply pulling the tape away. The advantages of using the Epiductive Tape were manyfold, namely,

(1) a uniform and stable skin-electrode contact was realizable;
(2) practically no pressure on the electrode was necessary, producing no indentation or puncturing of the skin;
(3) the electrode could conform to any irregular contour of the skin surface; and
(4) human factors were reduced to a minimum; no special manipulation on the part of both the investigator or the subject was necessary once the electrode was secured in position.

In view of these advantages, the epiductive tape was employed as a search electrode in place of the conventional dry plate electrode.

6.4 METHOD OF INVESTIGATION

Figure 6.1 shows the system for conductance measurement. A strip of activated epiductive tape (about 3" x 1") was pressed on the forearm. An electrode lead was wrapped in one end of the strip as connection cable. The arrangement for the indifferent (reference) site was the same as before.

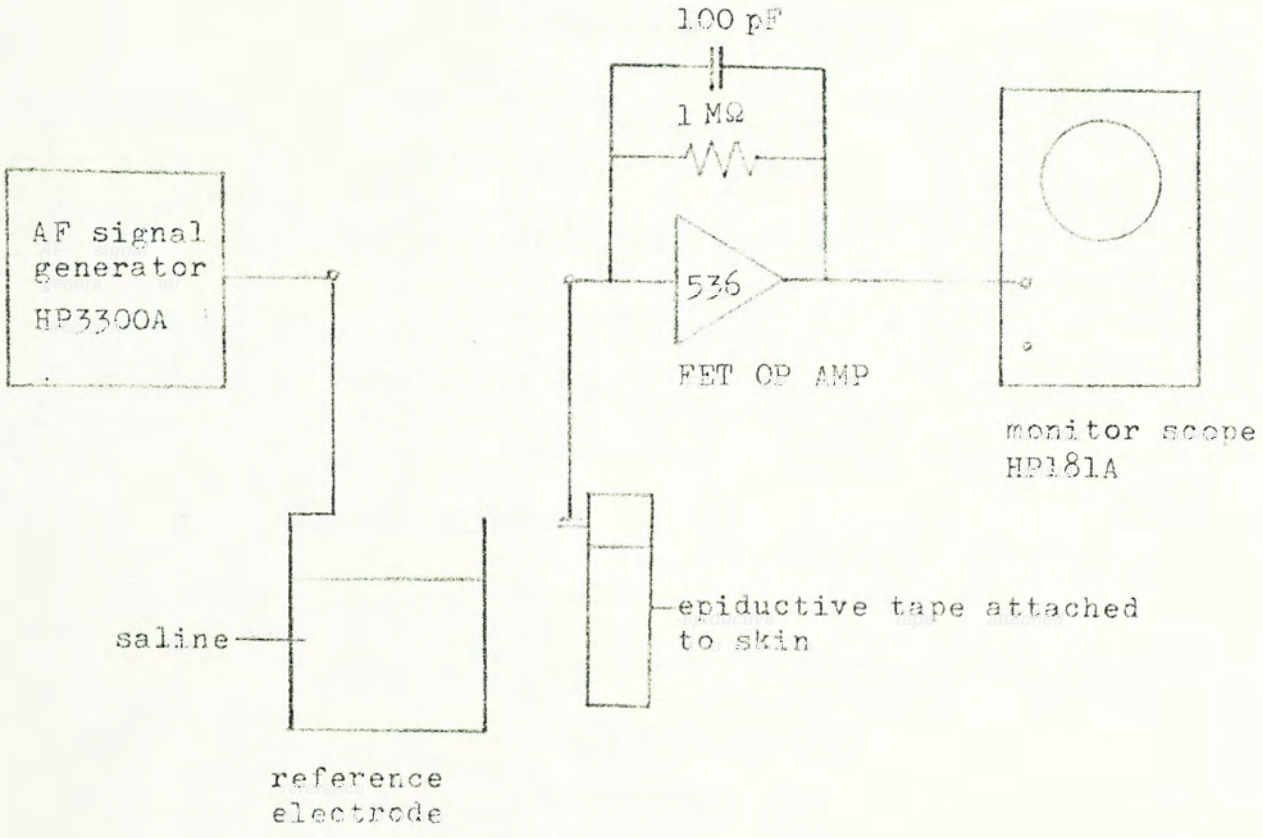

Fig. 6.1 Constant voltage method for locating conductance maxima on the skin

A constant voltage (0.5 Hz sine wave) was applied across the electrodes and the amount of current was read at the OP AMP output. The advantage of a constant voltage system was that the current density was independent of the surface area of contact. As the input voltage was gradually increased from zero, the current increased in non-linear manner but at an input voltage of about 10V a sudden step increase in current was observed. At this point the subject could feel a sharp pricking sensation at the electrode site similar to those described in Ryodoraku measurements. Here the use of a low frequency AC enabled the subject to identify the sensation easily: the pricking sensation just followed the input rythm closely, appearing at the input peaks and soothing at low or intermediate levels. Once the stinging sensation had occurred the input could be lowered to 2 - 5 volts and the sensation still remained. This resembled a breakdown phenomenon. If the input voltage level was maintained this could intensify to become more acute pain sensation. When the electrode tape was removed after a few minutes, tiny spots of less than 50 μm diameter were observed on the surface. These spots were then those having a lower threshold for the 'breakdown' phenomenon than the surrounding area (this will be explained in the next section). A small metal electrode (2 mm Ø) placed at such a spot showed that the conductance was more than the conductance of the surrounding areas. This could hardly be observed beforehand. A microscopic examination of these spots showed that most of them were not associated with hair follicles. If during the experiment the stimulation was prolonged

the spots would be blackened and become larger in size; in some cases even a small depression could be observed showing complete destruction of the top tissues. Since nearly all criticisms concerning electrode deficiencies had been eliminated by the use the use of the epiductive tape, we considered that these good conductance spots corresponded to those claimed by Nakatani.

In order to know the pattern of these spots two meridians (Lung 手太陰肺經, and Pericardium手厥陰心包經, Fig. 6.2) on the ventral side of the forearm were examined. Epiductive tapes were pressed along each meridian and the points having the lowest threshold for pain sensation were located. A total of 9 subjects, aged from 17 to 40, were studied using this method.

6.5 RESULTS AND DISCUSSIONS

6.5.1 Experimental results

In all 9 subjects it was found that good conductance spots associated with stinging sensation could be found in the vicinity of the two meridians. However, such points were characterized by the following observations:

(1) Although some of the points might be considered close to certain acupuncture points, most of them fell in an irregular pattern and all alienated from the acupuncture points and meridians.

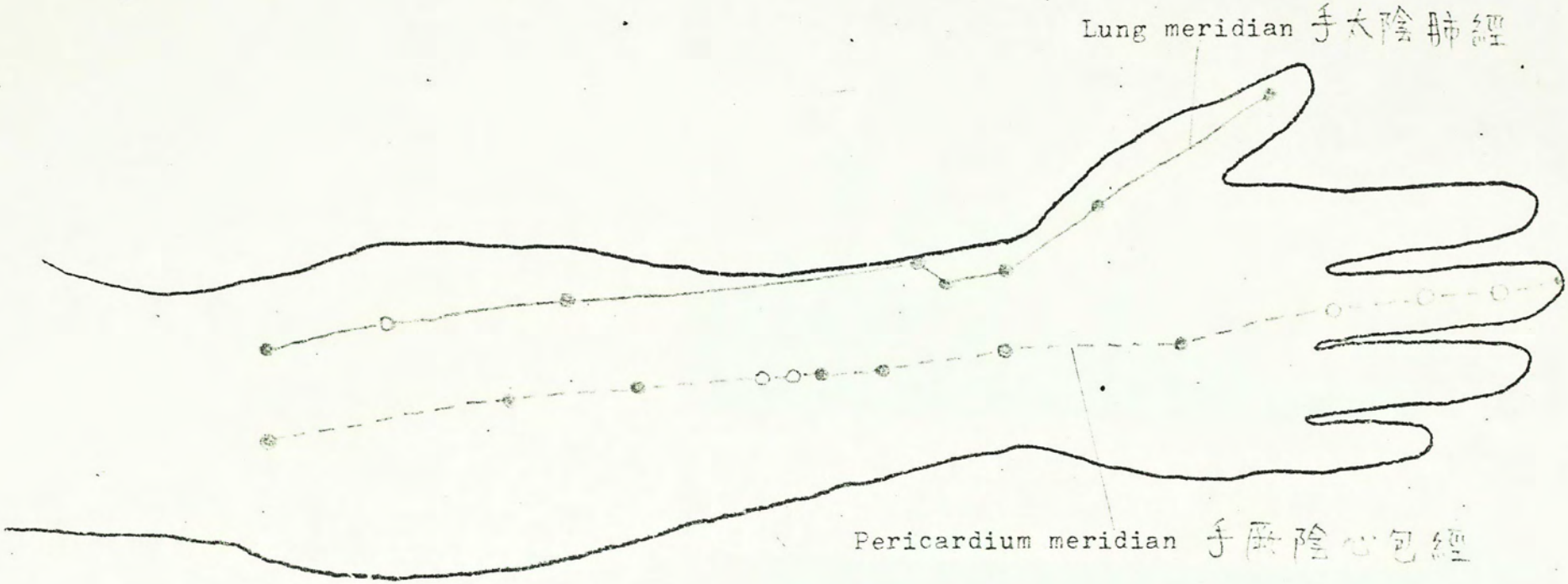

Fig. 6.2 The Lung and the pericardium meridians on the forearm

PALM AND VENTRAL SIDE OF FOREARM

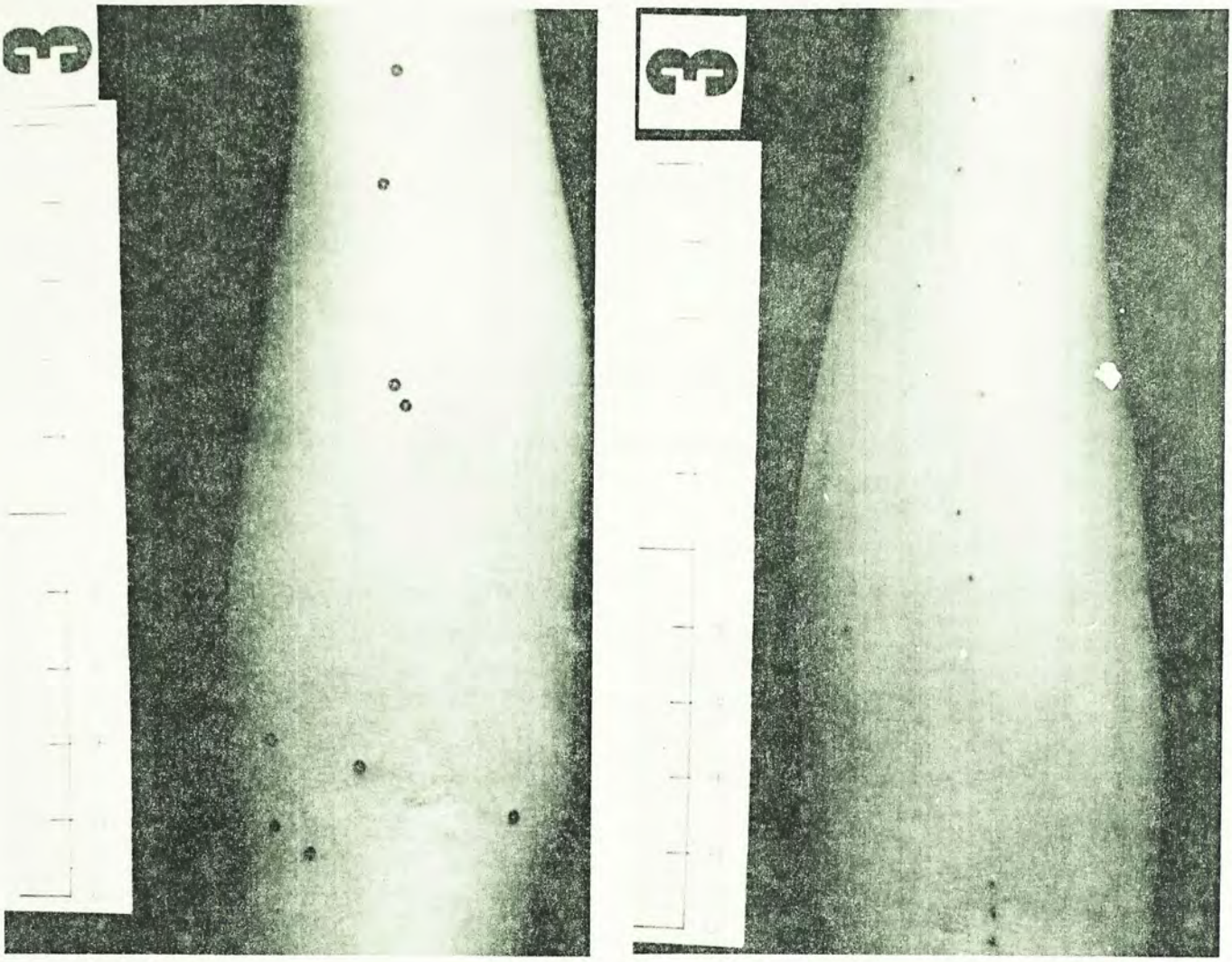

(a) (b)

Fig. 5.3 Spots of good conductance on (a) left and (b) right forearms showing the unsymmetrical pattern. The spots shown are along the pericardium meridian.

(2) The points located in all 9 individuals were all different. No general pattern could be derived on statistical basis.

(3) When other anatomically similar locations were examined, spots of good conductance could be found with similar ease, although no known acupuncture points and meridians were in association with these areas.

(4) In four individuals both left and right limbs were studied, but the pattern on either limb turned out to be unsymmetrical (Fig. 6.3).

From these evidence it was clear that even with our relatively small sample of cases no definite correlation between the observed spots of good conductance and the acupuncture points could be justified. This would be better understood if the nature of such spots were known.

6.5.2 Nature of good conductance spots

It was noted that the occurrence of acute pain sensation when passing an electric current transcutaneously was also discovered elsewhere. In electrocutaneous stimulation for sensory substitution for the deaf very sharp pricking sensation could be elicited by the signal (a series of rectangular current-limited pulses) even at a relatively low input level. In a thorough study of this artifact Mason and Mackay (60) concluded that the sensation was caused by localized thermal effect at some spots on the skin.

It was thus likely that the spots located in our case were due to a similar effect. In order to show this, it was noted that the threshold thermal density for pain resulting from radiant heat stimulation was $H = 1.05\ W\,cm^{-2}$ (61). Equating this to the power dissipated in a constant voltage system, the threshold voltage to produce thermal pain is

$$V = (RHA)^{1/2} \text{ volts}$$

where R is the resistance of the spot and A is its area. The average value of R was found to be of the order of 500 kΩ (after stimulation). Taking the diameter of the spot to be 50 μm, the threshold voltage would be about 3 volts. This is in good agreement with our previously noted value of 2 - 5 volts.

Before skin damage the resistance of the spot should be higher, and would therefore demand for a higher threshold voltage. In our experiment the initial threshold was about 8 to 18 volts. Substituting an average value of 13 volts into the above equation for the threshold voltage, the original specific resistance (product of resistance and area) of the spot can be calculated, giving

$$R_o A_o = \frac{13^2}{1.05} = 160\ \Omega cm^2$$

This value is many orders of magnitude smaller than our previous result for the specific resistance of the skin (about 1 $M\Omega\,cm^2$ on the average). This is why the burning effect

did not spread through the whole surface under the electrode tape. However, the skin might have local spots having relatively smaller resistance, and it was here that the thermal effect took place. These spots might be due to the presence of structural defects, scratches, or filled sweat glands. But the exact nature is still unknown. These became the most susceptible points on the skin, but because of their relatively small size and scarcity in number, they were hardly noticeable when using a macro surface electrode. If a large excitation was applied, these spots would be automatically 'developed' when localized thermal damage spread through the cellular structure in the immediate vicinity.

6.6 · CONCLUSION

From our earlier studies on skin impedance it has been found that the resistance mainly resides in the top part of the stratum corneum. As the structure here is mainly composed of extinct cells it is difficult to see how the electrical properties of these cells can be related to spots of acupuncture which are usually located 'deep within muscle' (57). However, if such a relation did exist, they would undoubtedly provide much convenience to our understanding of acupuncture. Probably this is the chief reason why this topic has received so much attention.

With the epiductive electrode a much more reliable method for conductance measurements is implementable. Being limited

by the supply of the electrode tape we were not able to take more samples for the study. However, this was not so much important since for this project we were more concerned with the techniques for reliable measurement than taking samples. Even so, the results signified a random nature in the spots of high conductance value, and no regularity in the observed pattern could be identified on the whole or on the individual basis. Consequently there is the reason to doubt Nakatani's claim for the Ryodoraku pattern.

We have also shown that the stinging sensation when a Ryodoraku point was located was in fact the result of thermal damage. This might at first develop in tiny spots of smaller electrical resistivity, and once started the burning effect became accumulative until all the neighbouring structure had been destroyed. After that the resistance of the entire small area was greatly reduced, so that the spots became more easily observable than before stimulation. This might be a more reasonable explanation for the so-called Ryodoraku.

CHAPTER SEVEN CONCLUSIONS AND DISCUSSIONS

7.1 EQUIVALENT MODELS

The impedance of the skin has been found to exhibit very interesting properties. In the frequency plots, the straight line portion in the intermediate frequency range has a slope less than unity, showing that a power-law relationship is involved. This is more explicitly shown in the complex impedance plots which has been found to be in the form of a circular-arc locus with the centre being displaced down from the real axis. These graphical representations, when put together, can be concisely explained by an equivalent electrical network consisting of a constant phase admittance and a shunt resistance. The constant phase admittance possesses frequency-dependent properties such that it has a constant phase angle and the magnitude varies as some powers ($\alpha<1$) of the frequency. This property cannot be explained by ordinary electrical components or any combinations of such components, and so it is not appropriate to treat the skin simply as a dielectric material. Sometimes it may be convenient to interpret the frequency characteristics as arising from a series of dielectric layers of

varying relaxation properties and that the relaxation time of each layer is governed by a certain distribution law (7, 37, 38). However, this does not explain why such a restriction is always valid. Furthermore, it is not appropriate to assume any particular form for the structural representation without due regards to its nature and physical significance. There is one important point which is most relevant to our understanding of a biological impedance. In a physiological system the flow of electric currents is acco lished by ionic movements in an electrolytic solution. This will make it very different from non-electrolytic materials in which electric currents are carried by free electrons (or holes). Since free ions must be present in pairs, either of them will respond to an applied field and their motions will be coupled to each other. The processes of ionic conduction and polarization will then be ascribed to a different nature as electronic conduction and polar relaxation, and hence the terms conductivity and dielectric constant should have different meanings. Any attempt to describe an electrolytic system as an ordinary conductor or dielectric is just to ignore the existence of the electrolytes.

In view of this, it will be more appropriate to consider the skin impedance as resulting from ionic conduction and polarization effects of the skin cell layers. As such the impedance will be in the form of a polarization capacitance combined with a resistance. This approach receives justification as one finds that a biological cell alone may possess similar frequency dispersion effects. Taking the cellular lamina as a structural unit, it is possible

to construct a structural equvalent model to describe the impedance makeup of the skin. From the skin-stripping experiment, it has been found that the impedance resides in the stratum corneum of the epidermis, and that the few cell layers in the stratum nearest to the surface determine the overall impedance. This result disproves the hypothesis for a definite 'water barrier' in the epidermis, but rather the impermeability is caused by the laminae structure of the entire stratum corneum, with increasing effects towards the surface. If sweat glands are present, they form a ready bypass for the current to discharge into the body internal circuit at the level of the dermis; the result is a marked reduction of the shunt resistance. The effect of some partially filled ducts is that the shunt resistance is appreciably higher at DC than at higher frequencies. In the impedance plane this will be demonstrated as a low frequency departure from the circular-arc locus.

7.2 PHYSICAL FACTORS AFFECTING SKIN IMPEDANCE

Of the many physical factors causing changes in the skin impedance, two processes are found to be fundamental. The first is the state of sweating. All physical factors (e.g. temperature, psychological state, humidity, etc.) that can affect sweating rate can be considered as secondary in producing variations of the skin impedance. In the palms and fingers, excessive sweating has another effect to block the sweat ducts, thereby increasing the

impedance. This 'automatic shutoff' mechanism appears to be the major cause for the restrained surface sweating in this region as compared to other parts of the body where a large quantity of surface sweating is possible.

The other factor to be considered is the effective contact area. It is believed that pressure and movement artifacts in using a dry electrode is mainly the result of variations of the unstable contact area. If a dry electrode has to be used, it is advisable to have perfectly cleaned surfaces on the skin and on the electrode. This may be conveniently achieved by skin-stripping and electrode surface polishing respectively.

Both sweating and change of contact area primarily affect the conductance pathway only. The polarization capacitance of the corneum is relatively unaffected.

7.3 ELECTROACUPUNCTURE

The occurrence of electropermeable points, or Ryodoraku, on the skin surface has been found to be associated with thermal breakdown of the stratum corneum. The breakdown leaves tiny spots on the skin surface of considerably reduced resistance, and simultaneously produces burning pain. Since no regular pattern for the electropermeable points can be identified, the occurrence of these points should be considered as surface defects rather than the result of electrophysiological correlates.

7.4 TRANSIENT ANALYSIS

The transient response of a biological impedance with phase constant α is a well-defined time function. For integral or simple fractions of α, it is possible to find a concise mathematical expression for the function, but for α to be an arbitrary constant, it has to be evaluated numerically at discrete time intervals. For α to be in the range (0.5, 1.0) the curves can be fitted to any experimental response curves to obtain the parameters characterizing the impedance function. This is provided by a simple iteration scheme making use of the converging properties of the response curves (the curves corresponding to different α values clusters around the 51% point). The ease with which the parameters can be estimated is of great importance if the transient method is to be a useful technique. In our experiment with the skin the method has proved to be satisfactory in providing the required accuracy and measurement speed.

7.5 SUGGESTIONS FOR FURTHER WORK

(1) The vol age transient technique implemented in our measurements suffered from several limitations: (a) the response time was not fast enough to cope with measurements of impedance functions having higher characteristic frequencies; (b) only discrete points in the response could be sampled for

extrapolation; (c) the measured result was easily affected by other series components.

A better scheme is to ultilize computer on-line processing. The response signal can be loaded to a mini-computer through an A/D converter and multiplexing circuits; the curve-fitting and iteration process can be executed simultaneously through soft-ware control. This facilitates a better measurement speed, accuracy and response time.

(2) The non-linear behaviour of the skin impedance consequent upon a large excitation signal is a subject of interest. The possible causes for this are (a) dielectric breakdown (62); (b) thermal damage (60); (c) water transport across the corneum (63). A thorough understanding of the basic mechanism will enable flexibilities in the application of transcutaneous therapy or sensory substitutes.

(3) More individual samples is needed to support or disqualify the avocated pattern of Ryodoraku. The method developed in this project has proved to be reliable and should be useful useful for further investigation.

REFERENCES

1. Rothman S., Physiology and biochemistry of the skin, The University of Chicago Press, Chicago 1954.

2. Champion R.H., Gillman T., Rook A.J., Sims R.T. (Eds), An introduction to the biology of the skin, Blackwell Scientific Publications, 1970.

3. Edelberg R., Electrical properties of skin, in H.R. Elden (Ed.), Biophysical properties of the skin, Vol. I, N.Y., Wiley, 1971.

4. Weiner J.S., Hellmann K., The sweat glands, Biological Review, 35, 1960.

5. Montagna W., Parakkal P.F., The structure and function of skin, 3rd Ed., Academic Press, N.Y., 1974.

6. Geddes L.A., Electrodes and the measurement of bioelectric events, Wiley-Interscience, N.Y., 1972.

7. Tregear R.T., Physical functions of skin, Academic Press, N.Y., 1966.

8. Lawler J.C., Davis M.J., Griffith E.C., Electrical characteristics of the skin, J. Invest. Dermatol., 34, 1960.

9. Suchi T., Experiments on electrical resistance of the human epidermis, Japanese J. Physiol., 5, 1955.

10. Rosendal T., Concluding studies on the conducting properties of human skin to AC, Acta Physiol. Scand., 9, 1945.

11. Gildemeister M., Die Elektrizitätserzengung der Haut und der Drüsen In Bethe, "Handbuch normalen pathologischen Physiologie" Bd VIII, Tl. 2, 1928.

12. Yokota T., Fujimori B., Impedance change of the skin during the galvanic skin reflex, Japanese J. Physiol., 12, 1962.

13. Fowles D.C. Mechanisms of electrodermal activity, in R. Thompson and M. Patterson (Eds.), Bioelectric recording techniques, Part C, Academic Press, N.Y., 1974.

14. Venables P.H. Martin I., Skin resistance and skin potential, in P. Venables and I. Martin (Eds.), Manual of psychophysiological methods, Wiley, N.Y., 1967.

15. Huhta J.C., Webster J.G., Interference in biopotential recording, in H.A. Miller and D.C Harrison (Eds.), Biomedical electrode technology, Academic Press, N.Y., 1974.

16. Swanson D.K., Webster J.G., A model for skin-electrode impedance, in H.A. Miller and D.C. Harrison (Eds.), Biomedical electrode technology, Academic Press, N.Y., 1974.

17. Khalafalla A.S., Turner L., Spyker D., An electrical model to simulate skin dielectric dispersion, Computers and Biomed. Research, 4, 1971.

18. Cole K.S., Membranes, ions and impulses, University of Calif. Press, Calif. 1968.

19 Schwan H.P., Electrical properties of tissue and cell suspensions, in J.H. Lawrence and C.A. Tobias (Eds.), Advances in biological and medical physics, Academic Press, Vol. 5, N.Y., 1957.

20 Cole K.S., Cole R.H., Dispersion and absorption in dielectrics, I, Alternating current characteristics, J. Chem. Physics, 9, 1941.

21. Cole K.S., Cole R.H., Dispersion and absorption in dielectrics, II, Direct current characteristics, J. Chem. Physics, 10, 1942.

22. Mauro A., Space charge regions in fixed charge membranes and the associated property of capacitance, Biophys. J., 2, 1962.

23. Sandblom J., Walker J.L., Eisenman G., The transient response and impedance locus of a mobile site membrane, Biophys. J., 12, 1972.

24. Cole K.S., Electrodiffusion models for the membrane of squid axon, Physiol. Rev., 45, 1965.

25. Kishimoto U., Transmembrane impedance of the chara cell, Japanese J. Physiol., 24, 1974.

26. Almasi J.J., Schmitt O.H., Automated measurement of bioelectric impedance at very lòw frequencies, Computers and Biomed. Research, 7, 1974.

27. Lane J.F., Electrical impedances of superficial limb tissues: epidermis, dermis, and muscle sheath, Ann. NY Acad. Sci., 170, 1970.

28. Sneddon I.H., The use of integral transforms, McGraw-Hill, N.Y., 1972.

29. Gradshteyn I.S., Ryzhih I.M., Table of integrals series and products, Academic Press, N.Y., 1965.

30. Fitzhugh R., Cole K.S., Voltage and current clamp transients with membrane dielectric loss, Biophys. J., 13, 1973.

31. Taylor R.E., Moore J.W., Cole K.S., Biophys. J., 1, 1960.

32. Moore J.W., Narahashi T., Poston R., Arispé N., Biophys. Soc. Annu. Meet. Abstr., 10, 1970.

33. Tregear R.T., Dirnhuber P., The mass of keratin removed from the stratum corneum by stripping with adhesive tape, J. Invest. Derm., 38, 1962.

34. Getzel W.A., Webster J.G., Minimizing silver-silver chloride electrode impedance, IEEE Trans. Biomed. Eng., BME-23, No. 1, 1976.

35. Hunter R., Williams M.G., Studies of epidermal regeneration by means of a strip method, J. Invest. Derm., 29, 1957.

36. Blank H.S., Smith J.G., Fischer R.W., The epidermal barrier: a comparison between scrotal and abdominal skin, J. Invest. Derm., 36, 1961.

37. Yamamoto T., Yamamoto Y., Electrical properties of the epidermal stratum corneum, Med. and Biol. Eng., Mar. 1976.

38. Yamamoto T., Yamamoto Y., Dielectric constant and resistivity of epidermal stratum corneum, Med. and Biol. Eng., Sept. 1976.

39. Wada M., Sudorific action of adrenadin on the human sweat glands and determination of their excitability, Science 111, 1950.

40. Lader M.H., Montagu J.D., The psycho-galvanic reflex: a pharmacological study of the peripheral mechanism, J. Neurol. Neurosurg. Psychiat., 26, 1962.

41. Almasi J.J., Schmitt O.H., Systematic and random variations of ECG electrode system impedance, Presented at international impedance meeting, New York Acad. Sci., N.Y., 1969.

42. Frost E., Orkin L.R., Localization of acupuncture sites, Pro. NIH Acupuncture Research Conf., DHEW Publication No. (NIH) 74-165, 1973.

43. Noordergraaf A., Silage D., Electroacupuncture, IEEE Trans. Biomed. Eng., BME-20, No. 5, 1973.

44. Sarkany I., Shuster S., Stammers M.C., Occlusion of the sweat pore by hydration, British J. of Dermat., 77, 1965.

45. Lavier J., Deutsche Zeitschrift für Akupunktur (West Germany), 9(3), 1960. Chinese translation from 針灸專輯，上海市醫藥科學技術情報站編，上海科學技術出版社，1962.

46. Kim B.H. (金鳳漢，關於經絡實質的研究，朝鮮醫學 (1)：5~13，1962.
Chinese translation: ibid.

47. 針刺麻醉資料綜述，全國針刺麻醉學習班選編組編，人民衛生出版社，1973.

48. 針刺麻醉原理的探討，同上.

49. 針刺麻醉的臨床應用，同上.

50. Saita H.S., Modern scientific medical acupuncture, J. Am. Osteopath. Assoc., 72, 1973.

51. Matsumoto T., Hayes M.F., Acupuncture, electric phenomenon of the skin and Postvagotomy Gastrointestinal Atony, Am. J. Surg., 125, 1973.

52. 七泉晃正，灸の臨床，6(2)，1959.
Chinese translation: 針灸專輯 (45).

53. Reichmanis M., Marino A.A., Becker R.O., Electrical correlates of Acupuncture points, IEEE Trans. Biomed. Eng., BME-22, 1975.

54. Reichmanis M., Marino A.A., Becker R.O., D.C. skin conductance variation at acupuncture loci, Am. J. Chinese Med., 4:1, 1976.

55. Becker R.O., Reichmanis M., Marino A.A., Spadaro J.A., Electrophysiological correlates of Acupuncture points and meridians, Psychoenergetic Systems, 1, 1976.

56. 經絡電阻測量的初步小結（摘要），北京醫學院基礎部、第三附屬醫院針麻組，錄自針刺麻醉原理的探討，(48).

57. 針灸學，上海中醫學院編，人民衛生出版社，1974

58. Leung K.Y. (梁鏡亮) (Ed.), Acupuncture Digest, Chinese Acupuncture Association, Hong Kong, 1967.

59. Burton C.V., Maurer D.D., Solvent-activated current passing tape electrode for transcutaneous electrical stimulation of the peripheral nervous system, IEEE Trans. Biomed. Eng., BME-23, No. 4, 1976.

60. Mason J.L., Mackay N.A.M., Pain sensations associated with electrocutaneous stimulation, IEEE Trans. Biomed. Eng., BME-23, No. 5, 1976.

61. Hardy H.D., Pain sensations and reactions, Baltimore, MD: Williams and Wilkins, 1952.

62. Gibson R.H., Electrical stimulation of pain and touch in the skin senses, D.R. Kenshalo (Ed.), Springfield, IL: Thomas, 1968.

63. Rein H., Electro-endosmosis in excised human skin, Z. Biol., 81, 1924.

PART TWO

INTRODUCTION

In our study on the skin impedance it was found that the impedance possessed a peculiar frequency dispersion effect, namely that it could be described by a constant phase frequency-dependent component. Later it was found that the overall impedance of the skin could be decomposed into cellular units of similar form. That is to say, in order to understand the nature of the skin impedance more completely, it would be neccessary to start from the cellular level - to find the nature of the impedance in a single biological cell. There is a wealth of literature on this topic, all pointing to the properties of the cell membrane. In general, three approaches have been used in characterizing ion permeation across the membrane (1): the electrodiffusion theory formulated by Nernst and Planck, the theory of irreversible thermodynamics, and the transition theory. We are more interested in the electrodiffusion model because this is more powerful in predicting the kinetic behaviour. In principle, a diffusion process will give rise to a frequency-dependent impedance. This effect has been noted in calculating the AC diffusion impedance of a p-n junction diode (2). We shall try to apply the electro-diffusion model in the consideration of a cell membrane. However,

we shall point out the misconception in the conventional development of the model. The misconception has been generally taken for granted, and inevitably has led to inconsistent results. With some modifications we shall show that the electrodiffusion model can be a powerful approach in predicting the membrane frequency characteristics.

CHAPTER EIGHT MEMBRANE IMPEDANCE

8.1 ELECTRODIFFUSION EQUATIONS

Consider a membrane system as shown in Fig. 8.1. The following assumptions are made:

(1) The membrane is of constant thickness d, is homogeneous, and is infinite in extent in the transverse plane.
(2) For simplicity the permeating ions are assumed to be of a single salt, and are univalent.
(3) The ions are completely dissociated (activity coefficient = 1).
(4) Ion mobilities are constant over the range considered and are the same within the membrane as in the free solution.
(5) Osmotic and hydrostatic pressures are assumed to be negligible. Ion convection is also negligible.

We are interested in knowing how the ions will permeate through the membrane. For an ionic species moving under the influences of a concentration gradient and an electric field, the

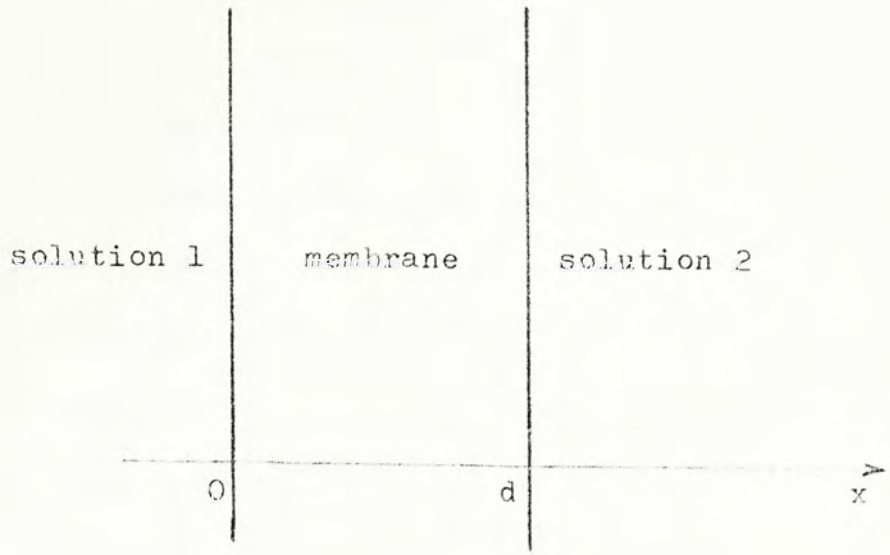

Fig. 8.1 A membrane separating two solutions.

Nernst-Planck equation gives the resultant flux. The ionic currents for a cation and an anion are respectively given by:

$$-J_p = D_p F \frac{\partial C_p}{\partial x} + F \mu_p C_p \frac{\partial \phi}{\partial x} \qquad (8.1)$$

$$-J_n = -D_n F \frac{\partial C_n}{\partial x} + F \mu_n C_n \frac{\partial \phi}{\partial x} \qquad (8.2)$$

where μ: ionic mobility

D: diffusion coefficient

C: ionic concentration

F: Faraday's constant

ϕ: electric potential

and the subscripts p and n refer to cations and anions respectively.

The Nernst-Planck equations are fundamental to the study of electrodiffusion processes inside a membrane. We shall proceed to solve these equations for the ionic fluxes and concentration and potential profiles. In doing so, two additional relations are helpful. The first is given by the continuity equations which describe the variations of ionic fluxes and the concentration profiles. The other is the Poisson's equation for the potential distribution. These are stated in the following equations:

$$\frac{\partial C_p}{\partial t} = -\frac{1}{F}\frac{\partial J_p}{\partial x} \qquad (8.3)$$

$$\frac{\partial C_n}{\partial x} = \frac{1}{F}\frac{\partial J_n}{\partial x} \qquad (8.4)$$

$$\frac{\partial^2 \phi}{\partial^2 x} = -\frac{F\rho}{\epsilon} \qquad (8.5)$$

where ρ = net charge density

ϵ = electric permittivity

If a steady current is maintained through the membrane, we have,

$$J_o = J_p + J_n \qquad (8.6)$$

Equations (8.3 - 8.6) are the constraints to be imposed in solving (8.1) and (8.2).

The continuity equations (8.3) and (8.4) can be stated in a more convenient form. Differentiating equations (8.1) and (8.2) with respect to x and substituting (8.3) and (8.4) for the LHS, we have

$$\frac{\partial C_p}{\partial t} = D_p \frac{\partial^2 C_p}{\partial x^2} + \mu_p \frac{\partial C_p}{\partial x}\frac{\partial \phi}{\partial x} + \mu_p C_p \frac{\partial^2 \phi}{\partial x^2} \qquad (8.7)$$

$$\frac{\partial C_n}{\partial t} = D_n \frac{\partial^2 C_n}{\partial x^2} - \mu_n \frac{\partial C_n}{\partial x}\frac{\partial \phi}{\partial x} - \mu_n C_n \frac{\partial^2 \phi}{\partial x^2} \qquad (8.8)$$

8.2 ELECTRONEUTRALITY OR SPACE CHARGE?

8.2.1 Microscopic electroneutrality

The primary goal in electrodiffusion analysis is to solve equations (8.1, 8.2) subject to the constraints of (8.3 - 8.6). It will readily be seen that these partial differential equations are not easily separable unless some simplifying assumptions can be made. Such assumptions may not be realistic , but so long as they are consistent within the framework of analysis the results can be tested experimentally for validity.

One simplest approximation to make is the use of the Laplace equation in lieu of the more rigorous Poisson equation (8.5). That is,

$$\frac{\partial^2 \phi}{\partial x^2} = 0 \qquad (8.9)$$

This is equivalent to stating that the principle of electroneutrality applies to the membrane not only as a whole (macroscopic electroneutrality) but also on a point-wise basis (microscopic electroneutrality). This assumption obviously affords a substantial mathematical simplification (3), and because of this it has become the basis of most studies concerning electrodiffusion (4).

Putting the Laplace equation (8.9) into the continuity equations (8.7) and (8.8), one gets

$$\frac{\partial C_p}{\partial t} = D_p \frac{\partial^2 C_p}{\partial x^2} + \mu_p \frac{\partial C_p}{\partial x} \frac{\partial \phi}{\partial x} \qquad (8.10)$$

$$\frac{\partial C_n}{\partial t} = D_n \frac{\partial^2 C_n}{\partial x^2} - \mu_n \frac{\partial C_n}{\partial x} \frac{\partial \phi}{\partial x} \qquad (8.11)$$

Equations (8.10) and (8.11) can be rearranged to eliminate terms containing the electric field component, giving (for $C_p = C_n$)

$$\mu_n \frac{\partial C_p}{\partial t} + \mu_p \frac{\partial C_n}{\partial t} = \mu_n D_p \frac{\partial^2 C_p}{\partial x^2} + \mu_p D_n \frac{\partial^2 C_n}{\partial x^2} \qquad (8.12)$$

Since microscopic electroneutrality is assumed we may write $C_p = C_n = C$. We note that the ionic mobilities and diffusion coefficients are related by the Einstein equation

$$D_p F = \mu_p RT \; ; \quad D_n F = \mu_n RT \qquad (8.13)$$

where R is the molar gas constant, and T is the absolute temperature. Consequently equation (8.12) becomes

$$\frac{\partial C}{\partial t} = D \frac{\partial^2 C}{\partial x^2} \qquad (8.14)$$

where $D = \dfrac{2 D_n D_p}{D_n + D_p}$ is the ambipolar diffusion coefficient.

Equation (8.14) can be solved directly once the boundary conditions and the type of forcing function are specified. In general, the steady-state concentration profile will be in the form (5)

$$C(x,t) = C_o + C'(x,t) \qquad (8.15)$$

where C_o is the mean concentration throughout the membrane in the zero current steady-state condition, and $C'(x,t)$ is the variable part of the concentration.

For a sinusoidal perturbation the second term of (8.15) can be written as

$$C'(x,t) = C'(x)\, e^{j\omega t} \qquad (8.16)$$

Hence equation (8.14) can be written as

$$j\omega C'(x,t) = \frac{\partial^2 C'(x,t)}{\partial x^2} \qquad (8.17)$$

and the solution immediately follows.

8.2.2 Several querries

The approach discussed above was generally adopted by many authors (for example, Sandblom et al., Ref. 6) as being analogous to the transport of electric charges in semiconductors. Before we examine it more closely we shall quote some arguments put forward by Agin (7) in opposition to the assumption of microscopic electroneutrality. They are summarized as follows:

(1) Microscopic electroneutrality is a satisfactory approximation only if the following conditions can hold:

(a) In the time domain, the relaxation time of the substance is very much shorter than the time span of a certain event.

(b) In the space domain, substantial depa ures from electroneutrality may occur only over very short distance of the

order of a few Debye lengths (the Debye shielding length is a measure of the extent to which space charge can be held at the expense of thermal energy. For physiological systems it is on the order of several angstroms). If the space of interest is great enough such departures may be negligible.

However, the membranes are very poor conductors having a relaxation time of the order of milliseconds, and they are usually no more than several Debye lengths in thickness. Therefore it is quite doubtful if the assumptions can still be valid.

(2) At an interface between two phases the discontinuities of dielectric constant and charge density are such that a diffuse layer of accumulated charges is completely necessary on both sides of the boundary. For a thin structure like the membrane, the net charge density does not have room to decay to zero within the two bounding edges, so that the assumption of electroneutrality will be seriously violated.

(3) As the electric permittivity is of the order of 10^{-11}, (S.I units) extremely small values of charge density can still produce substantial divergence of the electric field.

From these considerations it would seem worthwhile to take heed of the unlimited use of the electroneutrality requirement in working out the electrodiffusion models. A detailed

discussion was presented by Cole (8) to review the inability of the classical electrodiffusion theory to describe the behaviour of the squid axon, and this led him to conclude that without some modifications the approach was completely unrealistic. As Agin saw it, a serious examination of the properties of space charge regions in the membrane might provide surer ground.

8.2.3 Inconsistencies arising from electroneutrality

Although the arguments advocated by Agin was sound enough to arouse suspicion in the validity of electroneutrality, it was not so powerful to disqualify the use of it completely. We shall show that the assumption of microscopic electroneutrality is self-contradictory and leads to trivial results.

For convenience the continuity equations (8.10, 8.11, 8.14) are rewritten here in terms of the variable part of the concentration

$$\frac{\partial C'}{\partial t} = D_p \frac{\partial^2 C'}{\partial x^2} + \mu_p \frac{\partial C'}{\partial x} \frac{\partial \phi}{\partial x} \qquad (8.18)$$

$$\frac{\partial C'}{\partial t} = D_n \frac{\partial^2 C'}{\partial x^2} - \mu_n \frac{\partial C'}{\partial x} \frac{\partial \phi}{\partial x} \qquad (8.19)$$

$$\frac{\partial C'}{\partial t} = D \frac{\partial^2 C'}{\partial x^2} \qquad (8.20)$$

where $C' = C'(x,t)$

At this point most authors would ignore (8.18, 8.19) and go on straight to solve (8.20) directly. However, a careful re-examination of all three equations shows that the system of equations are not consistent at all.

Let us first substitute (8.21, 8.22) into (8.18). This gives

$$j\omega\, C'(x)\, e^{j\omega t} = D_p \frac{\partial^2 C'(x)}{\partial x^2} e^{j\omega t} + \mu_p \frac{\partial C'(x)}{\partial x} \frac{\partial \phi_o}{\partial x} e^{(j\omega t)2}$$

Separating terms containing $e^{j\omega t}$ and $e^{2j\omega t}$, we have

$$j\omega C' = D_p \frac{\partial^2 C'}{\partial x^2} \qquad (8.23)$$

$$\frac{\partial C'}{\partial x} \frac{\partial \phi_o}{\partial x} = 0 \qquad (8.24)$$

Similarly equation (8.19) can be separated into

$$j\omega C' = D_n \frac{\partial^2 C'}{\partial x^2} \qquad (8.25)$$

$$\frac{\partial C'}{\partial x} \frac{\partial \phi_o}{\partial x} = 0 \qquad (8.26)$$

Equations (8.23, 8.25) can be satisfied simultaneously only if $D_p = D_n$ or

$$\frac{\partial^2 C'}{\partial x^2} = C' = 0 \qquad (8.27)$$

Since in general $D_p \neq D_n$, equation (8.27) results. This condition is also consistent with equation (8.24, 8.26) where the concentration gradient is then necessarily zero. From equations (8.15), (8.16), it is obvious that

$$C(x,t) = C_o \qquad (8.28)$$

Equation (8.28) states that under steady conditions the concentration of each ion species must be constant everywhere inside the membrane. If so the statement of (8.20) is nothing more than a tautology and the solution thereof must be totally irrelevant. This vital point was virtually ignored by many authors working in this field (3, 5, 6).

If the condition (8.27) is substituted into equations (8.1, 8.2), the ionic currents can be obtained as

$$J_p = - F \mu_p C_o \frac{\partial \phi}{\partial x}$$

$$J_n = - F \mu_n C_o \frac{\partial \phi}{\partial x}$$

Hence under electroneutrality condition the ions can only move under constant drift. This is obviously the case for an infinite volume of electrolytes, but for the membrane of only 100 Å in thickness this result is completely at variance. If only the drift component was present, the membrane would not have such properties as capacitance and potential at all. In conclusion we may say that the assumption of microscopic electroneutrality is identical to stating that the membrane is no different from the bulk of the electrolytic solution, and any attempt to infer a form for the concentration profile is as misleading.

8.3 SOLUTION OF NERNST-PLANCK EQUATIONS FOR A MEMBRANE IN SPACE CHARGE

8.3.1 A simple relation for ionic concentrations

If the simplifying assumption of electroneutrality is not permissible, it will be much more difficult to find a solution for the Nernst-Planck equations (8.1, 8.2). Since the Laplace equation (8.9) does not hold, the next lower order approximation applied to the situation of a membrane will be the Poisson equation (8.5). For a net space charge to occur, the ionic concentrations C_p and C_n are not the same, but can separately be written as (5)

$$C_p = C_o + p(x,t) \qquad (8.29)$$

$$C_n = C_o + n(x,t) \qquad (8.30)$$

where p and n are the perturbed ionic concentrations and C_o is the mean concentration. It should be noted that the mean ionic concentration (over the whole membrane) is assumed to the same for both cation and anion. This is necessary for the membrane to be electrically neutral macroscopically. In other words

$$\int_o^d \rho(x,t)\,dx = \int_o^d p\,dx - \int_o^d n\,dx = 0 \qquad (8.31)$$

where ρ is the net charge density. For a sinusoidal forcing function we have the linearized forms

$$p(x,t) = p(x)\, e^{j\omega t} \qquad (8.32)$$

$$n(x,t) = n(x)\, e^{j\omega t} \qquad (8.33)$$

Similarly, the Nernst-Planck equations (8.1, 8.2) and the continuity equations (8.7, 8.8) can be linearized by assuming p, n to be negligible compared with C_o. Thus,

$$-J_p = D_p F \frac{\partial p}{\partial x} + F \mu_p C_o \frac{\partial \phi}{\partial x} \qquad (8.34)$$

$$-J_n = -D_n F \frac{\partial n}{\partial x} + F \mu_n C_o \frac{\partial \phi}{\partial x} \qquad (8.35)$$

$$j\omega p = D_p \frac{\partial^2 p}{\partial x^2} + u_p C_o \frac{\partial^2 \phi}{\partial x^2} \qquad (8.36)$$

$$j\omega n = D_n \frac{\partial^2 n}{\partial x^2} - u_n C_o \frac{\partial^2 \phi}{\partial x^2} \qquad (8.37)$$

The last two equations can be put into the forms

$$\frac{j\omega p}{D_p} = \frac{\partial^2 p}{\partial x^2} + \frac{F C_o}{RT} \frac{\partial^2 \phi}{\partial x^2} \qquad (8.38)$$

$$\frac{j\omega n}{D_n} = \frac{\partial^2 n}{\partial x^2} - \frac{F C_o}{RT} \frac{\partial^2 \phi}{\partial x^2} \qquad (8.39)$$

where the Einstein relation (8,13) has been ultilized. Adding and subtracting (8.38) and (8.39) gives

$$\frac{\partial^2 (p+n)}{\partial x^2} = j\omega \, (p/D_p + n/D_n) \qquad (8.40)$$

$$\frac{\partial^2 \rho}{\partial x^2} = j\omega \, (p/D_p - n/D_n) + \frac{F^2 C_o}{RT\epsilon} \rho \qquad (8.41)$$

These equations are not easily separable unless when the following relation is satisfied:

$$p = k\, n \qquad (8.42)$$

This equation shows a simple relation between p and n, and will be ultilized for the solution of (8.38) and (8.39). We note that the

condition of microscopic neutrality, namely $p = n$, is a particular solution of (8.42) only. In general $k \neq 1$ and the exact value of k can be inferred from the solution of (8.38) and (8.39). Before this, we first note that the net charge density can be expressed in terms of k as

$$\rho = (k - 1)\, n = (k - 1)\, p / k \qquad (8.43)$$

Substituting the Poisson equation (8.5) into (8.36, 8.37) and using these expressions for ρ, we have

$$j\omega p = D_p \frac{\partial^2 p}{\partial x^2} - \frac{\mu_p C_o F}{\epsilon} \frac{(k - 1)}{k}\, p$$

$$j\omega n = D_n \frac{\partial^2 n}{\partial x^2} + \frac{\mu_n C_o F}{\epsilon} (k - 1)\, n$$

These two equations can be rearranged to give the simpler forms

$$\frac{\partial^2 p}{\partial x^2} = \frac{p}{L_p^2} \quad ; \quad \frac{\partial^2 n}{\partial x^2} = \frac{n}{L_n^2} \qquad (8.44)\ (8.45)$$

where

$$\frac{1}{L_p^2} = \frac{j\omega}{D_p} + \frac{\mu_p C_o F}{D_p \epsilon} \frac{(k - 1)}{k} \qquad (8.46)$$

$$\frac{1}{L_n^2} = \frac{j\omega}{D_n} + \frac{\mu_n C_o F}{D_n \epsilon} (k - 1) \qquad (8.47)$$

L_p, L_n are the diffusion lengths.

Equations (8.44, 8.45) are both simple second order differential equations with the solutions in the form

$$A e^{\frac{x}{L}} + B e^{-\frac{x}{L}}$$

Now if p and n are to be similarly proportional to each other everywhere in the membrane, it is necessary that $L_p = L_n$. Thus,

$$\frac{j\omega}{D_p} + \frac{\mu_p C_o F}{D_p \epsilon} \frac{(k-1)}{k} = \frac{j\omega}{D_n} - \frac{\mu_n C_o F}{D_n \epsilon} (k - 1)$$

from which

$$k^2 + \left\{ \frac{j\omega RT}{F^2 C_o} (D_n - D_p)/D_n D_p \right\} k - 1 = 0 \qquad (8.48)$$

This last equation specifies the value of k. Writing

$$1/D' = \frac{D_n - D_p}{D_n D_p} \qquad (8.49)$$

$$R_m^2 = \frac{RT\epsilon}{2 C_o F^2} \qquad (8.50)$$

where R_m is the Debye shielding length, (8.48) simplifies to

$$k^2 + \frac{2j\omega R_m^2}{D'} k - 1 = 0 \qquad (8.51)$$

Here an approximation for the above equation proves helpful. We note that the ionic mobilities of most ions in the membrane are of the order of 10^{-12} $m^2 s^{-1} V^{-1}$ (8) so that the diffusion coefficients at room temperatures are of the order of 10^{-14} $m^2 s^{-1}$. This implies

$$D' > 10^{-14} \ m^2 s^{-1}$$

The Debye shielding length R_m under physiological conditions is approximately 10 Å (4). From these values,

$$R_m^2 / D' < 10^{-4}$$

so that at moderate frequencies the middle term of (8.51) can be neglected. Consequently we may have a more convenient expression for k. That is,

$$k^2 - 1 = 0 \qquad (8.52)$$

giving $k = +1, -1$ (8.53)

It should be noted that the first solution in (8.53) is trivial (electroneutrality) and corresponds to free electrolytic solutions of immense volume. The second solution indicates another state of ionic transport in which a gain in the cation concentration is coupled to a loss in anion concentration, in equal quantity. The

reverse is also true. This strikingly simple expression for k suggests a very interesting feature of ionic transport involving two species - only two states can take place: either electroneutrality is maintained or a space charge is set up with equal and opposite changes in the two ionic concentrations. This statement is exact under DC steady state condition or if the diffusion coefficients of the two ion species are equal.

At higher frequencies equation (8.51) must be used and the complete solution for k is thus

$$k = -j\omega R_m^2 / D' \pm \sqrt{1 + (j\omega R_m^2 / D')^2} \qquad (8.54)$$

Putting this into equations (8.46) and (8.47) for the diffusion lengths, we find

$$1/L^2 = 1/L_n^2 = 1/L_p^2 \qquad (8.55)$$

$$= \tfrac{1}{2} \left\{ 1/R_m^2 + \frac{j\omega(D_n + D_p)}{D_n D_p} \mp 1/R_m^2 \sqrt{1 + (j\omega R_m^2 / D')^2} \right\} \qquad (8.56)$$

Two special cases are noted:

(1) In DC steady state, $\omega = 0$, then

$$L = \infty, \quad R_m \qquad (8.57)$$

corresponding to the neutrality and space charge condition respectively. The second solution is quite reasonable since the decay of a space charge is characterized by the Debye shielding length.

(2) $D_n = D_p$ For equal diffusion coefficients $k = \pm 1$ and the diffusion lengths are given by

$$1/L^2 = \begin{cases} j\omega/D & k = 1 \qquad (8.58) \\ j\omega/D + 1/R_m^2 & k = -1 \qquad (8.59) \end{cases}$$

Where $D = D_p = D_n$

8.3.2 Solutions for concentration profiles

Having found the value of k we may now proceed to solve for the concentration profiles. From equations (8.44, 8.45),

$$p = A_p e^{\frac{x}{L}} + B_p e^{-\frac{x}{L}}$$

$$n = A_n e^{\frac{x}{L}} + B_n e^{-\frac{x}{L}}$$

For the condition $p = k n$ to hold everywhere in the membrane, it is also necessary that

$$A_p = k A_n = A$$

$$B_p = k B_n = B$$

Hence we have

$$p = Ae^{\frac{x}{L}} + Be^{\frac{-x}{L}} = k n \qquad (8.60)$$

From equation (8.31)

$$\int_o^d (Ae^{\frac{x}{L}} + Be^{-\frac{x}{L}})\, dx = 0$$

Therefore $(A - B) = Ae^{\frac{d}{L}} - Be^{-\frac{d}{L}}$.

A solution for the above equation is $B = -Ae^{\frac{d}{L}}$.

Substituting into (8.60), we have

$$p = A\left(e^{\frac{x}{L}} - e^{\frac{d-x}{L}}\right) \qquad (8.61)$$

At $x = 0$, $p(0) = A\left(1 - e^{\frac{d}{L}}\right)$ (8.62)

and hence

$$p = p(0)\,\frac{\left(e^{\frac{x}{L}} - e^{\frac{d-x}{L}}\right)}{1 - e^{\frac{d}{L}}} \qquad (8.63)$$

It is interesting to note that the concentration profile is asymmetrical, i.e.,

$$p(x) = -p(d-x) \qquad (8.64)$$

Similarly $$n = n(0)\,\frac{\left(e^{\frac{x}{L}} - e^{\frac{d-x}{L}} \right)}{1 - e^{\frac{d}{L}}} \qquad (8.65)$$

where $$n(0) = k\,p(0) \qquad (8.66)$$

$$= -n(d) \qquad (8.67)$$

8.3.3 Solution for ionic currents

Once the concentration profile is specified, we may obtain a solution for the potential profile and from these results the total ionic current can be determined. From Poisson equation (8.5), and using the relation $\rho = p(k - 1)/k$

$$\frac{\partial \phi}{\partial x} = -\frac{F}{\epsilon} \int \rho \, dx$$

$$= -\frac{F}{\epsilon} \frac{(k-1)A}{k} \int \left(e^{\frac{x}{L}} - e^{\frac{d-x}{L}} \right) dx$$

$$= -\frac{F}{\epsilon} \frac{(k-1)\,AL}{k} \left(e^{\frac{x}{L}} + e^{\frac{d-x}{L}} \right) + \frac{\partial \phi_o}{\partial x} \qquad (8.68)$$

where $\frac{\partial \phi_o}{\partial x}$ is a constant field.

Integrating once more from 0 to d,

$$V = \int_0^d \frac{\partial \phi}{\partial x} dx = \frac{2FL^2(k-1)}{k\epsilon} p(0) + \frac{\partial \phi_o}{\partial x} d$$

where V is the potential difference across the membrane boundaries. Hence

$$\frac{\partial \phi_o}{\partial x} = \frac{V}{d} - \frac{2FL^2(k-1)}{kd\epsilon} p(0) \qquad (8.69)$$

Substituting into (8.68),

$$\frac{\partial \phi}{\partial x} = -\frac{F(k-1)}{k\epsilon} LA\left(e^{\frac{x}{L}} + e^{\frac{d-x}{L}} \right) + \frac{V}{d} - \frac{2FL^2(k-1)}{kd\epsilon} p(0) \qquad (8.70)$$

The concentration gradients are obtained by differentiating equation (8.61) and (8.65). Thus,

$$\frac{\partial p}{\partial x} = \frac{A}{L}\left(e^{\frac{x}{L}} + e^{\frac{d-x}{L}} \right) \qquad (8.71)$$

$$\frac{\partial n}{\partial x} = \frac{kA}{L}\left(e^{\frac{x}{L}} + e^{\frac{d-x}{L}} \right) \qquad (8.72)$$

As a result, the ~~ionic concentrations~~ current densities given by (8.34, 8.35) are now

$$-J_p = \frac{D_p FA}{L}\left(e^{\frac{x}{L}} + e^{\frac{d-x}{L}} \right) - \frac{F^2 \mu_p C_o}{\epsilon} \frac{(k-1)LA}{k}\left(e^{\frac{x}{L}} + e^{\frac{d-x}{L}} \right) + \frac{F\mu_p C_o}{d}\left\{ V - \frac{2FL^2}{\epsilon}\frac{(k-1)}{k} p(0) \right\} \qquad (8.73)$$

$$-J_n = \frac{-D_n F A k}{L}\left(e^{\frac{x}{L}} + e^{\frac{d-x}{L}} \right) - \frac{F^2 \mu_n C_o}{\epsilon} \frac{(k-1)LA}{k}\left(e^{\frac{x}{L}} + e^{\frac{d-x}{L}} \right)$$

$$+ \frac{F\mu_n C_o}{d}\left\{ V - \frac{2FL^2}{\epsilon}(k-1).n(0) \right\} \qquad (8.74)$$

In most cases the mobilities of the two ion species are not too much different, so that $D' \gg D_p \doteq 10^{-14}\ m^2 s^{-1}$. Also we are most interested in the frequency dispersion occuring at moderate or low frequencies. Consequently the equation (8.52) is a reasonable approximation. This gives $k = \pm 1$. From equation (8.56), the diffusion length is given by

$$1/L = \sqrt{1/R_m^2 + j\omega \frac{D_n + D_p}{2D_n D_p}}$$

$$= 1/R_m \sqrt{1 + j\omega\lambda} \qquad (8.75)$$

where $$\lambda = R_m^2 \frac{(D_n + D_p)}{2D_n D_p} \qquad (8.76)$$

With equations (8.53) and (8.75), the equations for the ionic currents then become

$$-J_p = -\frac{D_p F \rho(0)}{2 R_m} \frac{\left(e^{\frac{x}{L}} + e^{\frac{d-x}{L}} \right)}{\left(e^{\frac{d}{L}} - 1 \right)} \left(\frac{j\omega\lambda}{\sqrt{1+j\omega\lambda}} \right) - \frac{D_p F}{1+j\omega\lambda} \frac{\rho(0)}{d}$$

$$+ F\mu_n C_o \frac{V}{d} \qquad (8.77)$$

$$-J_n = -\frac{D_n F \rho(0)}{2R_m} \frac{\left(e^{\frac{x}{L}} + e^{\frac{d-x}{L}} \right)}{\left(e^{\frac{d}{L}} - 1 \right)} \left(\frac{j\omega\lambda}{1+j\omega\lambda} \right) - \frac{D_n F}{1+j\omega\lambda} \frac{\rho(0)}{d}$$

$$+ F\mu_n C_o \frac{V}{d} \qquad (8.78)$$

8.3.4 Membrane impedance

From equations (8.77), (8.78), the total current is

$$-J_o = -(J_p + J_n)$$

$$= (D_p + D_n) F \rho(d) \left\{ \frac{\left(e^{\frac{x}{L}} + e^{\frac{d-x}{L}} \right)}{\left(e^{\frac{d}{L}} - 1 \right)} \left(\frac{j\omega\lambda}{2R_m\sqrt{1+j\omega\lambda}} \right) + \frac{1}{d(1+j\omega\lambda)} \right\}$$

$$+ FC_o(\mu_p + \mu_n) \frac{V}{d} \qquad (8.79)$$

where for convenience $\rho(d)$ is used in place of $\rho(0)$ because for current injected in the negative direction $\rho(d)$ will be positive. The value of $\rho(d)$ is determined by the boundary condition at $x = d$, namely the current density must be continuous. This requires a knowledge of the boundary process pertaining to the membrane-solution interface. There are two hypothesis for the boundary process. One is to assume that in the steady state the membrane

surfaces are in Donnan equilibrium (3). In other words, the ionic concentrations on either side of the boundary, and just next to it, are related by the Nernst potential. Injection of current across the boundary is achieved by altering this potential. This is analogous to a pn junction in which excess charge carriers are injected across the junction by applying a bias potential. Another approach is to assume that the ionic concentration at the edge of the membrane is just proportional to the external concentration; the proportionality constant is given as the 'partition coefficient'. This approach was ultilized by Hodgin and Katz (9) in evaluating the resting membrane potential.

Since no definite description of the membrane boundary process is available we shall not involve in it in detail. But rather, we shall simply assume that the boundary charge density $\rho(d)$ is proportional to the externally applied potential. This is a reasonable assumption because in the linearized form the total ionic current must be proportional to the applied voltage. Similarly the transmembrane p.d. is also proportional to the external applied voltage. Denoting the latter by V_o, these imply

$$\rho(d) = a_1 V_o$$

$$V = a_2 V_o$$

where a_1, a_2 are constants.

It follows from equation (8.79) that at the boundary the current density is given by

$$-\frac{J_o(d)}{V_o} = (D_p + D_n)Fa_1\left\{\coth\frac{d}{2L}\left(\frac{j\omega\lambda}{R_m\cdot\sqrt{1+j\omega\lambda}}\right) + \frac{1}{d(1+j\omega\lambda)}\right\}$$

$$+ FC_o(\mu_p + \mu_n)\frac{a_2}{d} \qquad (8.80)$$

Equation (8.80) gives the membrane admittance. Several points can be noticed:

(1) There is an irrational part, given by the first term inside the large bracket, of the membrane admittance. This will give rise to frequency dispersion in the membrane impedance characteristic and may probably be the cause for the observed anomalous frequency dependent component.

(2) The term $1/j\omega\lambda$ indicates that the membrane may possess an inductive effect. This point has been noted by Cole (10) in experiments with the squid axon membrane, and remained unexplained. From (8.80) we note that for a thin membrane the inductive component may be quite significant at low frequencies.

(3) The last term of equation (8.80) corresponds to simple drift and is equivalent to a pure resistance.

These can be summarised in the equivalent circuit as illustrated in Fig. 8.2. The experimental equivalent circuit of Cole is also drawn for comparison. For convenience (8.80) is rewritten as

$$Y = \frac{J_o(d)}{V_o} = A_1 \left\{ \gamma \left(\frac{j\omega\lambda}{1+j\omega\lambda} \coth \gamma\sqrt{1+j\omega\lambda} \right) + \frac{1}{1+j\omega\lambda} \right\} + A_2 \qquad (8.81)$$

where A_1, A_2 are constants and $\gamma = d/2R_m$.

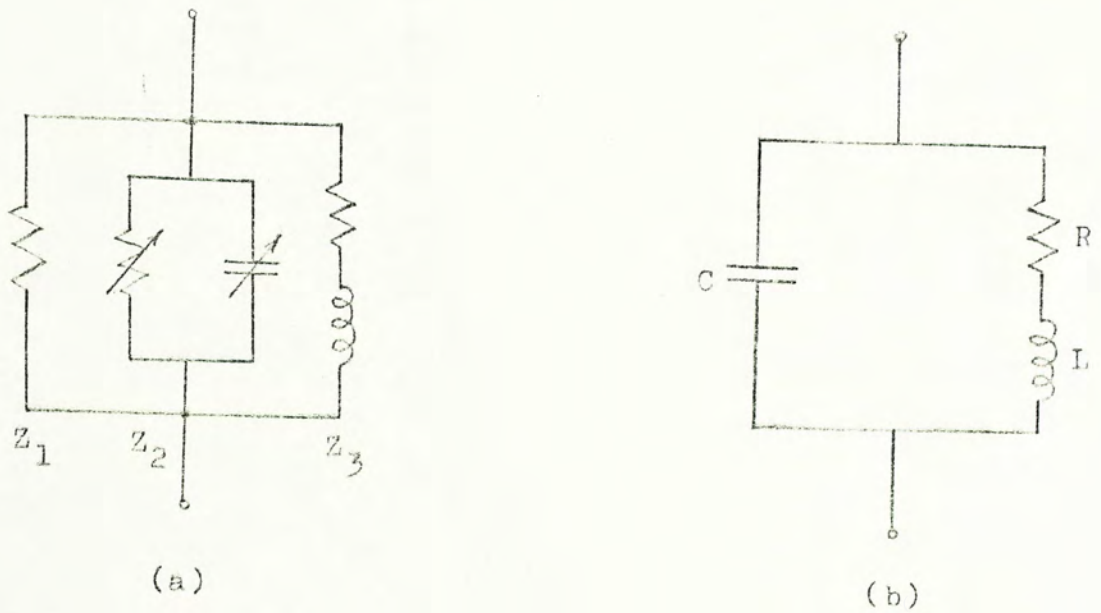

(a) (b)

Fig. 8.2 Equivalent circuit for membrane impedance.
(a) theoretical; (b) Squid axon membrane equivalent circuit.

Z_1- pure resistance; Z_2- frequency-dependent component;
Z_3- inductive component.

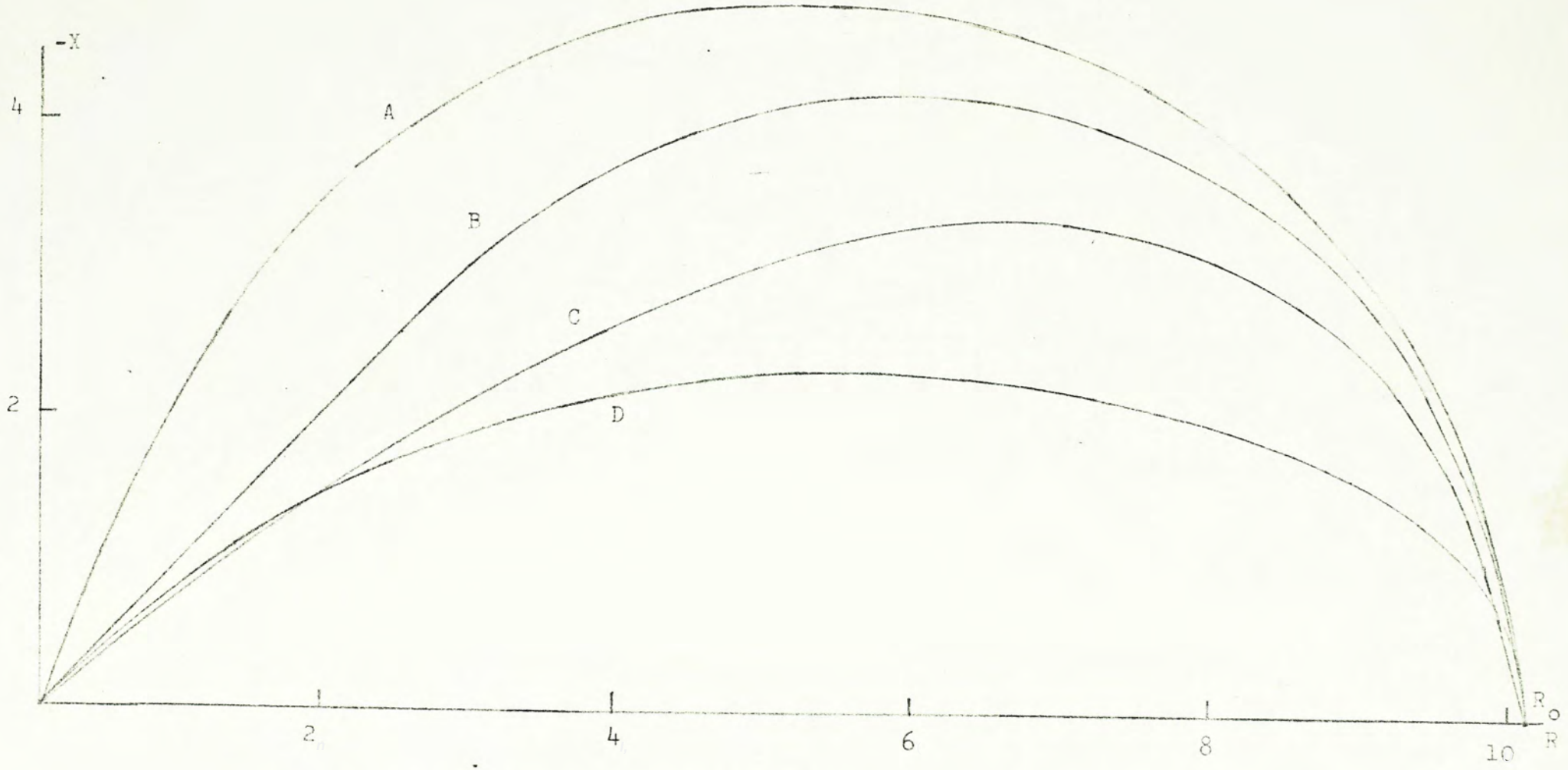

Fig. 8.3 Impedance locus calculated from equation (8.81). Units shown are arbitrary.

	A	B	C	D
A_2/A_1	.1	.1	10	10
γ	10	.1	10	.1

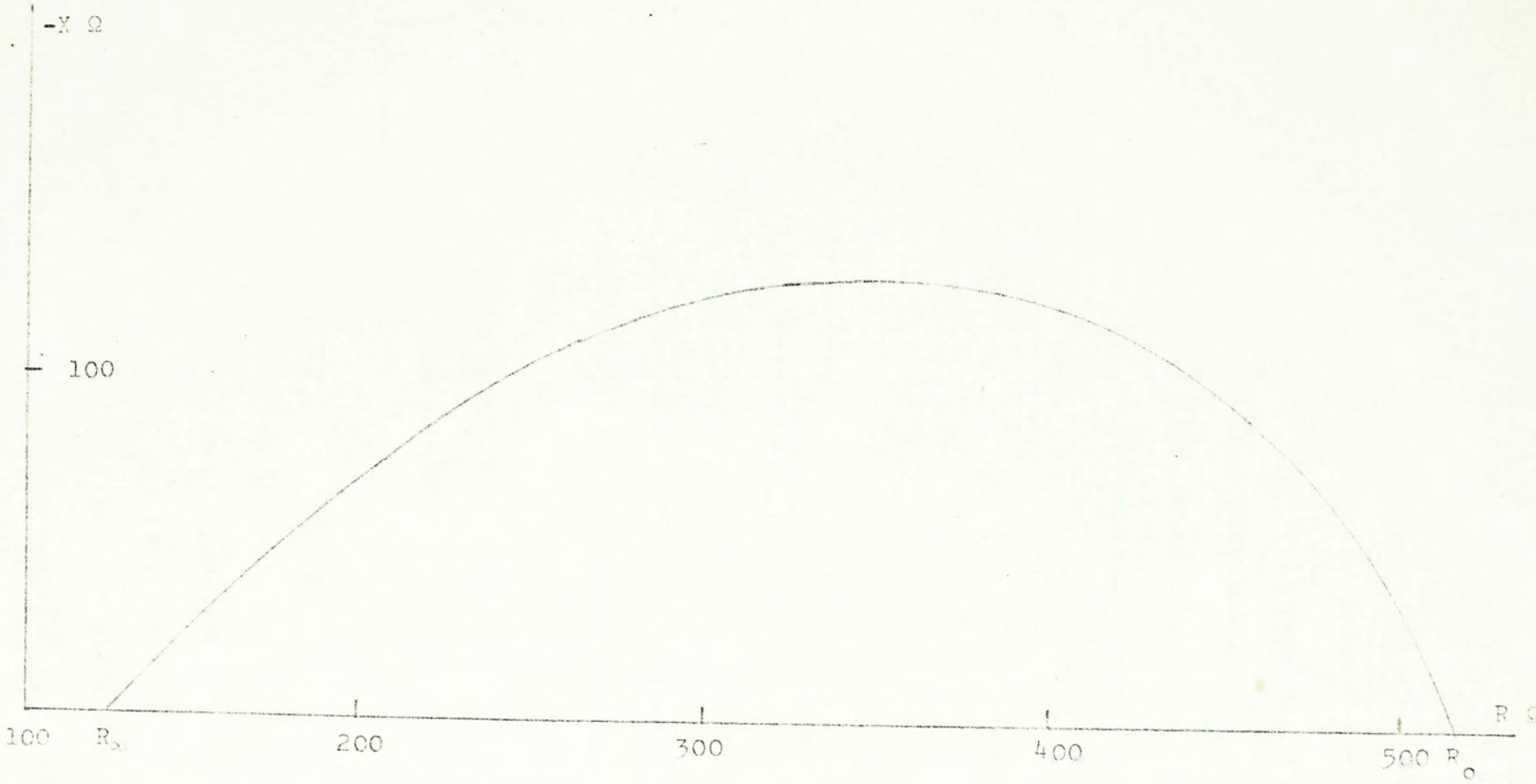

Fig. 8.4 Impedance measurements on the kelp, Laminaria shown on the complex impedance plane (10).

Equation (8.81) is evaluated numerically for different values of γ and A_1/A_2, and the results are presented in Fig. 8.3. It can be seen that the loci approximate to semi-circular arcs at low frequencies and at the high frequency end a constant phase angle is obtained for all loci. The shape is in general agreement with the results obtained for the plant cell membranes as illustrated in Fig. 8.4.

8.4 CONCLUSION

Microscopic electro-neutrality is valid only for a large and uniform volume of electrolytic solution. For a thin membrane in contact with an aqueous solution, the effect of space charge should be considered. The net space charge results from a difference in the concentration of the ionic species. If the two ionic concentrations can be related by a simple ratio the diffusion equations can be solved directly giving a frequency-dependent impedance with an inductive component.

Once the boundary process is known a complete solution for the membrane impedance would be possible. The approach can be extended to include more permeating ionic species. In the case of a membrane separating 2 ionic solutions of different concentrations and compositions, other membrane properties such as rectification and DC membrane potential could be evaluated. This would

definitely provide a better approximation than the simple assumption of electroneutrality.

If the cell membrane impedance can possess frequency-dependent characteristics there is no wonder why the impedance of the skin can be described by the same characteristics. However, for a skin stratum of many cellular laminae of inhomogeneous properties the situation will be more complicated. In this case each cell lamina may have a frequency characteristic of its own and hence a slight distribution effect results. Certainly more work would be necessary if a more precise description of the distribution effect is desired.

REFERENCES

1. Eisenman G., Sandblom J.P., Walker J.L., Membrane structure and ion permeation, Science, 155, Feb. 1967.

2. Feldman J.F., The physics and circuit properties of transistors, Wiley: N.Y., 1973.

3. Teorell T., Transport processes and electrical phenomena in ionic membranes, Progr. Biophys. Biophys. Chem., 3, 1953.

4. Plonsey R., Bioelectric phenomena, McGraw-Hill: N.Y., 1969.

5. Conti F., Eisenman G., The steady state properties of ion exchange membranes with fixed charges, Biophys. J., 6, 1966.

7. Agin D., Electroneutrality and electrodiffusion in the squid axon, Proc. Natl. Acad. Sci., 57, 1967.

8. Cole K.S., Electrodiffusion models for the membrane of squid axon, Physiol. Rev., 45, 1965.

9. Hodgin A.L., Katz B., The effect of sodium ions on the electrical activity of the Giant Axon of the Squid, J. Physiol., 108, 1949.

10. Cole K.S., Membranes, ions, and impulses, University of Calif. Press, Calif., 1968.

6. Sandblom J., Walker J.L., Eisenman G., The transient response and impedance locus of a mobile site membrane, Biophys. J., 12, 1972